Investigating the role of CD226 on $CD4^+$ T cells in the context of cancer

Doctoral thesis

to obtain a doctorate (PhD)

from the Faculty of Medicine

of the University of Bonn

Nazhifah Binte Salim

from Singapore

2026

Written with authorization of

the Faculty of Medicine of the University of Bonn

First reviewer: Prof. Dr. rer. nat Tobias Bald

Second reviewer: Prof. Dr. med. Christian Kurts

Day of oral examination: 13.05.2026

From the Institute of Experimental Oncology (IEO), Bonn

Table of Contents

List of Abbreviations

APCs	Antigen presenting cells
ADCC	Antibody-dependant cellular cytotoxicity
BC	Breast cancer
BCC	Basal cell carcinoma
BLIMP-1	B lymphocyte-induced maturation protein-1
CD	Cluster of differentiation
CD3	Cluster of differentiation 3
CD4	Cluster of differentiation 4
CD8	Cluster of differentiation 8
CD45	Cluster of differentiation 45
CD96	Cluster of differentiation 96
CD112	Cluster of differentiation 112
CD155	Cluster of differentiation 155
CD226	Cluster of differentiation 226
CRC	Colorectal carcinoma
cRPMI	Complete RPMI
CRISPR	Clustered regularly interspaced short palindromic repeats
crRNA	CRISPR ribonucleic acid
CTLs	Cytotoxic T lymphocytes
CTLA-4	Cytotoxic T lymphocyte associated protein 4
CM	Cutaneous carcinoma
CXCL	Chemokine (C-X-C motif) ligand

DAMPs	Danger-associated molecular patterns
DCs	Dendritic cells
DLN	Draining lymph nodes
DNAM-1	DNAX accessory molecule 1
Eomes	Eomesodermin
EA	Esophageal Adenocarcinoma
FOXO1	Forkhead box protein 1
FOXP3	Forkhead box protein 3
gD	Glycoprotein D
HCC	Hepatocellular Carcinoma
HSV	Herpes simplex virus
ICC	Intrahepatic Cholangiocarcinoma
ICI	Immune checkpoint inhibitor therapy
IDO	Indoleamine-2,3-dioxygenase
IFN-γ	Interferon gamma
ILCs	Innate Lymphoid Cells
IL	Interleukin
IL-2	Interleukin 2
IL-4	Interleukin 4
IL-7	Interleukin 7
IL-10	Interleukin 10
IL-13	Interleukin 13
IL-15	Interleukin 15
IL-17A	Interleukin 17A

IS	Immunological synapse
ITIMs	Immunoreceptor tyrosine-based inhibitory motif
LCMV	Lymphocytic choriomeningitis virus
LFA-1	Lymphocyte function-associated antigen 1
LN	Lymph Nodes
LPS	Lipopolysaccharides
MHC	Major histocompatibility complex
MDSCs	Myeloid-derived suppressor cells
MAGE-A3	Melanoma-associated antigen-3
NK	Natural Killer cells
NSCLC	Non-small cell lung cancer
NY-ESO-1	New York esophageal squamous cell carcinoma-1
PAMPs	Pathogen-associated molecular patterns
PBMCs	Peripheral blood mononuclear cells
PBS	Phosphate Buffered Saline
PCR	Polymerase Chain Reaction
PDAC	Pancreatic Ductal Adenocarcinoma
PD-1	Programmed cell death protein 1
PDL-1	Programmed cell death ligand 1
PKC	Protein Kinase C
PMA	Phorbol 12-myristate 13-acetate
PVR	Poliovirus receptor
RAG-2	Recombination activating gene 2
RBCs	Red blood cells

RCC	Renal cell carcinoma
RNP	Ribonucleoprotein
RTP	Room temperature
SCC	Squamous Cell Carcinoma
SD	Standard Deviation
SDS-PAGE	Sodium Dodecyl Sulfate Polyacrylamide Gel Electrophoresis
SEM	Standard Error Mean
S326	Serine 326
S329	Serine 329
sgRNA	Single-guide ribonucleic acid
T-bet	T-box transcription factor
TBS	Tris-buffered saline
Tcm	Central memory T cells
TCR	T cell receptors
Tem	Effector memory T cells
TGF-β	Transforming growth factor beta
Th cells	T helper cells
ThPOK	T-helper-inducing POZ/Krueppel-like factor
TIGIT	T cell immunoreceptor with Ig and ITIM domains
TILs	Tumour-infiltrating lymphocytes
TME	Tumour microenvironment
Tn	Naïve
TNF-α	Tumour necrotic factor alpha
tracrRNA	Tans activating CRISPR RNA

Tregs	Regulatory T cells
TRP-1	Tyrosinase-related protein 1
UM	Uveal Melanoma
VAV1	Vav Guanine Nucleotide Exchange Factor 1
WT	Wildtype
Y319	Tyrosine 319
Y322	Tyrosine 322

1. Introduction

1.1 Overview of the Immune System

1.1.1 Innate and Adaptive Immune System

The immune system consists of a network of specialized cells that cooperate to defend the host from foreign pathogens through orchestrated immune responses. This network is traditionally divided into two categories; innate and adaptive immunity. The innate immune network serves as the first line of defence against foreign pathogens, employing rapid non-antigen specific mechanisms for the clearance of pathogens and abnormal cells. Some key cellular components to this network include: natural killer (NK) cells and innate lymphoid cells (ILCs), macrophages, and dendritic cells (DCs).

NK cells mediate rejection of tumours and clearance of virus-infected cells. They exert granules, containing perforin and granzymes, inducing apoptosis of target cells (Kim et al. 2000). NK cells contribute to immune responses through functional activation and enhancement of antigen-presenting cells (APCs) or influence T-helper 1 (Th) responses within the adaptive immunity (Mocikat et al. 2003; Filipe-Santos et al. 2006). ILCs, on the other hand, can be more involved in regulatory roles, with distinct subsets (ILC-1, ILC-2, ILC-3). They orchestrate immune responses through specific cytokines production such as interferon-γ (IFN-γ), interleukin (IL)-4 and IL-17, ensuring homeostasis. Macrophages and DCs have phagocytic capabilities of engulfing antigens from the environment through recognition of danger-associated molecular patterns (DAMPs) and pathogen-associated molecular patterns (PAMPs) from infected or damaged cells. These cells further function as APCs by processing the engulfed antigens and presenting peptide fragments on either major histocompatibility complex (MHC) class I or II molecule. These peptide-MHC complexes are essential for the activation of B and T- cells; a key mechanism to trigger downstream adaptive immune responses.

The adaptive immunity - consisting of B and T cells - is antigen-specific and has immunological memory. It functions primarily to distinguish between “non-self” and “self” antigens, as well as eliminating specific pathogens. The acquired immunological memory obtained allows robust elimination of specific pathogen after repeated exposures. Hence, the adaptive immune network serves as an essential basis for effective immunization

against diseases. B cells arises from the bone marrow, and governs humoral or antibody-mediated immunity. Upon encountering foreign antigens, B cells become activated and undergo clonal expansion as well as differentiation into memory B cells or antibody-secreting plasma cells. Memory B cells persists long-term with retention of antigen-specific receptors, allowing active recall of responses upon antigen re-exposure. In contrast, plasma cells are relatively short-lived but are critical in directing antibody-dependant cellular cytotoxicity (ADCC); a mechanism where target pathogens are bounded by antibodies, marking them for destruction by other immune cells (Yeap et al. 2016).

1.1.2 T cells and cell-mediated immunity

T cells are bone marrow-derived leukocytes that undergo maturation in the thymus. These matured T cells are further categorised based on the expression of cluster of differentiation (CD) receptors – primarily $CD4^+$ and $CD8^+$ T cells. Mature T cells express unique T-cell receptors (TCRs), enabling antigen-specific recognition. Activation of T cells occurs through encounter with peptide antigens presented on MHC molecules on APCs. This is them followed by clonal expansion and subsequently differentiation into either cytotoxic T lymphocytes (CTLs; $CD8^+$ cells) or T-helper (Th) $CD4^+$ T cells. $CD8^+$ CTLs recognises peptide antigen presented on MHC-I molecules, and can pursue direct destruction of virus-infected cells or malignant cells; through secretion of perforin-granzyme or mediate apoptosis of target cells through Fas-FasL (Foulds et al. 2002).

In contrast, $CD4^+$ Th cells play the pivotal support role in maximizing immune responses. Consisting of various subsets, $CD4^+$ Th cells are very heterogenous, characterized through expression of distinct transcription factors and cytokine profiles (Table 1). These Th cells conventionally do not perform cytotoxic or phagocytic activities. Instead, they orchestrate immune responses through modulating functions of other immune cells. Unlike the CTLs, Th cells recognises peptide antigens presented on MHC-II molecules by professional APCs. Following activation, Th subsets secrete an array of cytokines that modifies effector cell differentiation, proliferation and function of immune cells.

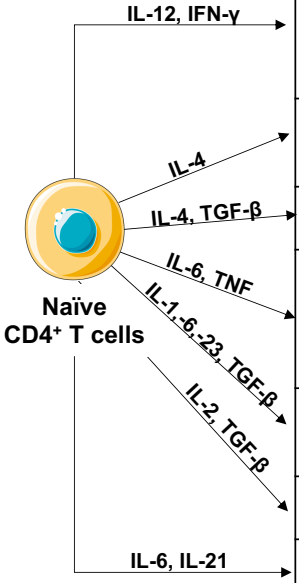

CD4 Subset	Transcription factors	Functions	Cytokine Profile
Th1	T-bet	• Activates bactericidal activities of macrophages • Enhances immunity against intracellular pathogens	IFN-γ, TNF-α
Th2	GATA-3	• Stimulates B-cells • Recruits mast cells, eosinophils and basophils to target parasites	IL-4, IL-5, IL-13
Th9	PU.1	• Enhances CD4⁺ T cell expansion • Recruits mast cells to target parasites	IL-9, IL-21
Th22	AhR	• Distinct functions unclear but have been shown to promote repair of epithelial barriers and heighten responses against pathogens (Aujla et al. 2008; Eyerich et al. 2009)	IL-22
Th17	RORγt	• Recruits neutrophils to target extracellular bacteria or fungi	IL-17, IL-21, IL-22, IL-25, IL-26
T regulatory cells (Treg)	FOXP3	• Regulates T cell responses and proliferation	IL-10, TGF-β
T follicular helper (Tfh)	Bcl-6	• Stimulated production of high-affinity antibodies from B cells	IL-4, IL-21

Table 1.1: Summary table depicting CD4⁺ T cell subsets and its characteristics. Differentiation of naïve CD4⁺ T cells are driven by different cytokines and these Th subsets harbour distinct transcription factors, functions and cytokine profiles. Table summarised from Golubovskaya and Wu (2016); Montauti et al. (2024).

1.1.3 The immune system in cancer

Cancer refers to a large group of diseases that constitutes abnormal growth of cells due to malignant transformation. The concept of tumour immunosurveillance, defined by Burnet and Thomas, proposes that the immune system bears vigilance towards elimination of emerging malignant cells (Burnet 1971; Thomas 1982). This was exemplified in a study employing the immunodeficient Recombination activating gene 2 protein knockout ($RAG2^{-/-}$) mice, where engraftment of sarcomas from donor wildtype (WT) mice were successful in these $RAG2^{-/-}$ mice; emphasising the prime role of the adaptive immunity in cancer (Shankaran et al. 2001). Concurrently, this study also demonstrated the influence of the immune system in developing low immunogenicity tumours, yielding its subsequent disease progression. This paradoxical phenomenon led to the cancer immunoediting model which harbours three phases – elimination, equilibrium and escape (Dunn et al. 2002).

The first elimination phase represents the cooperation between the immune network in the clearance of malignant cells. However, certain tumour variants may still persist, where

they progress into the equilibrium phase. In this phase, the variants then remain dormant and are clinically unapparent long-term. Finally, these dormant variants then obtain immune evasive capabilities due to genetic and epigenetic changes from the extended immune pressure. They employ various strategies to obtain a reduced immunogenicity such as; reduced antigen presentations, downregulation of immune checkpoint molecules, as well as impairing cytokine responses. With the dormancy broken, these unrestrained tumour variants manifests to be clinically apparent.

1.2 CD4 T cells in cancer

1.2.1 Multifaceted roles of Th subsets in cancer

As mentioned, $CD4^+$ T cells are heterogenous as they comprise of various polarised subsets (Table 1). Early cancer studies primarily focused on $CD8^+$ T cells due to their direct cytotoxic killing abilities, and that many cancer entities lack MHC-II expression. In recent years, studies have begun to unveil the importance of $CD4^+$ T cells as important contributors of immune responses in the tumour microenvironment (TME).

Th1 cells secretes mainly IFN-γ and tumour necrotic factor alpha (TNF-α), which are pivotal in driving anti-tumour responses (Liew 2002; Corthay et al. 2005; Dobrzanski 2013). These cytokines enhance CTL function through various ways including; modulating gene profiles, downregulating inhibitory molecules, and sustain CD27 co-stimulation with DCs (Ahrends et al. 2017). This was further exemplified by Hoepner et al. (2013) where brain tumour-bearing mice exhibited better tumour control following co-transfer of Th1-CTLs cells (Hoepner et al. 2013). Th1 cells also orchestrates promotion of cytotoxic mediators (e.g granzyme B and perforin) from immune cells (Tau et al. 2001; Takeda et al. 2002; Maimela et al. 2019), which further modulates tumour immunogenicity through regulation of their checkpoint molecules, including Programmed cell-death ligand 1 (PDL-1) and Chemokine (C-X-C motif) ligand 9 (CXCL9) (Freeman et al. 2021). Additionally, IFN-γ concurs MHC upregulation, thereby promoting tumour antigen presentation, and subsequently drives macrophage polarisation towards the proinflammatory M1 phenotype (Tau et al. 2001). More importantly, the presence of Th1 cells in tumours associates with favourable clinical outcome across most cancer variants (Bindea et al. 2013; Fridman et al. 2017). Paradoxically, chronic Th-1-driven inflammation can support tumour progression instead, through induction of IDO (indoleamine-2,3-dioxygenase) enzyme or

recruitment of the myeloid-derived suppressor cells (MDSCs) to the TME, dampening the overall anti-tumour responses (Lee et al. 2003; Muller et al. 2008).

Th2-driven cytokines were initially reported to promote tumour angiogenic functions and suppression of anti-tumour responses (Tataroğlu et al. 2004; Chraa et al. 2019). However, there are evidences demonstrating tumour regression by Th2 cells. IL-4, the hallmark Th2 cytokine, can induce necrosis in solid tumours (Volpert et al. 1998), and correlates with reduced vascularisation and tumour growth (Saleh et al. 1997). Furthermore, IL-4 mediates anti-tumour functions through eosinophils and macrophages (Tepper et al. 1992), whereas IL-13, another prime Th2 cytokine, mediates through neutrophils and macrophages (Ma et al. 2004). Ironically, in some cases, IL-13 dampens anti-tumour functions via inhibition of IFN-γ secretion from immune cells, impairing overall CTLs efficacies (Terabe et al. 2000). Despite this, clinical data have shown an association between Th2 immunity and efficacy of immune checkpoint inhibitor therapy (ICI). Blomberg et al. (2023) reported increased frequencies of intratumoural eosinophils in ICI patient responders, which further enhanced tumoricidal effects from CTLs, and attuned the TME to favour tumour control (Blomberg et al. 2023).

Th17 and its characteristic cytokine, IL-17, have been observed in serum, peripheral blood mononuclear cells (PBMCs), and in the TME of various cancers (Chang 2019). Th17 harbours both cancer-promoting or -inhibiting capabilities, depending on the cancer type. The pro-tumorigenic function of Th17 is usually linked to chronic inflammation (Punt et al. 2015). In inflammation-associated cancers such as colon, lung, gastric or liver cancers, elevated levels of Th17 tumour-infiltrating lymphocytes (TILs) are associated with unfavourable prognosis (Zhang et al. 2009; Chen et al. 2010; Tosolini et al. 2011; Yamada et al. 2012). In contrast, ovarian cancer patients with higher Th17 TILs showed significantly higher survival rates as compared to the latter; likely due to IL-17-associated anti-angiogenic chemokines such as CXCL2 or CXCL9 (Kryczek et al. 2009).

Regulatory T cells (Tregs), are perhaps the most studied subset in cancer. Conventionally, Tregs function to maintain immune tolerance and homeostatic responses. However, in the TME, Tregs supports tumour growth via inhibition of various mechanisms of anti-tumour immunity (Woo et al. 2002; Gobert et al. 2009; Spranger et al. 2013). They downregulate effector cell mechanisms via engagement of inhibitory molecules as Cytotoxic T-

lymphocyte associated protein 4 (CTLA-4) and Programmed cell death protein 1 (PD-1), or secretion of anti-inflammatory cytokines (Paterson et al. 2015; Wing et al. 2019). Upon chemotactic recruitment to the TME, secretion of IL-10 and Transforming growth factor beta (TGF-β) represses CTL functions, impair other Th subset differentiation, and restrain effector cell proliferation through IL-2 deprivation (Liu et al. 2011; Boyman and Sprent 2012; Wang et al. 2012). Tumour-derived Tregs also upregulate other immune checkpoint molecules and subsequently promotes tumour progression through limiting effector cell function (Yu et al. 2009; Sakuishi et al. 2013). Indeed, accumulation of Tregs in patients associates with poor prognosis across cancers (Liu et al. 2017). Therefore, research efforts were channelled towards diminishing suppressive mechanism of Tregs to enhance overall anti-tumour immunity (Quezada et al. 2006; Tan et al. 2020).

Collectively, these studies highlight the multi-faceted role of $CD4^+$ T cells in cancer. However, due to its complexity, Th cell functions in many cancer studies concerning CTLs, are overlooked; despite $CD8^+$ T cells dependency on Th functions.

1.2.2 Cytotoxic $CD4^+$ T cells

Early evidences of $CD4^+$ T cytotoxic cells were initially overlooked as *in-vitro* artefacts, as cytotoxicity was believed to be $CD8^+$ CTLs exclusive (Cenerenti et al. 2022). However, later *in-vivo* studies demonstrated the presence of antigen specific $CD4^+$ CTLs in both mouse and humans in various settings (Lukacher et al. 1985; Maimone et al. 1986). Since then, research interest in $CD4^+$ CTLs concerning cancer have expanded; though their ontogeny, mechanisms and plasticity still remains elusive. Extensive single-cell RNA sequencing analyses of TILs revealed $CD4^+$ CTLs harbor cytolytic molecules such as granzymes, perforin, and other granule-associated proteins (e.g, NKG7, granulysin), both in tumour and in circulation of patients with various solid tumours (Puram et al. 2017; Azizi et al. 2018; Guo et al. 2018; Zhang et al. 2018, 2019; Zhou et al. 2020; Cachot et al. 2021).

Functionally, $CD4^+$ CTLs were shown to perform direct tumoricidal function in an MHC-II-dependent manner in a preclinical study using melanoma models (Quezada et al. 2010). In line with this, antigen-specific $CD4^+$ CTLs, targeting New York esophageal squamous cell carcinoma-1 (NY-ESO-1) or Melanoma-associated antigen-3 (MAGE-A3), also exhibited direct granzyme-dependent cytotoxicity against tumour cells that received IFN-γ pre-stimulation or engineered to express MHC-II (Cachot et al. 2021). Adoptive transfer

of tumour-specific $CD4^+$, such as Tyrosinase-related protein 1 (TRP-1) $CD4^+$ T cells, in combination with CTLA-4 or CD137 agonists, into lympophenic mice promoted proliferation and tumour clearance (Quezada et al. 2010; Hirschhorn-Cymerman et al. 2012; Akhmetzyanova et al. 2016). Recently, it was shown that CD4+ T cells are required for eradication of MHC-I deficient melanoma tumours which have escaped CD8+ CTL mechanisms; both via direct recognition of MHC-II^+ tumour cells and indirect mechanisms involving interaction with MHC-II^+ $CD11c^+$ APCs (Kruse et al. 2023). This was also further supported by a study by Bawden et al. (2024) where the authors revealed interactions of $CD4^+$ T cells with tumour-associated APCs. Eradication of melanoma cells by the $CD4^+$ T cells was mainly through TNF-α and FasL interactions (Bawden et al. 2024). Collectively, these studies exhibited some of the diverse cytotoxic mechanisms of cytotoxic CD4 T cells; nevertheless, they underscore the therapeutic potential of $CD4^+$ T cells in cancer therapy.

Several combinations of transcription factors have been proposed to define cytotoxic $CD4^+$ T cells; such as T-box transcription factor (T-bet), Eomesodermin (Eomes), T-helper-inducing POZ/Krueppel-like factor (ThPOK), and B lymphocyte-induced maturation protein-1 (BLIMP-1) (Qui et al. 2011; Kitano et al. 2013; Weiskopf et al. 2015; Serroukh et al. 2018; Śledzińska et al. 2020). While ThPOK drives $CD4^+$ lineage commitment, its downregulation, in combination with T-bet and Runx3 signaling, has been suggested to be essential for cytotoxic $CD4^+$ T cell differentiation (Mucida et al. 2013). Eomes, known for promoting IFN-γ production in $CD8^+$ CTLs, appeared to be crucial for granzyme B production by cytotoxic Th1 cells post CD134 and CD137 co-stimulation (Qui et al. 2011). BLIMP-1 is recently proposed as a marker of cytotoxic $CD4^+$ T cells as it is associated with enhanced granzyme B production and cytotoxic differentiation. Interestingly, in this study, the authors also demonstrated that T-bet expression was required for overall function but not specifically for cytotoxic function of tumour-reactive CD4 T cells (Śledzińska et al. 2020). Despite these findings, the ontogeny of cytotoxic $CD4^+$ T cells still remains to be controversial across different disease context, especially in cancer (Oh and Fong 2021).

1.4 CD226 (DNAM-1) in Cancer Immunity

1.4.1 CD226 Axis

The DNAX accessory molecule 1 (DNAM-1) or CD226, was first described by Burns et al., in 1985 and Shibuya et al., later pioneered in the investigation of its roles in lymphocyte adhesion and function (Burns et al. 1985; Shibuya et al. 1996). CD226 is expressed on a multitude of immune cells including T, NK and B cells, monocytes and platelets. Thorough characterisation of CD226 in T and NK cells revealed it to be a crucial co-stimulatory receptor for signalling via its shared ligands – CD155 (poliovirus receptor; PVR) and CD112 (Nectin-2) (Shibuya et al. 1996; Dardalhon et al. 2005; Gilfillan et al. 2008). CD226 also belongs to a smaller immune regulatory network – often termed as CD226 axis – which also includes TIGIT (T cell immunoreceptor with Ig and ITIM domains) and CD96 (TACTILE), where they compete to bind CD155 (Figure 1.1).

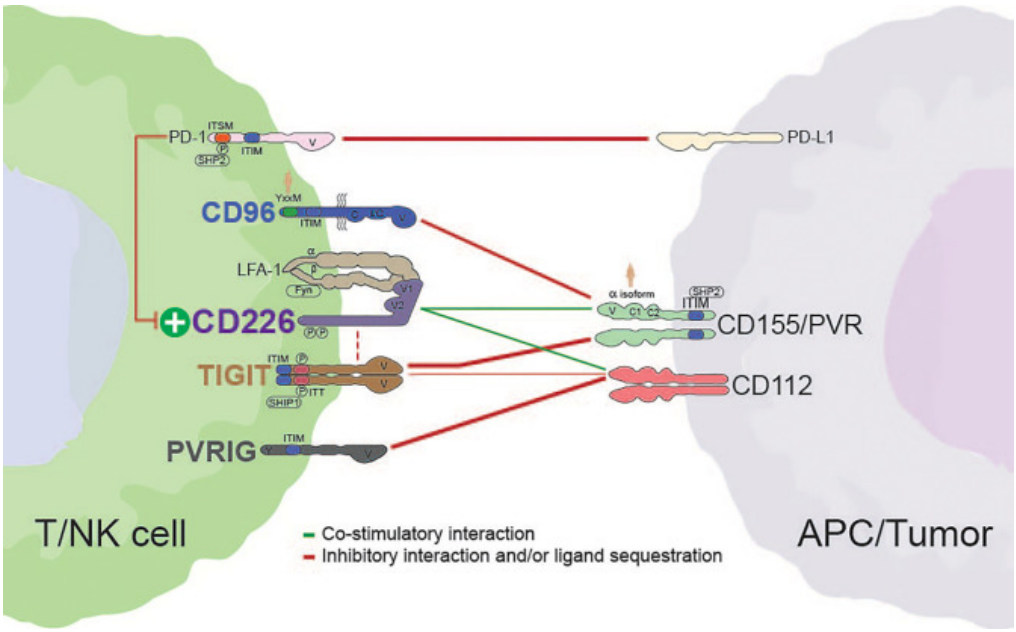

Figure 1.1: Interactions within the CD226 axis
Line thickness represents binding affinity. Upon ligand binding, phosphorylation at the cytoplasmic tail of CD226 and TIGIT/CD96, transmit co-stimulatory or co-inhibitory signals respectively. Picture taken from Conner et al. (2022).

CD226 harbours 3 domains: an extracellular domain, a transmembrane domain. and a cytosolic domain. The extracellular domain governs ligand recognition, adhesion as well as immune synapse formation. The cytosolic domain contains 2 conserved phosphorylation residues: tyrosine 319 (Y319) and serine 326 (S326) in mice, and tyrosine

322 (Y322) and serine 329 (S329) in humans. Signalling cascades following phosphorylation by Fyn (a src kinase) and protein kinase C (PKC) at these sites have modifying roles on overall effector cell function. For instance, in mouse, phosphorylation at Y319, but not S326, regulates NK cell function and cytotoxicity (Zhang et al. 2015). In humans, phosphorylation at S329 was shown to be crucial for ligand binding and co-localisation with Lymphocyte function-associated antigen 1 (LFA-1) in lipid rafts for effective immunological synapse (IS) formation in both NK and T cells (Shibuya et al. 1998, 1999). This interaction is especially important in NK cells, with LFA-1 then enabling phosphorylation of Y322 and advancing downstream signalling, ultimately driving effector functions (Kim and Long 2012).

1.4.2 Role of CD226 in NK and T cells in cancer

CD226 was established to be vital in anti-tumour function, especially in NK and T cells. CD226-deficient mice had impaired overall cytotoxicity and failed to control tumour growth and these tumours exhibited upregulated expression of CD155 and CD112 (Iguchi-Manaka et al. 2008). In NK cells, CD226 engagement with its ligands is crucial for NK cell-mediated cytotoxicity. This ligation preserves stable interaction between NK cells and tumour cells, allowing efficient granule polarization and degranulation (Kim et al. 2017).

With cancer studies predominantly focused on $CD8^+$ CTLs, it has become more apparent that CD226 bears a larger striking role in $CD8^+$ T cells. Increased CD226-expressing $CD8^+$ TILs in gastric cancer patients correlated with increased IFN-γ expression and ultimately, better clinical outcome. However, the observed increased CD226 expression was also paralleled with TIGIT upregulation, highlighting the regulatory mechanism of the CD226 axis (Huang et al. 2023). When co-expressed, TIGIT binds with higher affinity to CD155 than CD226, thereby promoting a preferential immunosuppressive signal. TIGIT disrupts CD226 homodimerization through cis interactions, hindering CD226-driven downstream signalling (Stengel et al. 2012). Recently, PD-1 was also reported to be involved in CD226 regulation as CD226 also serves as a substrate involved in the PD-1 signalling cascade (Banta et al. 2022).

Preclinical studies have further emphasized the importance of CD226 expression on $CD8^+$ TILs in cancer therapy. For example, in non-small cell lung cancer (NSCLC) patients, effective anti-tumour responses following PD-1/PD-L1-targeted therapy and anti-TIGIT

treatment requires the availability of CD226-expressing $CD8^+$ T cells (Banta et al. 2022). Similarly, melanoma patients with high CD226-expressing $CD8^+$ T cells had extended progression-free survival rates after ICI therapy (Braun et al. 2020). Finally, a deficiency in CD226 expression negates therapeutic mechanisms of anti-CD137, anti-GITR and anti-CTLA-4 in various tumour models (Wang et al. 2018; Braun et al. 2020). These past extensive studies certainly poised CD226 as an agonistic target for immunotherapy. However, therapeutic targeting of CD226 still remains a challenge as its diverse expression on immune cells, poses potential risks of complex pharmacological responses. To date, only one anti-CD226 agonist (LY3435151, Eli Lilly) reached phase 1 clinical trials, but was later terminated due to unspecified reasons (Conner et al. 2022). Although one can speculate reasons for the termination, the interest to further understand and manipulate CD226 and its axes for cancer therapy still remains.

Overall, these findings emphasize the indispensable role of CD226 in driving effective anti-tumour responses, particularly in $CD8^+$ CTLs and NK cells. However, despite these in-depth researches, the roles and regulations of CD226 in $CD4^+$ T cells concerning anti-tumour immunity has yet to be fully elucidated. Given the growing interest in both the cytotoxic and regulatory capabilities of $CD4^+$ T cells in TME, understanding CD226's influence on $CD4^+$ T cells presents as a research gap and potentially a promising avenue for clinical research.

1.4.3 Emerging roles of CD226 in $CD4^+$ T cells

As aforementioned, Tregs function to impede anti-tumour responses. Early cancer studies concerning the CD226 axis in CD4+ T cells were therefore focused on modulating the regulatory functions of Tregs. Shown in one study, melanoma-derived Tregs with a low CD226/TIGIT expression ratio were highly suppressive, and correlated with poorer clinical outcome upon ICI therapy (Fourcade et al. 2018). Thereby, providing a rationale for immunotherapies to enhance CD226 activation whilst blocking TIGIT to modulate Tregs' suppressive functions in cancer. Mechanistically, in NK cells, activation of downstream CD226 signaling represses Forkhead box protein 1 (FOXO1), a negative regulator of NK cell function. This transcription factor is also responsible for Treg differentiation through Forkhead box protein 3 (FOXP3) regulation – resulting in IFN-γ production as well as reduced inhibitory function (Ouyang et al. 2012; Du et al. 2018). While these pathways

were individually explored in NK cells and Tregs, it remains unclear whether CD226 directly modulates FOXO1 in Tregs. Recently, opposing studies have further suggested conflicting roles for CD226 in Treg stability (Sato et al. 2021; Ma et al. 2023). Hence, the precise role of CD226 in Treg suppressive function remains largely debatable.

With an expanding interest of $CD4^+$ T cells in anti-tumour immunity, the mechanism and function of CD226 in this context is still yet to be fully understood, despite the presence of $CD226^+$ $CD4^+$ T cells in tumours (Huang et al. 2023). Shibuya et al., demonstrated that CD226 is further required for efficient Th1 polarization in human $CD4^+$ T cells, through its association with LFA-1 upon activation (Shibuya et al. 1996). This was also similarly reported by Dardalhon et al. (2005), where *in-vivo* administration of blocking CD226 antibody hindered Th1 expansion (Dardalhon et al. 2005). Engagement of CD226 was further shown to mobilize Vav Guanine Nucleotide Exchange Factor 1 (VAV1) allowing synergy with TCR signals and promotes IL-17 production in primary human $CD4^+$ T cells (Gaud et al. 2018). Beyond regulation by TIGIT and PD-1, previous data from our lab demonstrated that ligation with CD155 promotes phosphorylation at the tyrosine residue, directing downstream ubiquitination involving the E3 ubiquitination ligase Cbl-b (Braun et al. 2020). This cascade subsequently resulted in internalization and degradation of CD226 in $CD8^+$ T cells. Ultimately, these $CD226^{Low}$ $CD8^+$ T cells became dysfunctional. Whether a similar mechanism operates in $CD4^+$ T cells, remains unknown. Overall, these findings highlight the need to further understand the contribution of CD226 in $CD4^+$ T cells, especially in the context of cancer.

1.5 Thesis Aims

Many cancer studies historically overlooked $CD4^+$ T cell functions, predominantly focused on $CD8^+$ T cells due to their direct killing capabilities and the lack of MHC-II expression in various tumour entities. This has poised $CD8^+$ T cells as prime candidates for cancer immunotherapy, especially in immune checkpoint blockade or adoptive transfer therapies. In recent years, accumulating evidences have since unveiled the critical contributions of $CD4^+$ T cells in in sustaining and maximizing anti-tumour responses in many cancers through diverse mechanisms. This includes an emerging interest in cytotoxic $CD4^+$ T cell subsets, whose ontogeny and functions remains elusive – further complicating the $CD4^+$ T cell pool in cancer.

Our lab and many others have described the relevance of CD226 and its downstream mechanisms of anti-tumour functions in $CD8^+$ T cells. However, the role and regulation of CD226 in $CD4^+$ T cells, especially in the context of anti-cancer responses, remains to be interrogated. Understanding this would leverage opportunities to harness the CD226 axis for future therapeutic advantages,

We therefore hypothesize that CD226 expression in tumour-reactive $CD4^+$ T cells is required for accelerating effective anti-tumour responses with aims summarized as follows:

1. Characterise CD226 expression on $CD4^+$ T cells in cancer.
2. Decipher the regulation of CD226 in $CD4^+$ T cells in the TME.
3. Investigate the functional relevance of CD226 in tumoricidal $CD4^+$ T cells

2. Materials and methods

2.1 Materials

2.1.1 Fluorochrome-conjugated antibodies

Table 2.1: Overview of fluorochrome-conjugated antibodies

Antibody	**Conjugate**	**Clone**	**Source**	**Identifier**
Anti-mouse CD3ε	BUV395	145-2C11	BD Biosciences	Cat#: 564144 RRID: AB_2738618
Anti-mouse NK1.1	BUV395	PK136	BD Biosciences	Cat#: 563565 RRID: AB_2738278
Anti-mouse CD45.2	BUV395	104	BD Biosciences	Cat#: 564616 RRID: AB_2738867
Anti-human CD8	BUV395	RPA-T8	BD Biosciences	Cat#: 563795 RRID: AB_2722501
Anti-human TCR αß	BUV395	IL26	BD Biosciences	Cat#: 745569 RRID: AB_2722501
Anti-human CD45	BUV395	HI30	BD Biosciences	Cat#: 563792 RRID: AB_2869519
Anti-mouse CD4	BUV496	GK1.5	BD Biosciences	Cat#: 612952 RRID: AB_2813886
Anti-mouse CD4	BUV805	GK1.5	BD Biosciences	Cat#: 612900 RRID: AB_2827960
Anti-human CD3	BUV805	UCHT1	BD Biosciences	Cat#: 612895 RRID: AB_2870183
Anti-mouse PD-1 (CD279)	BUV615	RMP1-30	BD Biosciences	Cat#: 752354 RRID: AB_2875871
Anti-human CD4	BUV615	OKT4	BD Biosciences	Cat#: 612988 RRID: AB_2870259
Anti-mouse CD8α	BUV737	53-6.7	BD Biosciences	Cat#: 612759

				RRID: AB_2870090
Anti-mouse CD62L	BUV737	MEL-14	BD Biosciences	Cat#: 612833 RRID: AB_2870155
Anti-mouse TCRß	BUV737	H57-597	BD Biosciences	Cat#: 612821 RRID: AB_2870145
Anti-human CD25	BUV737	2A3	BD Biosciences	Cat#: 612807 RRID: AB_2916878
Anti-human T-bet	BV785	4B10	Biolegend	Cat#: 644835 RRID: AB_2721566
Anti-mouse CD226	BV786	10-E5	BD Biosciences	Cat#: 744611 RRID: AB_2871596
Anti-mouse CD226	BV711	10-E5	BD Biosciences	Cat#: 750915 RRID: AB_2875002
Anti-mouse CD183 (CXCR3)	BV605	CXCR3-173	Biolegend	Cat#: 126523 RRID: AB_2561353
Anti-human CD197 (CCR7)	BV605	G043H7	Biolegend	Cat#: 353223 RRID:AB_11124325
Anti-mouse CD137 (4-1BB)	BV650	1AH2	BD Biosciences	Cat#: 740499 RRID: AB_2740222
Anti-mouse TIGIT	BV650	1G9	BD Biosciences	Cat#: 744212 RRID: AB_2742061
Anti-mouse MHC-II (I-A/I-E)	BV650	M5/114.15.2	Biolegend	Cat#: 107641 RRID: AB_2565975
Anti-mouse CD45.1	BV650	A20	Biolegend	Cat#: 110736 RRID: AB_2562564
Anti-mouse IL-17A	BV650	TC11-18H10.1	Biolegend	Cat#: 506930 RRID: AB_2686975
Anti-human RORγt	BV650	Q21-559	BD Biosciences	Cat#: 563424 RRID: AB_2738197
Anti-mouse TCRß	BV510	H57-597	Biolegend	Cat#: 109233

				RRID: AB_2562349
Anti-mouse CD19	BV510	6D5	Biolegend	Cat#: 115556 RRID: AB_2562136
Anti-human CD25	BV510	BC96	Biolegend	Cat#: 302639 RRID: AB_2629671
Anti-mouse RORγt	BV421	Q31-378	BD Biosciences	Cat#: 562894 RRID: AB_2687545
Anti-mouse T-bet	BV421	OK136	Biolegend	Cat#: 644816 RRID:AB_10959653
Anti-mouse CXCR4	BV421	L276F12	Biolegend	Cat#: 146511 RRID: AB_2562788
Anti-mouse CD127 (IL-7Ra)	BV421	A7R34	Biolegend	Cat#: 135027 RRID: AB_2563103
Anti-mouse FOXP3	eFluor 450	FJK-16s	eBioscience	Cat#: 48-5773-82 RRID: AB_1518812
Anti-human TIGIT	eFluor 450	MBSA43	eBioscience	Cat#: 48-9500-42 RRID: AB_2637413
Anti-mouse CD112 (Nectin-2)	BV421	829038	BD Biosciences	Cat#: 748046 RRID: AB_2872507
Anti-mouse CD107a (LAMP-1)	BV421	1D4B	Biolegend	Cat#: 121618 RRID:AB_10896064
Anti-mouse Granzyme B	Pacific Blue	GB11	Biolegend	Cat#: 515408 RRID: AB_2562196
Anti-human IL-17A	Pacific Bluie	BL168	Biolegend	Cat#: 512311 RRID: AB_961393
Anti-mouse MHC-I ($H\text{-}2D^b$)	BV421	KH95	BD Biosciences	Cat#: 743535 RRID: AB_2741567
Anti-mouse CD4	PerCP	RM4-5	BD Biosciences	Cat#: 553052 RRID: AB_394587

Anti-mouse TNF-α	PerCP/Cy5.5	MP6-XT22	Biolegend	Cat#: 506322 RRID: AB_961434
Anti-mouse GATA3	Alexa Fluor 647	L50-823	BD Biosciences	Cat#: 560068 RRID: AB_493319
Anti-human IL-10	Alexa Fluor 647	JES3-9D7	Biolegend	Cat#: 501414 RRID: AB_1645316
Anti-mouse CD25	Alexa Fluor 700	PC61	Biolegend	Cat#: 102024 RRID: AB_493709
Anti-mouse CD69	APC	H1.2F3	eBioscience	Cat#: 17-0691-82 RRID: AB_1210795
Anti-mouse CD155 (PVR)	APC	TX56	Biolegend	Cat#: 131510 RRID:AB_10640453
Anti-mouse Perforin	APC	S16009A	Biolegend	Cat#: 154303 RRID: AB_2721462
Anti-mouse Blimp-1	APC	5E7	Biolegend	Cat#: 150007 RRID:AB_2728186
Anti-mouse IL-10	APC	JES5-16E3	Biolegend	Cat#: 505009 RRID: AB_315363
Anti-human CD69	APC	FN50	Biolegend	Cat#:310909 RRID: AB_314844
Anti-human CD155 (PVR)	APC/Fire 750	SKIL4	Biolegend	Cat#: 337626 RRID: AB_2800897
Anti-mouse KLRG-1	PE/Cy7	2F1	eBioscience	Cat#: 25-5893-82 RRID: AB_1518768
Anti-mouse CD44	PE/Cy7	IM7	Biolegend	Cat#: 103030 RRID: AB_830787
Anti-mouse Ki-67	PE/Cy7	16A8	Biolegend	Cat#: 652426 RRID: AB_2632693
Anti-human IFN-γ	PE/Cy7	45.B3	Biolegend	Cat#: 502528 RRID: AB_1626154

Anti-human CD45RA	PE/Cy7	HI100	Biolegend	Cat#: 304126 RRID:AB_10708879
Anti-human CD112	PE/Cy7	TX31	Biolegend	Cat#: 304126 RRID:AB_10708879
Anti-human GATA3	PE/Cy7	L50-823	BD Biosciences	Cat#: 560405 RRID: AB_1645544
Anti-mouse IL-13	PE	eBio13A	eBioscience	Cat#: 12-7133-41 RRID:AB_10852712
Anti-mouse IFN-γ	PE	XMG1.2	Biolegend	Cat#: 505808 RRID: AB_315402
Anti-mouse EOMES	PE	Dan11mag	eBioscience	Cat#: 12-4875-80 RRID: AB_1603278
Anti-mouse CD45.1	PE	A20	Biolegend	Cat#: 110707 RRID: AB_313496
Anti-human IL-13	PE	JES10-5A2	Biolegend	Cat#: 501903 RRID: AB_315198
Anti-mouse CD3ε	FITC	145-2C11	Biolegend	Cat#: 100306 RRID: AB_312671
Anti-mouse TCRß	FITC	H57-597	Biolegend	Cat#: 109206 RRID: AB_313429
Anti-mouse CD45.1	FITC	A20	Biolegend	Cat#: 110706 RRID: AB_313495
Anti-human FOXP3	KIRAVIA Blue 520	206D	Biolegend	Cat#: 320132 RRID: AB_2876623

2.1.2 Viability Dyes

Table 2.2: Overview of viability dyes

Viability Dyes	**Source**	**Identifier**
LIVE/DEAD™ Fixable Near-IR Dead Cell Stain Kit	Invitrogen™	Cat#: L10119
LIVE/DEAD™ Fixable Blue	Invitrogen™	Cat#: L23105
Zombie NIR™ Fixable Viability Kit	Biolegend	Cat#: 423106

2.1.3 Antibodies for T cell activation

Table 2.3: Overview of antibodies used for T cell activation

Antibody	**Clone**	**Source**	**Identifier**
Purified anti-human CD3	OKT3	Biolegend	Cat#: 317315 RRID: AB_1877070
Purified anti-human CD28	CD28.2	Biolegend	Cat#: 302902 RRID: AB_314303
Purified anti-mouse CD28	37.51	Biolegend	Cat#: 102102 RRID: AB_312866
Purified anti-mouse CD3	145-2C11	Biolegend	Cat#: 100302 RRID: AB_312667
Ultra-LEAF™ Purified anti-mouse CD3 Antibody	17A2	Biolegend	Cat#: 100238 RRID: AB_2561487

2.1.4 Mice

Table 2.4: Overview of mouse strains

Mouse Strain	**Description**
C57BL/6 (B6 WT)	Purchased from Charles River. Mice expressing MHC class I H-2^b, MHC class II I-A^b, and the congenic marker Ly5.2 (CD45.2)
C57BL/6.CD226-deficient (*Cd226*^{KO}) mice	Mice bred with genetic B6 background and carries a deletion of the *Cd226* gene.
C57BL/6,*Cd226*^{Y319F} *mice* (*Cd226*^{Y319F})	Mice bred with genetic B6 background harbouring a point mutation in the tyrosine residue (Y319F) of CD226.
C57BL/6.*Cbl-b*^{C373A} *(Cbl-b*$^{\Delta R}$*)*	Mice bred with genetic B6 background harbouring a loss-of-function mutation in the RING finger domain abrogating the E3 ubiquitin-ligase function
C57BL/6.gDT-II X SJL-PtprcaPep3b/BoyJ (gDT-II)	Mice generated on a B6 background expressing I-Ab restricted T cell receptor (Vα3.2 Jα 16/Vß2 Dß2.1 Jß2.1) specific for HSV-1-derived glycoprotein D peptide ($gD_{(315-327)}$, IPPNWHIPSIQDA), and the congenic marker CD45.1.

2.1.5 Cell lines

Table 2.5: Overview of cell lines

Cell line	**Origin**	**Description**	**Source**
B16.F1	Mouse Melanoma	Subline of B16.F10 that possess lower metastatic potential	Hölzel Lab, Uniklinikum Bonn.
B16.F10	Mouse melanoma	Parental cell line used for the generation of B16.gD variants	Bald Lab, QIMR Berghofer, Australia

B16.F10.gD (B16.gD)	Mouse melanoma	Polyclonal B16F10 cell line retrovirally transduced with construct containing HSV-derived glycoprotein D.	Generated in-house by Emma Bawden, Hölzel lab, Uniklinikum Bonn.
B16.gD.*Ciita*$^{-/-}$ (B16.gD.CIITA^{KO})	Mouse melanoma	Polyclonal B16.gD cell line with genetic disruption of *Ciita* gene. Generated from vector Px459-*Ciita*.	Generated in-house by Emma Bawden, Hölzel lab, Uniklinikum Bonn.
B16.gD.*Ciita*^{WT} (B16.gD.CIITA^{WT})	Mouse melanoma	Control B16.gD cell line generated with empty Px459 vector.	Generated in-house by Emma Bawden, Hölzel lab, Uniklinikum Bonn.
CHO-K1	Hamster	A derivative of the parental Chinese Hamster Ovary (CHO) cell line, established from an ovarian biopsy of an adult female Chinse Hamster	ATCC, #CCL-61
CHO-OKT3	Hamster	CHO-K1 generated to express OKT3 single-chain variable fragment (scFV)	Generated in-house by Johannes Siewart, Bald Lab, Uniklinikum Bonn
CHO-OKT3-hCD112	Hamster	CHO-K1 generated to express OKT3 scFv and human CD112	Generated in-house by Johannes Siewart, Bald Lab, Uniklinikum Bonn
CHO-OKT3-hCD155	Hamster	CHO-K1 generated to express OKT3 scFv and human CD155	Generated in-house by Johannes Siewart, Bald Lab, Uniklinikum Bonn

2.1.6 Cell culture medium

Table 2.6: Overview of cell culture medium

Cell culture Medium	**Source and Composition**
Complete RPMI (cRPMI)	RPMI 1640 medium + GlutaMAX™ (Gibco™, Cat#: 61870036) containing: o 10% Fetal Calf Serum (FCS)

	○ 100 U/mL Penicillin (Gibco™, Cat#: 15140122) ○ 100 µg/mL Streptomycin (Gibco™, Cat#: 15140122) ○ 10 mM NEAA (Gibco™, Cat#: 111140050) ○ 1 mM ROTI®Cell HEPES (Roth, Cat#: 9157.1) ○ 1mM Sodium Pyruvate (Gibco™, Cat#: 11360070) ○ 2 µM β-Mercaptoethanol (Gibco™: Cat#: 21985-023)

2.1.7 Buffers

Table 2.7: Overview of buffers

Buffers	**Source and Composition**
Sterile 1X Phosphate Buffered Saline (PBS)	Purchased from Gibco™ (Cat#: 10010023)
FACS Buffer	1X PBS (made in-house, Institute of Experimental Oncology) containing: ○ 2% FCS ○ 2mM EDTA
Digestion media	RPMI 1640 containing: ○ 1mg/ml collagenase D ○ 1mg/ml DNAseI
1X Lämmli Buffer	120mM 1M Tris-HCl ph 6.8 20% Glycerol 4% SDS 20mM β-Mercaptoethanol 0.02% Bromophenol-Blue
10x Sodium Dodecyl Sulfate Polyacrylamide Gel Electrophoresis (SDS-PAGE) running buffer	25mM TRIS 192mM Glycine 0.1% SDS

10x Tris-buffered saline (TBS)	150mM NaCl 50mM TRIS
1x TBST	1x TBS 0.05% Tween-20
1x Transfer Blotting Buffer	25mM TRIS 192mM Glycine 15% Isopropanol

2.1.8 Peptides and recombinant proteins

Table 2.8: Overview of peptides and recombinant proteins

Peptide and Recombinant Proteins	**Source**	**Identifier**
Recombinant human IL-2 (Aldeskeulin)	Novartis Pharma	Cat#:1-22475
Recombinant mouse IL-7	Peprotech Inc.	Cat#: 217-17-50UG
Recombinant mouse IL-15	Peprotech Inc.	Cat#: 210-15-50UG
Recombinant mouse IFN-γ	Peprotech Inc.	Cat#:315-05
Recombinant mouse CD155-Fc	Sino Biological	Cat#: 50259-M03H
Recombinant mouse CD112-Fc	Biolegend	Cat#: 776504
$gD_{(315-327)}$, Sequence: IPPNWHIPSIQDA	Synthesised through JPT Peptide Technologies	-
LCMV GP_{61-80} Sequence:GLKGPDIYKGVYQFKSVEFD	Gift from Teresa Steffen (AG Baumjohann, Uniklinikum Bonn)	-

2.1.9 Commercially available kits

Table 2.9: Overview of commercially available kits used

Commercially available kits	**Source**	**Identifier**
Cytofix/Cytoperm™ Fixation/Permeabilization Solution Kit	BD Biosciences	Cat#: 554714 RRID: AB_2869008
Dynabeads™ Antibody Coupling Kit	Invitrogen™	Cat#: 8802-6841-7
EasySep™ Mouse CD4+ T Cell Isolation Kit	StemCell Technologies	Cat#: 19852
EasySep™ Human CD4+ T Cell Isolation Kit	StemCell Technologies	Cat#: 17952
Foxp3 Transcription Factor Staining Buffer Set	Invitrogen™	Cat#: 00-5523-00
MagniSort™ Mouse CD4 Positive Selection Kit	Invitrogen™	Cat#: 8802-6841-7
Lonza™ P3 Primary Cell 4D-Nucleofector™ X Kit L	Lonza™	Cat#: V4XP-3024
Lonza™ P4 Primary Cell 4D-Nucleofector™ X Kit L	Lonza™	Cat#: V4XP-4024
Pierce BCA Protein Assay Kit	Thermo Scientific	Cat#: 23225
Tumour Dissociation Kit	Miltenyl Biotec	Cat#: 130-095-929

2.1.10 Chemical and reagents

Table 2.10: Overview of chemicals and reagents

Chemical and Reagents	**Source**	**Identifier**
Alt-R® CRISPR-Cas9 trans activating CRISPR RNA (tracrRNA)	Integrated DNA Technologies (IDT)	Cat#: 1073191

BD GolgiPlug™	BD Biosciences	Cat#: 555029
Mouse Beta Actin monoclonoal antibody	Santa Cruz	Cat#: SC47778
Peroxidase AffiniPure® Goat Anti-Mouse IgG (H+L)	Jackson Immunoresearch	Cat#: 115-035-003 RRID:AB_10015289
Peroxidase AffiniPure® Goat Anti-Rabbit IgG (H+L)	Jackson Immunoresearch	Cat#: 111-035-003 RRID: AB_2313567
Collagenase D	Sigma-Aldrich	Cat#: 11088858001
DNAse I	Roche	Cat#: 4536282001
Dynabeads Human T-activator CD3/CD28	ThermoFischer Scientific	Cat#: 111.31D
EDTA 0.5M	Invitrogen™	Cat#: 10458654
EnGen® Spy Cas9 NLS	New England Biolabs	Cat#: M0646M
ROTI®Histofix	Roth	Cat#: P087.5
H20 Ampuwa Water	Fresenius Kabi	Cat#: B102407
ImmunoCult Human CD3/CD28 T Cell Activator	StemCell Technologies	Cat#: 10991
Ionomycin	Sigma-Aldrich	Cat#: 13909-1ml
PageRuler Prestained Protein Ladder	ThermoScientific	Cat#: 26616
Protease phosphatase inhibitory cocktail	Cell Signaling Technology	Cat#: 5872S
Phorbol 12-myristate 13-acetate (PMA)	Sigma-Aldrich	Cat#: 1585-1mg
Rabbit anti-mouse CD226	Abcam	Cat#: ab212011

Clone: EPR20710		
Red blood cell lysis buffer (Hybri-Max)	Sigma-Aldrich	Cat#: R7757-100ml
Trypsin-EDTA (0.25%)	Gibco™	Cat#: 25200056
Trypan Blue Solution (0.4%)	Sigma-Aldrich	Cat#: 93595
UltraComp eBeads™ Plus Compensation Beads	Invitrogen™	Cat#: 01-3333-42

2.1.11 Consumables

Table 2.11: Overview of consumables used

Consumables	**Source**	**Identifier**
Cell culture flasks (T25, T75, T175)	Sarstedt	Cat#: 83.3910.003; 83.3911;
Cell culture plates (6-, 12-, 24-, 48-, 96-well)	Sarstedt	Cat#: 92406; 92412; 92424; 92448; 92096; 92697.
Cell strainer, 40µm	PluriSelect	Cat#:43-50040-50
Cell strainer, 70µm	PluriSelect	Cat#:43-57070-50
EDTA-coated Microcuvette	Sarstadt	Cat#:CB300LH
EasyEights™ EasySep™ Magnet	StemCell Technologies	Cat#: 18103
Polypropylene round-bottom FACS tubes (5mL)	Sarstedt	Cat#:55.1579
Polymerase Chain Reaction (PCR) stripes and lids (8-well)	Axygen	Cat#: PCR-0208-C, PCR-02CPC-C

Pipette tips, TipOne®	Star Lab	Cat#: S1112-1720, S1113-1710, S1110-3700,
Serological pipettes	Greiner Bio-One Corning® Costar Stripettes	Cat#: 4467, 4488, 4489

2.1.12 Laboratory Equipment

Table 2.12: Overview of laboratory equipment

Equipment	**Source/Company**
ChemiDoc MP Imaging system	Bio-Rad
Countess 3 Automated Cell Counter	Invitrogen
Cytek Aurora Spectral Cytometer	Cytek
FACSAria™ III Cell Sorter	BD Biosciences
BD FACSAria™ Fusion Flow Cytometer	BD Biosciences
FACSCanto II Flow Cytometer	BD Biosciences
LSRFortessa Cell Analyzer	BD Biosciences
Thermocycler	Bio-Rad
4D-Nucleofector Core Unit	Lonza™
4D-Nucleofector X Unit	Lonza™
BioRad's Mini Trans-Blot® Cell system	BioRad
Odyssey® DLx Imaging System	LI-COR Biosciences®

2.1.13 Software

Table 2.13: Overview of software used

Software	**Source/Company**
Benchling Online Platform	Benchling
FACS Diva	BD Biosciences
Flow Jo v10.7.1	Tree Star Inc.
GraphPad Prism v10	Graphpad
SpectroFlo®	Cytek
Image Studio	LI-COR Biosciences®

2.2 Methods

2.2.1 Mice

Wildtype (WT) C57BL/6 mice were purchased from Charles River, Jackson. C57BL/6 CD226-deficient ($CD226^{KO}$) mice, C57BL/6 $CD226^{Y319F}$ mice, Cbl-b ‘‘knock-in’’ mice (C373A; Cbl-$b^{\Delta R}$) and gDT-II X SJL-PtprcaPep3b/BoyJ (gDT-II) mice were bred in house and maintained at the in iFET Animal Facility (Uniklinikum Bonn). Experiments were conducted using sex- and aged-matched mice that are greater than 6 weeks of age, in accordance to national and institutional guidelines.

2.2.2 Cell lines and cell cultures

All CHO-K1 variants and B16 melanoma cell lines were cultured with complete RPMI medium, at 37°C, 10% CO_2. B16F10.gD (B16.gD) were generated via retroviral transduction of parental B16F10 with full-length gD as described in Bawden et al. (2024). The polyclonal cell line B16.gD.$Ciita^{KO}$ was generated using CRISPR-Cas9 protocol, also as described in Bawden et.,al, 2024. All B16.gD cell lines were generated by Emma Bawden, while all CHO-K1 cell variants were generated in-house by Johannes Siewert. All cell lines were expanded for experimental use and routinely tested negative for mycoplasma.

2.2.3 *In-vivo* tumour model

B16F1 cells ($1x10^5$ cells) were injected subcutaneously into mice in a final volume of 100 µl of 1X PBS. Tumour growth was monitored throughout the duration of experiment using digital callipers. Tumour volume was calculated using the following formula: ($(width^2 \times length)/2$). Mice were euthanized when tumours have reached $100mm^2$ in size, following ethical guidelines.

2.2.4. Blood sample preparation

Blood was sampled through heart puncture upon sacrifice using CO_2, into EDTA-coated tubed. Blood samples were then treated with 1 ml red blood cell (RBC) lysis buffer for 15 mins at room temperature (RTP) and washed twice with FACS buffer (2% FCS, 2mM EDTA). The lysis treatment was repeated twice, before a final resuspension in FACS buffer.

2.2.5 Spleens and lymph node sample processing

Mouse spleen and lymph nodes were mashed through 70 µm cell strainers to obtain single cell suspensions. For lymph nodes: cells were washed with FACS buffer and pelleted through centrifugation (400xg, 5mins), before use for further assays. For spleens: cell suspensions were pelleted and treated with 1 ml of RBC lysis buffer for 15 mins (RTP), and washed twice with FACS buffer, before proceeding to subsequent downstream experiments.

2.2.6 Tumour samples

Tumours were harvested from mice and mashed through 70 µm cell strainers to obtain single cell suspension. Cell suspensions were centrifuged (500xg, 5mins) and resuspended in 5 ml of digestion media (RPMI containing 1mg/ml collagenase D and 1mg/ml DNAseI). Samples were then incubated in the shaker incubator at 37°C for 45 mins. Subsequently, samples were washed with FACS buffer and passed through 40 µm cell strainers. After a final centrifugation (500xg, 5mins), cell pellets were resuspended in FACS buffer or cRPMI before further experiments or analysis.

2.2.7 Mouse T cell activation and function assay

For *in-vitro* activation, 96-well U-bottom culture plates were coated with 2 µg/ml of soluble mouse anti-CD3 and anti-CD28 in 1X PBS at 4°C, overnight. The single-cell suspensions from processed spleens and lymph nodes were seeded at $2x10^5$ cells per well in cRPMI containing recombinant human IL-2 (100 U/ml). For cytokine production assays, Golgi/Plug (containing brefeldin A) was added during the final 4 hours of respective time points. Cells were then subsequently harvested and stained for flow cytometric analysis using standard protocols.

2.2.8 Flow cytometry and flow cytometry-based sorting

Single cell suspensions were firstly incubated with a staining cocktail containing anti-CD16/CD32 (TruStain FcX) and a viability dye in 1X PBS, at 4°C for 15 mins, in the dark. An unstained and a viability control is included in every experiment and acquisition. Viability control was prepared by heat-treating cells at 65°C for 15 mins to induce cell death. Cells were then washed, followed by a surface stain with a cocktail containing the respective fluorochrome-conjugated monoclonal antibodies (prepared in FACS buffer), at

4°C for 20 mins, in the dark. For experiments concerning surface staining only, samples were washed and subsequently with 100 µl of 4% paraformaldehyde (Histofix) and further incubated at 4°C for 30 mins. Finally, samples were resuspended in a volume of 200 µl of FACS buffer prior to acquisition.

For intracellular cytokine or transcription factor detection, surface-stained cells were washed and permeabilized using either the Fixation/Permeabilization Kit for intracellular targets, or the Foxp3 Transcription Factor Staining Buffer Set for intranuclear targets, following the manufacturers' protocols. Upon permeabilization, cells were stained intracellularly with antibody cocktail prepared in the respective Perm/Wash buffers (1X), at 4°C for 30 mins in the dark. Cells were then washed with 1X Perm/wash buffer and finally resuspended in 200 µl of FACS buffer before acquisition. All samples were acquired either on the Aurora (Cytek), LSRFortessa (BD Bioscience), or FACSCanto (BD Biosciences). Flow cytometry data were analysed on FlowJo software.

For flow cytometric sorting: single cell suspension of respective samples were subjected to surface staining protocols as aforementioned. The stained samples were either sorted via FACSAria Fusion (BD Bioscience) or FACSAria III (BD Biosciences). All sorting procedures were executed by personnel of the Flow Cytometry Core Facility (University Hospital Bonn).

2.2.9 Co-culture with CD155-Fc dynabeads for surface CD226 analysis

Mouse anti-CD3 (clone 145-2C11; 5 µg/ml per mg beads), anti-CD28 (clone 37.51; 5 µg/ml per mg beads), and recombinant mouse CD155 fused to the Fc region of human IgG1 (CD155-Fc) were conjugated to Dynabeads through the Dynabeads™ M-270 Epoxy Bead Coupling Kit (Invitrogen), following the manufacturer's protocol. CD155-Fc was conjugated at varying concentrations— 0.05, 0.5, and 5 mg/ml per 5mg beads—to assess dose-dependent effects. Control beads ("Stim beads") were conjugated only with mouse anti-CD3 and anti-CD28. As an additional control, Dynabeads were also conjugated with anti-CD3, anti-CD28, and recombinant mouse CD112-Fc (BioLegend) in place of CD155-Fc. The respective conjugated beads were used at 1 µl/well with $2X10^5$ splenocytes/well in 96-well U-bottom plate in a final volume of 200 µl of complete RPMI (cRPMI) medium. At respective time points following co-cultures, cells were harvested, and Dynabeads were

removed using the EasySep™ Magnet (StemCell). Surface expression of CD226 was then analysed through flow cytometry.

2.2.10 Immunoblot

After co-cultures with beads, cells were harvested and washed with 1X PBS, and lysed with 1X Lämmli buffer. Lysates were heated (95°C, 5 mins) and stored at -20°C, Proteins were separated on 8%, 10%, or 12% SDS-PAGE gels at 140V 100 minutes (100V at initial 10-15 mins), and subsequently transferred to a 0.2 μM pore size nitrocellulose membrane using Mini Trans-Blot® Cell system at 100V for 1 hour. Membrane blockings were done with 5% BSA in TBS-T at 4°C, overnight. After which the membrane was incubated primary anti-CD226 antibodies overnight at 4°C; loading controls were added for 1 hour at RTP. After washing (3x, 5mins each, TBS-T), the membranes were incubated with secondary antibodies (1:15000) in 5%BSA/TBS-T for 1 hour at RTP in the dark. Finally, the membrane was washed twice with TBS-T and one final TBS wash. Imaging was captures using the Odyssey® DLx Imaging System and processed with Image Studio software.

2.2.11 Human T cells activation assays

Peripheral blood mononuclear cells (PBMCs) were thawed and treated with DNAseI (Roche) for the removal of dead cells (30mins) before experiment. Cells were plated in 96-well U-bottom plate (in cRPMI), at $2X10^5$ cells per well. T cell activation was performed through co-culture with CD3/CD28 stimulator beads (Thermo Fischer Scientific) at a ratio of 1:1, following manufacturer's protocol. In experiments concerning the assessment of cytokine production, GolgiPlug was added into cultures at the final 4 hours of the respective time points. Cultures were incubated (37°C, 5% CO_2) and harvested at respective timepoint for flow cytometric analysis.

2.2.12 Generation of CD226-targeting sgRNA-Cas9 RNP complex

Both mouse or human CD226-targeting CRISPR-RNA (crRNA) were designed using the Benchling online platform, and synthesized by Integrated DNA Technologies (IDT). Candidate crRNAs were selected based on low off-target (>50) and high on-target (>60) scores. Single-guide RNA (sgRNA) was firstly generated via annealing of single-stranded crRNA with a trans-activating tracrRNA (IDT) in a 1:1 molar ratio to obtain a 100 μM gRNA

duplex stock. The mixture is heated at 95°C for 5 mins, and then cooled to RTP for duplex formation. Next, to assemble the ribonucleoprotein (RNP) complex; 120 pmol/µl of the duplexed gRNA was combined with 60 pmol of Cas9 protein (New England Biolabs) in RNase/DNase-free PCR tubes. The mixture was then incubated in a thermal cycler (Bio-rad) at 37°C for 15 mins. The RNP complex was then cooled to RTP (10mins) before use in nucleofection.

2.2.13 Nucleofection procedures

Prior to every nucleofection experiment: mouse or human $CD4^+$ T cells were enriched using the EasySep™ negative isolation kit (StemCell Technologies) following manufacturer's protocol. Enriched cells are then seeded into a 6-well plate, pre-coated with soluble anti-CD3 and anti-CD28, to be activated for 48 hours. Following activation, cells were harvested and washed twice with 1X PBS before resuspension with the respective nucleofector solutions (Lonza).

For each reaction, 82 µl of the respective relevant Nucleofector™ solution (Lonza) was combined with 18 µl of Supplement 1. The specific solution and programs used for either mouse or human T cells are summarized in the table below:

Cell Type	**Nucleofector Solutions**	**4D-Nucleofector Program**
Mouse T cells	P4 Primary cells 4D-Nucleofector® solution	CM-137
Human T cells	P3 Primary cells 4D-Nucleofector® solution	EH-115

Up to $2x10^7$ cells were resuspended in 100 µl of the supplemented Nucleofector™ solution and combined with the pre-assembled RNP complex. For Mock controls, cells were nucleofected with Cas9 alone. Nucleofection was performed using 100 µL Nucleocuvette® vessels with the respective 4D-nucleofector (Lonza) programs. Post-nucleofection, pre-warmed cRPMI was added into the vessels, and rested at 37°C for 25 mins. Cells were then transferred to new culture plates containing pre-warmed cRPMI supplemented with recombinant human IL-2 (100 U/ml) and were further incubated for additional 48 to 72 hours. Knockout efficiencies of CD226 were determined via flow cytometry, prior to every downstream experimental application.

2.2.14 Enrichment of $CD4^+$ T cells from gDT-II mice

Spleens and lymph nodes of gDT-II mice were harvested and processed (as mentioned above) into single cell suspension. The lymphocytes were then subjected to negative $CD4^+$ T cell isolation using the EasySep™ Mouse $CD4^+$ T cell isolation kit (StemCell Technologies) following manufacturer's instructions. After which, supernatants obtained from the negative selection were collected for positive enrichment using the MagniSort™ Mouse $CD4^+$ T cell enrichment kit (Invitrogen) according to standard protocol. Enriched $CD4^+$ T cells are either used immediately for further assays, or cultured further in cRPMI supplemented with recombinant human IL-2 (100 U/ml) at 37°C, 5% CO_2. Purity of the enriched $CD4^+$ T cells was confirmed through flow cytometry.

2.2.15 MHC-I/II assessment of B16 cell lines

Expanded B16 cell lines in culture flasks were detached using 0.25% Trypsin-EDTA. Culture flasks were rinsed twice with 1X PBS to collect the detached B16 cells into tubes, where they were centrifuged (400xg, 5mins), and resuspended in cRPMI medium. The B16 cell lines are then plated into 96-well flat-bottom plates ($1x10^4$ per well), with or without IFNγ (1000 U/ml) treatment and incubated further for 72 hours. The respective B16 cells were then surface stained for MHC-I or MHC-II and assessed via flow cytometry.

2.2.16 *In-vitro* activation of gDT-II cells

$CD4^+$ T cells from gDT-II mice were enriched as previously described above. Splenocytes from a WT mouse were collected, washed twice with sterile 1X PBS and incubated with 10 µM of $gD_{(315–327)}$ peptide (IPPNWHIPSIQDA) for 45 minutes in the incubator (37°C, 5% $CO_{2)}$. After incubation, the peptide-pulsed splenocytes were washed twice with sterile 1X PBS and combined with previously enriched gDT-II $CD4^+$ T cells, into T25 flasks. Cells were co-cultured in cRPMI medium supplemented with 0.15 µg/mL lipopolysaccharides (LPS) and incubated (37°C, 5% CO2) for the next 5 to 7 days. After 48 hours from the initial co-culture, cells were split 1:2, and recombinant human IL-2 (100 U/ml, Aldeskeulin) was added every 24 hours. The activated gDT-II cells were flow sorted to obtain a pure $CD4^+$ T cell population before including in further *in-vitro* experiments.

2.2.17 Generation of $CD226^{KO}$ gDT-II $CD4^+$ T cells

$CD4^+$ T cells from gDT-II mice were firstly enriched and activated as described above. At day 6 post-activation, cells were harvested and subjected to CRISPR-cas9-mediated gene editing via nucleofection, as described previously in section 2.2.9. To ensure high purity of CD226-expressing or non-expressing cell populations, the nucleofected cells were flow sorted following specific surface markers. CD226 knockout ($CD226^{KO}$) were defined as live, $CD45.1^+$ $CD3^+$ $CD4^+$ $CD226^-$ cells. On the other hand, Mock-treated controls were sorted via live, $CD45.1^+$ $CD3^+$ $CD4^+$ $CD226^+$ cells. These sorted populations were then rested overnight in IL-2 supplemented cRPMI in the incubator, before usage for further co-culture experiments.

2.2.18 *In-vitro* functional assay for gDT-II cells

Expanded B16 cell lines were seeded into 96-well flat-bottom plates ($1x10^4$ per well), with or without mouse IFN-γ (1000 U/ml) treatment for 72 hours. Before co-culture with gDT-II cells, the B16 cells were gently washed with 1X PBS to remove residual IFNγ. *In-vitro* activated $CD4^+$ gDT-II cells (described above) were harvested in cRPMI and co-cultured with the B16 cells at 1:1 ratio. Co-cultures were incubated for 6 hours, in which GolgiPlug was added during the 4 hours of the period. Cells were then collected for flow cytometric analysis.

2.2.19 Statistical Analysis

All statistical analyses were conducted using GraphPad Prism software. Data are presented as mean ± standard deviation (SD), or standard error mean (SEM), depending on the respective experiment conducted. Unless noted, differences between two groups were assessed using an unpaired Student's *t*-test. For multiple group analyses, one-way or two-way ANOVA was applied, followed by Tukey's post hoc test for multiple comparisons. A *p*-value below 0.05 was considered statistically significant. Statistical significance is represented as: $p < 0.05$ = *; $p < 0.01$ = **; $p < 0.001$ = ***; $p < 0.0001$ = ****.

3. Results

3.1 CD226 and TIGIT expression patterns in T cell subsets

We firstly sought to characterise the baseline expression patterns of CD226 and TIGIT in T cell subsets from spleen, lymph nodes (LN) and blood from WT mice (Figure 3.1A). Our analysis revealed distinct expression patterns of CD226 and TIGIT on both $CD4^+$ and $CD8^+$ T cells across these organs (Figure 3.1B). Overall, $CD8^+$ T cells were observed to have consistently higher CD226 expression levels (with approximately 95% $CD226^+$ $CD8^+$ T cells), as compared to $CD4^+$ T cells across all organs (Figure 3.1C). On the other hand, $CD4^+$ T cell displayed varying CD226 expression levels, especially among its respective memory compartments (Figure 3.1D). Naïve (Tn) $CD4^+$ T cells showed low or limited CD226 expression, with no significant differences observed across the organs. The central (Tcm) and effector memory subsets (Tem), however, accounted for the majority of the CD226 positive cells within the $CD4^+$ T cell population; with blood-derived $CD4^+$ Tems exhibiting the highest level of CD226 among the three organs. Conversely, uniformly high levels of CD226 were detected in of $CD8^+$ memory T cells across the different organs, with the lowest expression exhibited in Tem cells from the spleen (Figure 3.1D).

In contrast to CD226, TIGIT expression levels were considerably lower in both T cell populations among all organs (Figure 3.1E). Only 5-10% of $CD4^+$ T cells and less than 2% of $CD8^+$ T cells showed TIGIT expression. Similar to the CD226 expression profile among the memory subsets from both $CD4^+$ and $CD8^+$ T cells, effector memory (Tem) showed the highest proportion of TIGIT positive cells, followed by central (Tcm) memory cells, while naïve T cells (Tn) had the lowest TIGIT expression across all organs (Figure 3.1F). These varying levels of CD226 and TIGIT expression in T cells at baseline provides some foundational understanding of how these receptors can be involved in further functions.

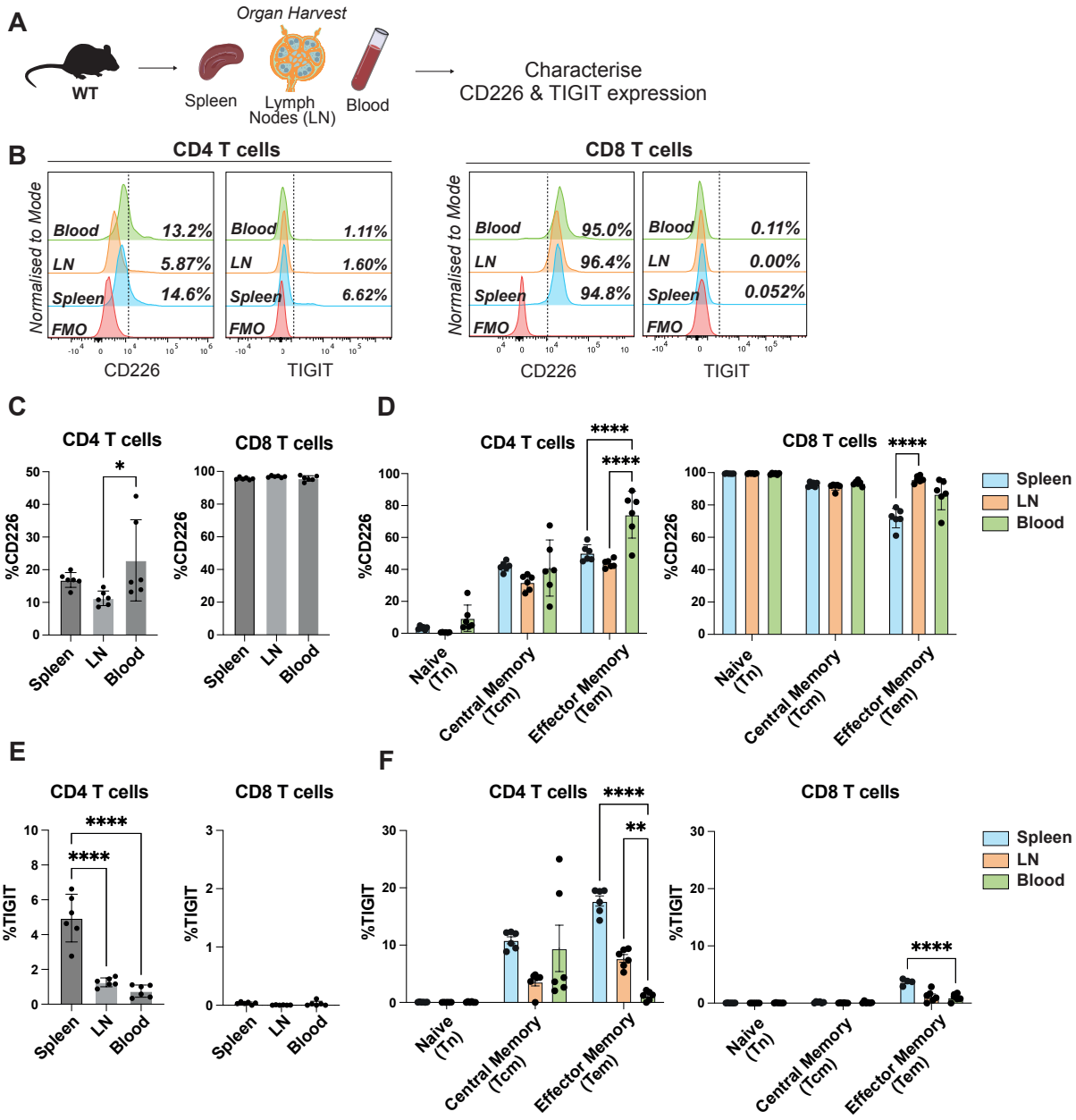

Figure 3.1: Characterisation of CD226 and TIGIT expression on T cells from WT mice **(A)** Schematic depicting the organs harvested for analysis of CD226 and TIGIT expression on T cells. **(B)** Representative FACS histograms showing surface expression of CD226 and TIGIT on $CD4^+$ and $CD8^+$ T cells. **(C)** Quantification of $CD226^+$ $CD4^+$ and $CD8^+$ T cells. **(D)** Frequency of $CD226^+$ cells within $CD4^+$ and $CD8^+$ T cells memory subsets. **(E)** Quantification of $TIGIT^+$ $CD4^+$ and $CD8^+$ T cells. **(F)** Frequency of TIGIT+ cells within $CD4^+$ and $CD8^+$ T cells memory subsets. Memory subsets were defined as follows: Naive (Tn) = $CD62L^+CD44^-$, central memory (Tcm) = $CD62L^+CD44^+$, effector memory (Tem) = $CD62L^-CD44^+$. (WT, n = 6, mean ± SEM, representative of 2 experiments). Statistics: one-way ANOVA with post hoc Tukey's for multiple comparisons (C, D, E, F); *p < 0.05, **p < 0.01, ***p < 0.001, ****p < 0.0001.

3.2 Upregulation of surface CD226 and cytokine production upon activation

CD226 functions as a co-stimulatory receptor on NK and T cells (Shibuya et al. 2003; Gaud et al. 2018; Weulersse et al. 2020). To specifically investigate its correlation to early $CD4^+$ T cell activation, CD226 surface expression and cytokine production by $CD4^+$ T cells from WT or CD226-deficient (*$Cd226^{KO}$)* mice was assessed, following TCR stimulation (with anti-CD3/CD28 antibodies) over various time points (Figure 3.2A). Upon stimulation, a significant increase in CD226 expression in WT cells was observed at all time points as compared to baseline (Day 0) (Figure 3.2B). This upregulation was also accompanied by significantly increased frequencies of CD226-positive $CD4^+$ T cells, which peaked at 48 hours post-stimulation. The geometric mean fluorescence intensity (gMFI) of CD226 also showed significantly elevating level as compared to baseline; which also peaked at the 48 hours' time point.

To examine if the upregulation of CD226 in $CD4^+$ T cells observed would also affect cytokine production, we compared cytokine expression profiles and kinetics that are characteristic of various $CD4^+$ T cell subsets (Th1: TNF-α, IFN-γ; Th2: IL-13; Th17: IL-17A; Tregs: IL-10) between WT and *$Cd226^{KO}$* mice. TNF-α levels peaked at 72 hours post-stimulation in both WT and *$Cd226^{KO}$* cells, but with no significant differences observed between the two groups at any of the time points of the experiment (Figure 3.2C and 3.2H). Similarly, IFN-γ production from both groups increased in a time-dependent manner; but with WT cells exhibiting significantly higher IFN-γ levels than *$Cd226^{ko}$* mice at 72 hours post-stimulation (Figure 3.2D and 3.2I). On the other hand, IL-13, IL-17A and IL-10 production remained low (fewer than 3% of the total $CD4^+$ T cell population) from both groups across all time points (Figure 2E-2G, Figure 2J-2L). Interestingly, despite the low levels, *$Cd226^{KO}$* cells conveyed higher expression of these cytokines at 48 hours as compared to WT cells, with IL-10 levels even gaining statistical significance. Curation of CD226-negative and -positive $CD4^+$ T cell populations within the WT cells at 48 hours post-stimulation (at CD226 peak expression levels) showed that CD226-positive $CD4^+$ T cells were the main contributors to the detected levels of cytokines (Figure 3.2M-3.2P). Collectively, these findings may indicate that CD226 can influence cytokine production in $CD4^+$ T cells, particularly cytokines characteristic of Th1 subsets, during early stages of T cell activation which can potentially modulate future functions.

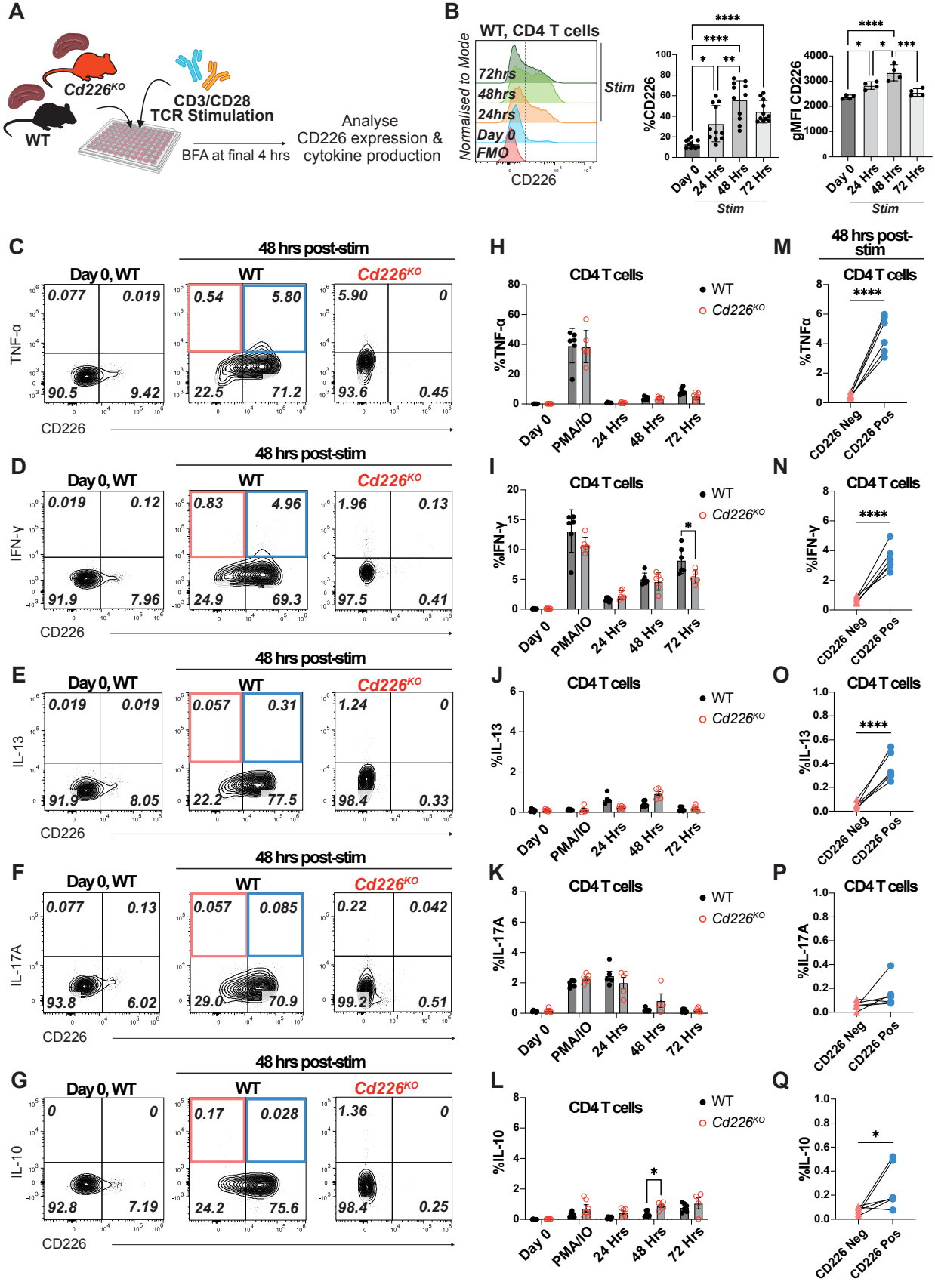
A
Cd226KO
WT
CD3/CD28
TCR Stimulation
BFA at final 4 hrs
Analyse
CD226 expression &
cytokine production
B
WT, CD4 T cells
Normalised to Mode
72hrs
48hrs
24hrs
Day 0
FMO
Stim
CD226
%CD226
gMFI CD226
Day 0
24 Hrs
48 Hrs
72 Hrs
Stim
C
D
E
F
G
48 hrs post-stim
Day 0, WT
WT
Cd226KO
TNF-α
IFN-γ
IL-13
IL-17A
IL-10
CD226
H
I
J
K
L
CD4 T cells
%TNF-α
%IFN-γ
%IL-13
%IL-17A
%IL-10
PMA/IO
M
N
O
P
Q
%TNFα
CD226 Neg
CD226 Pos

Figure 3.2: Upregulation of surface CD226 expression involves cytokine production **(A)** Schematic illustration for *in-vitro* T cell stimulation from WT and *Cd226^{ko}* splenocytes. **(B)** Representative histograms showing surface CD226 expression on WT CD4$^+$ T cells upon TCR stimulation, with corresponding quantifications. (WT, n = 4-11, mean ± SD, cumulative of 3 experiments). **(C-G)** Representative dot plots showing cytokine production by total CD4$^+$ T cells from WT and *Cd226^{ko}* mice at baseline (day 0) and 48 hours post-stimulation. **(H-L)** Quantification of the respective cytokines produced by total CD4$^+$ T cells from WT and *Cd226^{ko}* mice. PMA/ionomycin (PMA/IO) positive control values were taken from the 48-hour timepoint of the experiment. **(M-Q)** Quantification of the respective cytokines from CD226-positive and -negative CD4$^+$ T cells at 48 hours post-stimulation from WT cells. All data shown concerning cytokine production is representative of 2 experiments. (WT, n = 6, mean ± SEM). Statistics: one-way ANOVA with post hoc Tukey's for multiple comparisons (B, D), unpaired Student's T-test (E); *p < 0.05, **p < 0.01, ***p < 0.001, ****p < 0.0001.

3.3 CD4$^+$ tumour-infiltrating lymphocytes expresses CD226

In recent years, many studies have demonstrated the functional contributions of CD4$^+$ T cells in anti-tumour immunity, including in metastatic melanomas, thus highlighting their role in tumour control (Quezada et al. 2010; Schietinger et al. 2010; Gaud et al. 2018; Poncette et al. 2022). We therefore sought to further characterise CD226 expression on CD4$^+$ T cells in the tumour context. B16F1 cells were injected subcutaneously into WT mice, where the tumours, spleen and draining lymph nodes (DLN) were harvested at various experimental end points (Figure 3.3A). CD4$^+$ T cells from the tumours and spleens had similar proportions of CD226-expressing cells (approximately 15% in both tissues), with those in DLN bearing the lowest level of CD226 expression (approximately 5%) (Figure 3.3B). Similarly, no apparent differences were observed for TIGIT expression in CD4$^+$ T cells from the tumours and spleen (approximately 8~10%), with DLN exhibiting the lowest proportion of TIGIT-expressing CD4$^+$ T cells. Within the total CD4$^+$ T cell population, we further curated the frequencies of distinct Th subsets defined by their lineage-specific transcription factors (Th1: T-bet; Th2: GATA-3; Th17: RORγt; Tregs: FOXP3) (Figure 3.3C). In the tumour, CD4$^+$ T cells were predominantly composed of Th1 (T-bet$^+$) (approximately 50%) and Treg cells (FOXP3$^+$) (approximately 40%); with significantly higher frequencies as compared to those in the spleen or DLN (Figure 3.3C). In contrast, Th17 (RORγt$^+$) and Th2 (GATA-3$^+$) were present at lower levels as compared to both the Th1 and Treg populations, although these proportions were still elevated in comparison to their proportions in the spleen or DLN (Figure 3.3C).

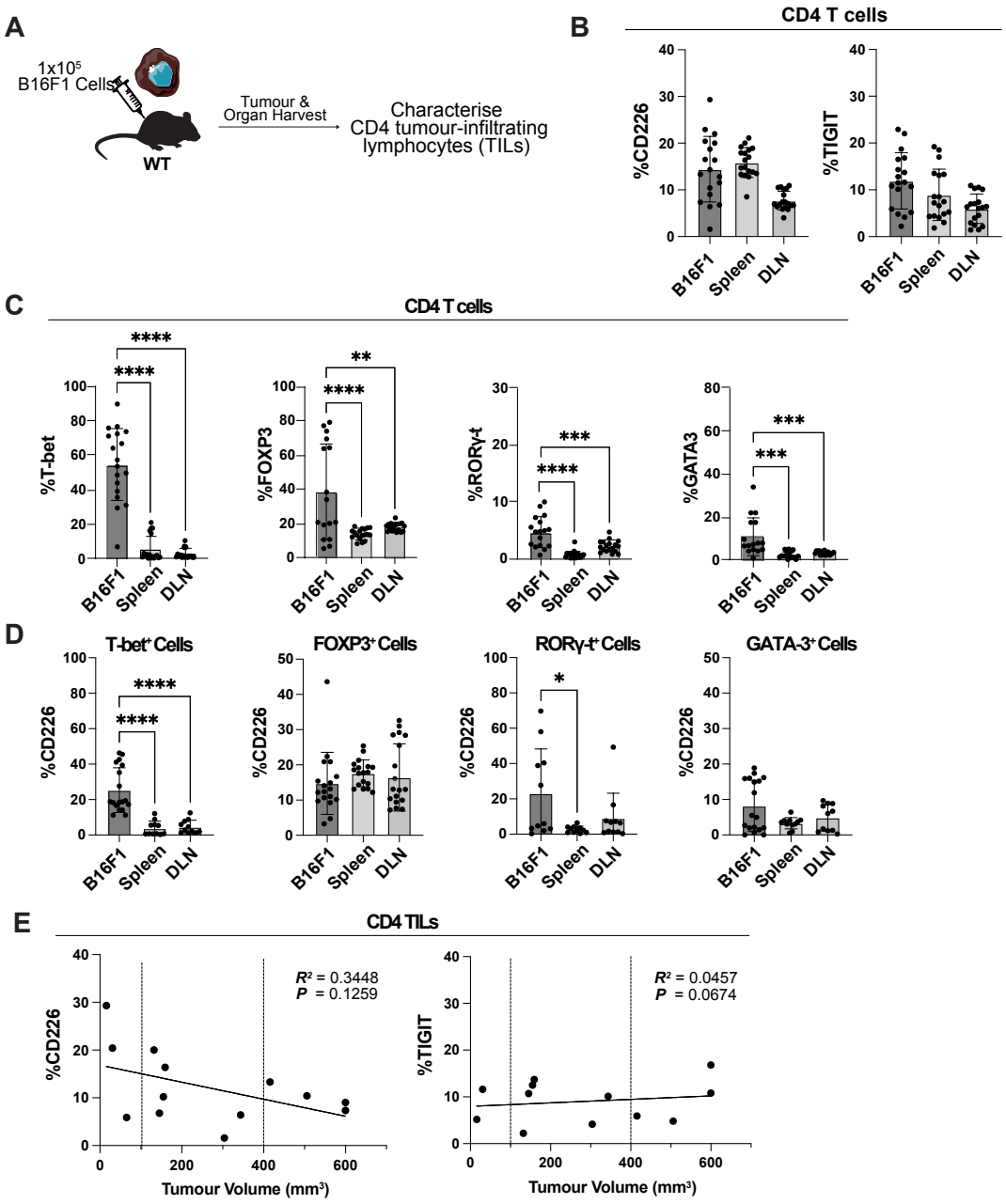

Figure 3.3: CD226 expression profile on CD4⁺ T cells isolated from melanoma-bearing mice

(A) Schematic illustration of *in-vivo* experimental setup involving the injection of B16F1 melanoma cells. **(B)** Quantification of CD226⁺ and TIGIT⁺ CD4⁺ T cells in B16F1 tumours, spleens and draining lymph nodes (DLN) of the tumour-bearing mice (WT, n=18, mean ± SD, cumulative of 4 independent experiments). **(C)** Quantification of indicated transcription factors characteristic for specific T-helper subsets; Th1: T-bet, FOXP3: Tregs, Th17: RORγt, Th2: GATA-3. **(D)** Quantification of surface CD226 expression from the respective Th subsets shown (WT, n=18, mean ± SD, cumulative of 4 independent experiments). (**E)** Frequencies of CD226⁺ and TIGIT⁺ CD4⁺ T cells in correlation with tumour volume. Statistics: one-way ANOVA with post hoc Tukey's for multiple comparisons (C and D).

Spearman rank correlation coefficient (E); *p < 0.05, **p < 0.01, ***p < 0.001, ****p < 0.0001.

We next assessed CD226 expression levels from these respective Th subsets (Figure 3.3D). Among the Th1 populations, the largest proportion of CD226-positive cells were exhibited by those in the tumour, with statistical significance when compared to those in the spleen or DLN. Th17 cells displayed similar trend, showing elevated levels of CD226-positive cells in the tumour. Opposingly, CD226-positive cells frequencies within the Tregs and Th2 population remained rather uniform across the organs.

We have previously shown that elevated levels of CD155 in tumours contributed to the loss of CD226 surface expression in CD8 TILs (Braun et al. 2020). To probe if similar mechanisms could also occur in the $CD4^+$ TILs, we reviewed CD226 and TIGIT expression levels in correlation to tumour volume (Figure 3.3E). Although the correlation between CD226 expression and tumour volume did not present statistical significance, there was an apparent trend towards a negative correlation (R^2= 0.3448), Hence, suggesting similar mechanisms of CD226 downregulation in $CD4^+$ TILs following tumour progression. In contrast, TIGIT expression levels were relatively consistent across all tumour volumes, which may illustrate that TIGIT on $CD4^+$ TILs remain undeterred upon tumour burden.

3.4 Ligation with CD155 drives surface downregulation of CD226 in T cells

To further investigate the underlying CD155-induced mechanism of CD226 downregulation in $CD4^+$ T cells, we established an *in-vitro* assay utilising beads coated with either anti-CD3/CD28 (Stim), or in combination with varying concentrations of mouse recombinant CD155 (Stim+CD155). As the recombinant mouse CD155 is fused to the C-terminal Fc region of the human IgG1 tag, confirmation of successful CD155 conjugation to the beads were confirmed by flow cytometry (Figure 3.4A). Incubation of WT naive T cells with Stim+CD155 beads (5ug/ml CD155) showed extensive loss of surface CD226 for both $CD4^+$ and $CD8^+$ T cells, as compared to those stimulated with control Stim beads (Figure 3.4B). Simultaneously, the early activation marker, CD69, was significantly upregulated following incubation with both beads group, demonstrating efficient T cell activation from the anti-CD3/CD28 conjugation (Figure 3.4C).

To assess if this effect is CD155 dose-dependent, we generated new sets of beads comprising of titrated CD155-fc concentrations (5ug/ml, 0.5ug/ml, 0.05ug/ml) and repeated the *in-vitro* assays (Figure 3.4D). Indeed, we observed significant surface CD226 reduction in both T cells by 360 minutes post incubation with beads conjugated with 0.5ug/ml and 5ug/ml CD155-fc; with 5ug/ml CD155-fc eliciting the most prominent effect (Figure 3.4E and 3.4F). Conversely, beads conjugated with 0.05ug/ml CD155-fc did not exhibit any apparent effect on CD226 expression levels and were hence omitted from further experiments (data not shown). Collectively, these data suggest that CD155 can elicit a dose-dependent downregulation of surface CD226 on $CD4^+$ T cells, emulating similar observations made in $CD8^+$ T cells. However, it is important to note that $CD8^+$ T cells had a more pronounced surface CD226 loss, which could be due to their higher baseline CD226 expression as compared to $CD4^+$ T cells.

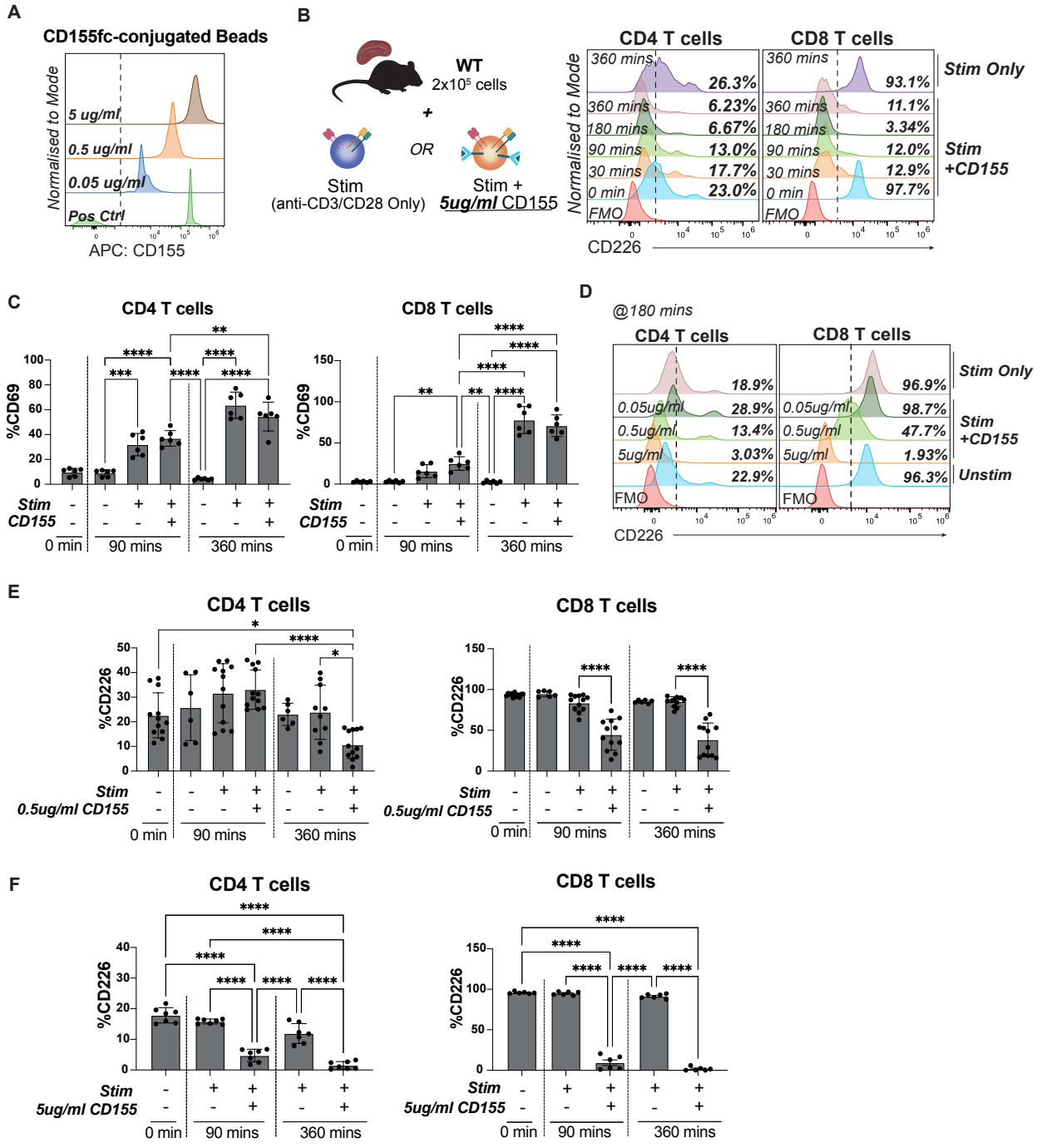

Figure 3.4: Surface CD226 is downregulated upon ligation with CD155, in a dose- and time-dependant manner

(A) Representative histogram plots showing titration of CD155 coupled to the dynabeads. **(B)** Representative histogram plots showing CD226 expression in splenic T cells stimulated with CD3/CD28 (stim) ± 5ug/ml CD155-coated beads, at various timepoints. **(C)** Representative histogram plots showing CD226 expression in both splenic T cells with CD3/CD28 (stim) ± CD155-coated beads at 180 minutes post incubation, with differing CD155 concentrations used for conjugation. **(D)** Quantification of $CD69^+$ $CD4^+$ and $CD8^+$ T cells stimulated with respective dynabeads at various timepoints. (WT, n= 3 per group,

mean ± SD, cumulative of 2 independent experiments). **(E)** Quantification of $CD226^+$ $CD4^+$ and $CD8^+$ T cells after stimulation with respective control (Stim only) and 0.5ug/ml CD155-conjugated beads at various timepoints. (WT, n=3 per group, mean ± SD, cumulative of 4 independent experiments). **(F)** Quantification of $CD226^+$ $CD4^+$ and $CD8^+$ T cells after stimulation with respective control (Stim only) and 5ug/ml CD155-conjugated beads at various timepoints. Unstimulated control at respective timepoints was not included in this experiment (WT, n=3 per group, mean ± SD, cumulative of 2 independent experiments). Statistics: one-way ANOVA with post hoc Tukey's for multiple comparisons. *p < 0.05, **p < 0.01, ***p < 0.001, ****p < 0.0001

3.5 Selective surface CD226 downregulation via CD155 engagement

CD112 (PVRL2 or Nectin-2), similar to CD155, belongs to the nectin and nectin-like family of immunoglobulin superfamily receptors, and presents as another ligand for CD226 (Stamm et al. 2018). High CD112 expression has been reported in several cancers, and has been associated with modulating and dampening T cell functions (Miao et al. 2013; Whelan et al. 2019; Zeng et al. 2021). Additionally, expression of CD112 on tumour cells correlates with angiogenesis and metastasis (Miao et al. 2013; Oshima et al. 2013; Bekes et al. 2019). Given that CD226 also binds to CD112, we therefore questioned if CD112 ligation could also induce downregulation of surface CD226 on T cells. To address this, we further generated CD112-fc (5ug/ml) conjugated beads (Stim+CD112), in parallel with CD155-conjugated beads, and performed similar *in-vitro* experiment as previously described (Figure 3.5A). Our data suggests that neither $CD4^+$ or $CD8^+$ T cells presented profound surface CD226 loss with Stim+CD112 beads at 360 minutes post incubation, as compared to the distinct downregulated CD226 levels observed with Stim+CD155 beads (Figure 3.5B and 3.5C) Interestingly, we instead observed a trend towards upregulated surface CD226 expression in $CD4^+$ T cells at 180 mins and 360 minutes post-incubation, reaching statistical significance at 360-minute timepoint, as compared to unstimulated controls. These data suggest that, in contrast to CD155, CD226 downregulation in T cells is no mediated through CD112 ligation, and may instead promote different modulatory effects, especially in $CD4^+$ T cells.

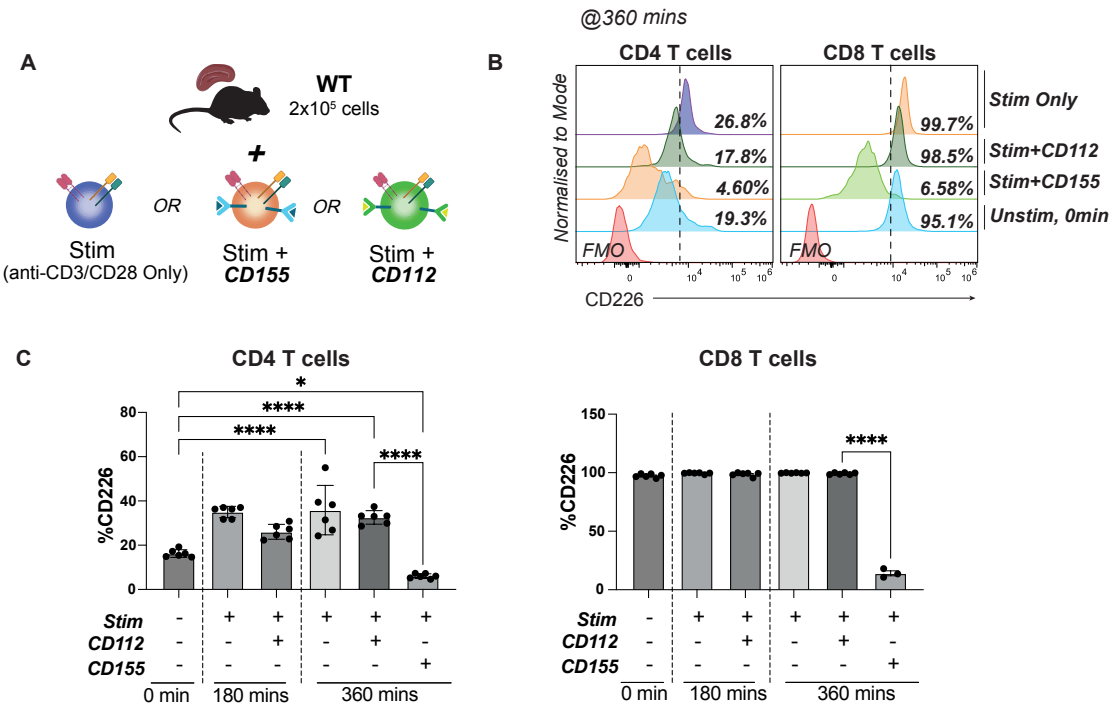

Figure 3.5: Selective downregulation of surface CD226 by CD155, but not CD112

(A) Schematic of *in-vitro* co-culture experiment with CD3/CD28 (Stim) beads ± CD155- or CD112-conjugated beads. **(B)** Representative histogram plots showing CD226 expression in both splenic CD4$^+$ and CD8$^+$ T cells with CD3/CD28 (Stim) ± CD155- or CD112-conjugated beads at 360 minutes post stimulation. **(C)** Quantification of CD226$^+$ CD4$^+$ and CD8$^+$ T cells after stimulation with respective control (Stim only), and CD155- or CD112-conjugated beads at various timepoints. (WT, n=3 per group, mean ± SD, cumulative of 2 independent experiments). Statistics: one-way ANOVA with post hoc Tukey's for multiple comparisons. *p < 0.05, **p < 0.01, ***p < 0.001, ****p < 0.0001.

3.6 CD155-ligation mediates Y319 phosphorylation and ubiquitination by Cbl-b

It was previously reported that the Y319 phosphorylation site is vital for CD226 signalling in NK cells and subsequent NK cells killing mechanisms. Additionally, through the use of mice bearing a point mutation at Y319 (*Cd226*^{Y319F}), we have previously demonstrated that this point mutation concurred for enhanced anti-tumour efficacy from CD8$^+$ TILs, with CD226 from *Cd226*^{Y319F} CD8$^+$ T cells being more resistant to CD155-mediated downregulation. However, its importance and mechanism in CD4$^+$ T cells specifically, has not been addressed. We performed similar beads experiments as previously described, with T cells isolated from *Cd226*^{Y319F} mice (Figure 5A). For technical purposes, we selected beads conjugated with 0.5ug/ml CD155 for these experiments, as higher concentrations (e.g 5ug/ml) accrued to accelerated of surface CD226 expression across

all time points for both mouse strains, concealing any genotype-specific responses (data not shown) (Figure 3.6A). Surface CD226 levels from *Cd226*^{Y319F} CD4^{+} T cells exhibited slight downregulation resistance following incubation with Sim+CD155 beads, as compared to those from the WT mice, although no statistical significance was obtained (Figure 3.6B and 3.6C). Consistent with our earlier observations and in clear contrast to the CD4^{+} T cells, *Cd226*^{Y319F} CD8^{+} T cells displayed significantly more pronounced resistance to CD155-induced surface CD226 loss than its WT counterpart (Figure 3.6B and 3.6C).

Phosphorylation at the Y319 residue recruits the Cbl-b E3 ubiquitin ligase downstream, which is important for post-transcriptional regulation in T cell. To investigate the role of Cbl-b in the mechanistic regulation of CD226 in CD4^{+} T cells, we utilized *Cbl-b*^{C373A} mice (*Cbl-b*$^{\Delta R}$), possessing a loss-of-function mutation in the RING finger domain, abolishing the E3-ligase function. We then repeated the previously described *in-vitro* beads stimulation assays with T cells from these mice (Figure 3.6D). Similar to findings with the Cd*226*^{Y319F} mice, CD226 expression from *Cbl-b*$^{\Delta R}$ T cells showed resistance against CD155-mediated downregulation compared to WT controls. This was also statistically significant for the CD4^{+} T cells at 180 minutes post-incubation. As expected from previous results, this effect was more pronounced in the CD8^{+} T cells. Subsequent immunoblot analysis revealed decreased levels of total CD226 protein content upon incubation with Stim+CD155 beads as compared to Stim or unstimulated controls. Thereby, suggesting degradation of CD226 upon CD155 ligation in CD4^{+} T cells (Figure 3.6E and 3.6F). Collectively, these data suggests that the mechanism of regulation of CD226 in CD4^{+} T cells through CD155 ligation, may mirror to those previously observed in CD8^{+} T cells; although with nuance distinctions in magnitude and response kinetics.

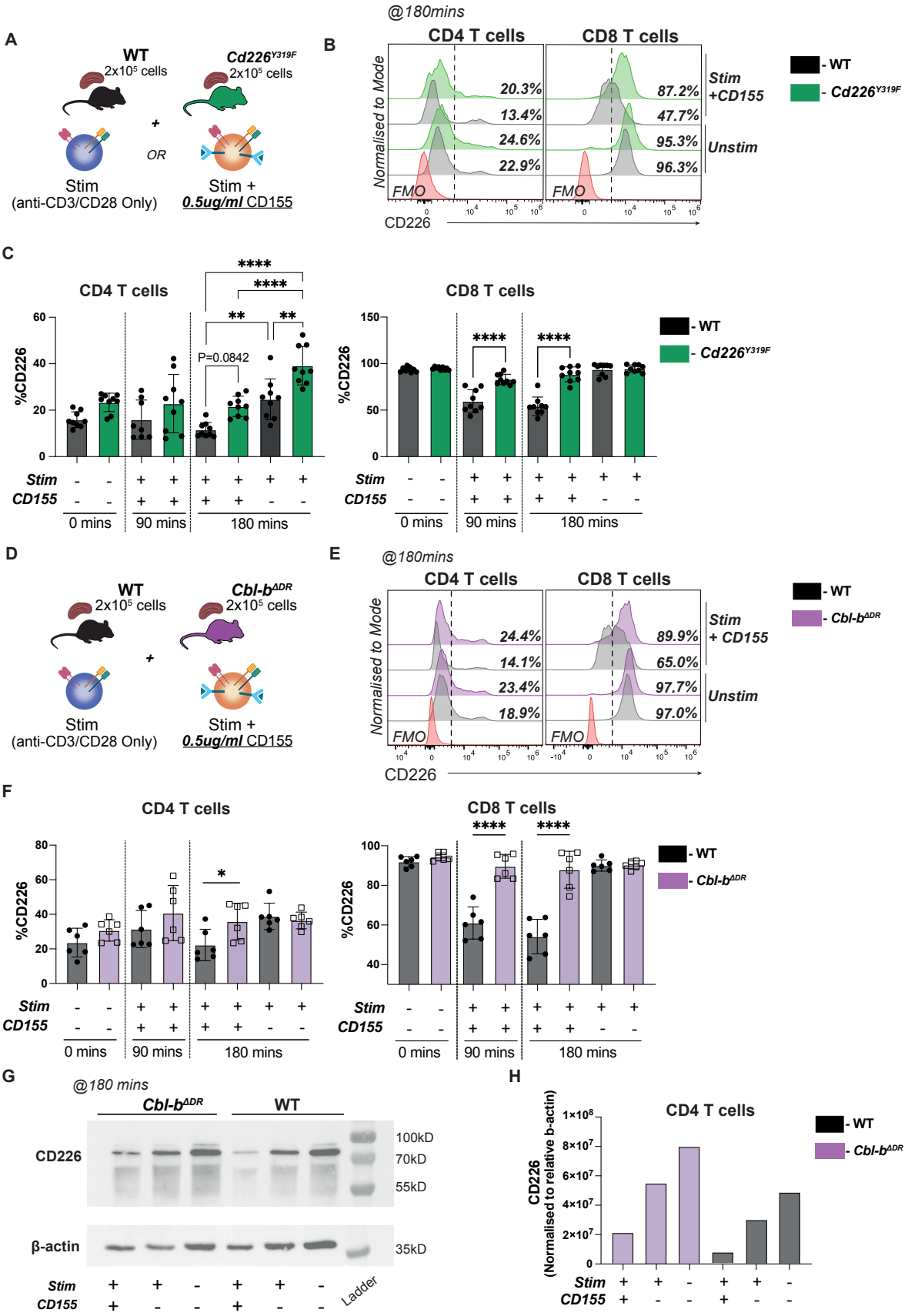
A
WT
2x10⁵ cells
Cd226Y319F
2x10⁵ cells
+
OR
Stim
(anti-CD3/CD28 Only)
Stim +
0.5ug/ml CD155
B
@180mins
CD4 T cells
CD8 T cells
Normalised to Mode
20.3%
13.4%
24.6%
22.9%
87.2%
47.7%
95.3%
96.3%
Stim +CD155
Unstim
FMO
CD226
- WT
- Cd226Y319F
C
CD4 T cells
CD8 T cells
%CD226
P=0.0842
****
**
Stim
CD155
0 mins
90 mins
180 mins
- WT
- Cd226Y319F
D
WT
2x10⁵ cells
Cbl-bΔDR
2x10⁵ cells
+
Stim
(anti-CD3/CD28 Only)
Stim +
0.5ug/ml CD155
E
@180mins
CD4 T cells
CD8 T cells
Normalised to Mode
24.4%
14.1%
23.4%
18.9%
89.9%
65.0%
97.7%
97.0%
Stim + CD155
Unstim
FMO
CD226
- WT
- Cbl-bΔDR
F
CD4 T cells
CD8 T cells
%CD226
*
****
Stim
CD155
0 mins
90 mins
180 mins
- WT
- Cbl-bΔDR
G
@180 mins
Cbl-bΔDR
WT
CD226
β-actin
100kD
70kD
55kD
35kD
Stim
CD155
Ladder
H
CD4 T cells
CD226
(Normalised to relative b-actin)
1×10⁸
8×10⁷
6×10⁷
4×10⁷
2×10⁷
0
Stim
CD155
- WT
- Cbl-bΔDR

Figure 3.6: CD226 ligation with CD155 induces Y319 phosphorylation and Cbl-b mediated ubiquitination in T cells
(A) Schematic of *in-vitro* co-culture experiment of splenic T cells from WT or *Cd226*^{Y319F} mice, with CD3/CD28 (Stim) beads ± CD155-conjugated beads. **(B)** Representative histogram plots showing CD226 expression in splenic CD4$^+$ and CD8$^+$ T cells from WT and *Cd226*^{Y319F} mice with CD3/CD28 (Stim) ± CD155-conjugated beads at 180 minutes post stimulation. **(C)** Quantification of CD226$^+$ CD4$^+$ and CD8$^+$ T cells from WT and *Cd226*^{Y319F} mice, after stimulation with CD3/CD28 (Stim only-, and CD155-conjugated beads at various timepoints. (WT, n=3 per group, mean ± SD, cumulative of 3 independent experiments). **(D)** Schematic of *in-vitro* co-culture experiment of splenic T cells from WT or *Cbl-b*$^{\Delta DR}$ mice, with CD3/CD28 (Stim) beads ± CD155-conjugated beads. **(E)** Representative histogram plots showing CD226 expression in splenic CD4$^+$ and CD8$^+$ T cells from WT and *Cbl-b*$^{\Delta DR}$ mice with CD3/CD28 (Stim) ± CD155-beads at 180 minutes post stimulation. **(F)** Quantification of CD226$^+$ CD4$^+$ and CD8$^+$ T cells from WT and *Cbl-b*$^{\Delta DR}$ mice after stimulation with CD3/CD28(Stim only-, and CD155-conjugated beads at various timepoints. (WT, n=3 per group, mean ± SD, cumulative of 2 independent experiments). **(G)** Representative immunoblot showing CD226 in CD4$^+$ T cells isolated from WT and *Cbl-b*$^{\Delta DR}$ mice with **(H)** respective quantifications. β-actin used as loading control. (Representative of 3 independent experiments). Statistics: one-way ANOVA with post hoc Tukey's for multiple comparisons. *p < 0.05, **p < 0.01, ***p < 0.001, ****p < 0.0001.

3.7 CD4$^+$ T cells isolated from gDT-II mice effectively are effectively primed towards memory phenotype

The relevance of CD226$^+$ CD4$^+$ T cells in anti-tumour immunity remains largely unknown. To investigate this, we employed the use of a TCR transgenic mouse model (gDT-II mice). gDT-II mice harbor a TCR recognising the MHC-II restricted epitope of the Herpes simplex virus (HSV)-derived glycoprotein D (gD) (Bedoui et al. 2009). In conjunction to these transgenic T cells, we incorporated a B16.F10 melanoma cell line that has been engineered to express the full-length HSV-derived gD protein (B16.gD) (Figure 3.7A) (Bawden et al. 2024). At baseline, the frequency of immune cells (T cells, NK cells, B cells) from gDT-II mice did not differ from WT mice (Figure 3.7B), however with a slightly higher CD4+ Tem population in the gDT-II mice (Figure 3.7C). Additionally, there was also no difference in the expression level of CD226 on both CD4$^+$ and CD8$^+$ T cells between the two strains (Figure 3.7).

We next sought to characterise the gDT-II CD4$^+$ T cells following activation (Figure 3.7E). *In-vitro* priming of gDT-II CD4$^+$ T cells was performed via co-culture of enriched gDT-II CD4$^+$ T cells and gD peptide-pulsed WT splenocytes – serving as APCs - in the presence

of IL-2 and LPS (Figure 3.7E). Pure enrichment of gDT-II CD4+ T cells was achieved through sequential negative and positive isolation protocols (Figure 3.7F). Following gD-priming, the $CD4^+$ T cells displayed a phenotypic transition from the naïve state towards a memory state, particularly skewing towards the Tcm phenotype (Figure 3.7G). This transition was accompanied by an overall significant increase in CD226 expression level in total $CD4^+$ T cells, with higher levels displayed particularly in the Tcm and Tem subsets compared to respective controls. Interestingly, the Tn subsets also displayed a modest increased in CD226 expression levels, though remained low overall (Figure 3.7H and 3.7I). Further stratification revealed that gD-primed cells displayed significantly elevated T-bet levels and negligible FOXP3 expression levels as compared to controls; suggesting that the majority of the gD-primed $CD4^+$ T cells are Th1 cells (Figure 73.J). Additionally, these cells showed some characteristics attributed to cytotoxicity, through an increase in BLIMP-1 levels and a decrease in Eomes and KLRG1 expression (Figure 3.7K).

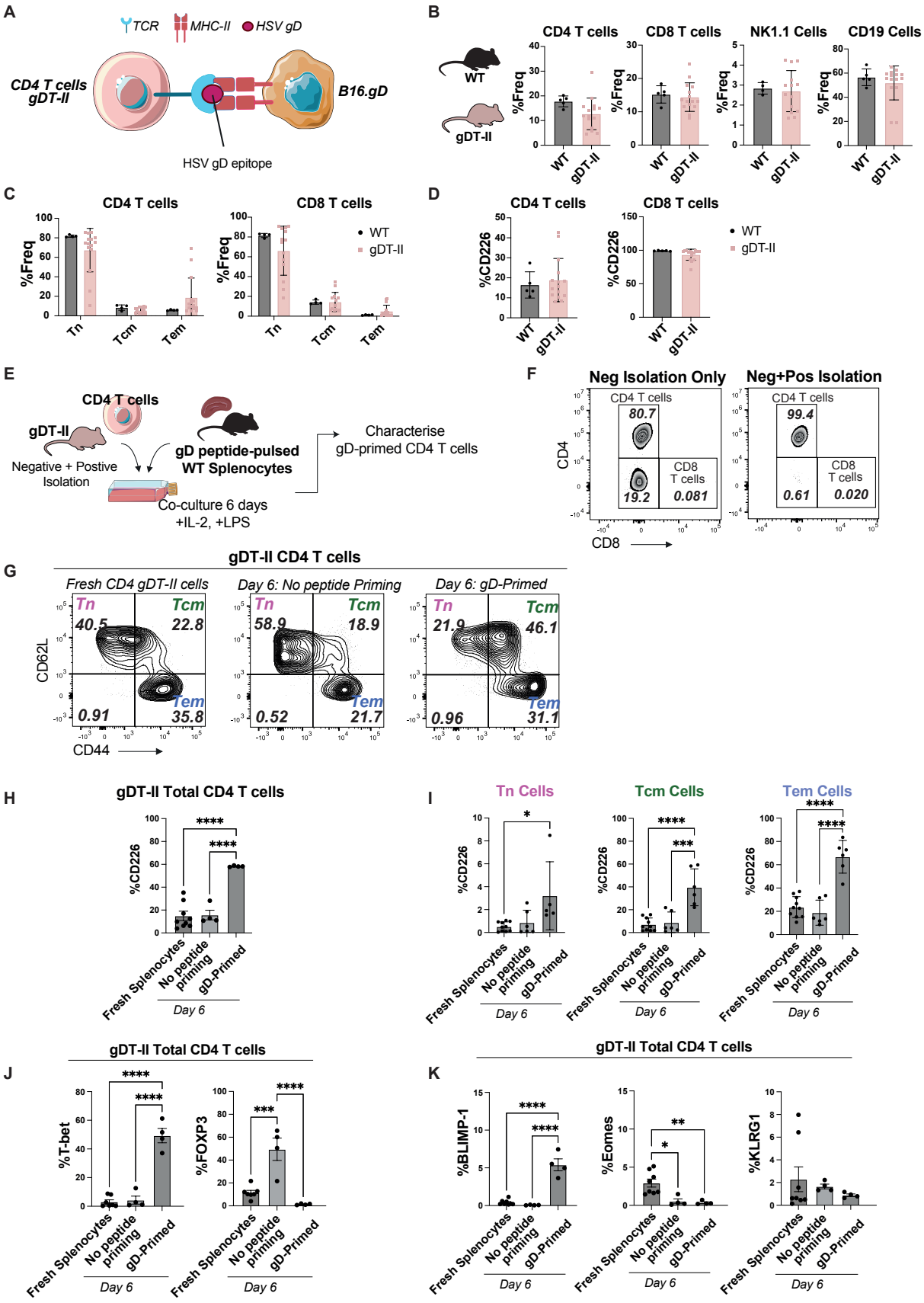
A
TCR
MHC-II
HSV gD
CD4 T cells gDT-II
B16.gD
HSV gD epitope
B
WT
gDT-II
CD4 T cells
CD8 T cells
NK1.1 Cells
CD19 Cells
%Freq
C
CD4 T cells
CD8 T cells
%Freq
Tn
Tcm
Tem
WT
gDT-II
D
CD4 T cells
CD8 T cells
%CD226
WT
gDT-II
E
CD4 T cells
gDT-II
Negative + Postive Isolation
gD peptide-pulsed WT Splenocytes
Co-culture 6 days +IL-2, +LPS
Characterise gD-primed CD4 T cells
F
Neg Isolation Only
Neg+Pos Isolation
CD4 T cells
80.7
19.2
CD8 T cells
0.081
99.4
0.61
0.020
CD4
CD8
G
gDT-II CD4 T cells
Fresh CD4 gDT-II cells
Day 6: No peptide Priming
Day 6: gD-Primed
Tn
Tcm
Tem
40.5
22.8
0.91
35.8
58.9
18.9
0.52
21.7
21.9
46.1
0.96
31.1
CD62L
CD44
H
gDT-II Total CD4 T cells
%CD226
Fresh Splenocytes
No peptide priming
gD-Primed
Day 6
I
Tn Cells
Tcm Cells
Tem Cells
J
gDT-II Total CD4 T cells
%T-bet
%FOXP3
K
gDT-II Total CD4 T cells
%BLIMP-1
%Eomes
%KLRG1

Figure 3.7: Characterisation of the gDT-II neoantigen system
(A) Schematic the gDT-II model, where $CD4^+$ T cells from gDT-II cells recognises gD-expressing B16.F10 melanoma cells (B16.gD). **(B)** Frequencies of splenic T cells, NK cells, and B cells in WT (n=4) and gDT-II (n=15) mice. (mean ± SD, cumulative of three experiments) **(C)** Memory subset distribution of $CD4^+$ and $CD8^+$ T cells in (n=4) and gDT-II (n=15) mice. Memory subset were defined as follows: Naive (Tn) = $CD62L^+CD44^-$, central memory (Tcm) = $CD62L^+CD44^+$, effector memory (Tem) = $CD62L^-CD44^+$. (mean ± SD, cumulative of 3 experiments) **(D)** Quantification of CD226+ T cells in WT (n=4) and gDT-II (n=15) mice. (mean ± SD, cumulative of three experiments). (**E)** Schematic depicting *in-vitro* gDT-II activation protocol. **(F)** Representative flow plots for $CD4^+$ T cell isolated using combined negative and positive selection protocols. **(G**) Representative flow plots showing memory subset distribution of gDT-II $CD4^+$ T cells at fresh isolation and day 6 post-cultures ± gD-priming. **(H-I)** Quantification of $CD226^+$ total $CD4^+$ T cells from gDT-II mice **(H),** and the respective memory subsets **(I),** at fresh isolation and day 6 post-cultures ± gD-priming. **(J-K)** Quantification of T-bet^+ and $FOXP3^+$ **(J)**, cytotoxic markers (Blimp-1, Eomes, KLRG1) **(K)** after fresh isolation and day 6 post-cultures ± gD-priming. (Fresh, n= 8; Day 6: n= 4-15; mean ± SEM, 2 experiments). **(**Statistics: one-way ANOVA with post hoc Tukey's for multiple comparisons (H-K). *p < 0.05, **p < 0.01, ***p < 0.001, ****p < 0.0001.

3.8 IFN-γ stimulation upregulates MHC-I and -II expression on B16 melanoma variants

As mentioned previously, gDT-II $CD4^+$ T cells can recognise the MHC-II restricted epitope of the HSV gD protein. To model this interaction, we incorporated a B16.F10 melanoma cell line that has been engineered to express the full-length HSV-derived gD protein (B16.gD), present on both MHC-I and MHC-II (Bawden et al. 2024). To assess MHC-I/II expression on the B16 melanoma variants for the gD antigen, the cells were stimulated with IFN-γ for 72 hours (Figure 3.8A). Following stimulation, both the parental B16.F10 WT and B16.gD cells displayed upregulation of MHC-I and MHC-II expression (Figure 3.8A and 3.8B). To address the role of MHC-II expression in the anti-tumour $CD4^+$ T cell functions, a B16.gD cell line deficient of MHC-II (B16.gD.*Ciita*^{KO}; $CIITA^{KO}$), through the disruption of the *Ciita* gene, was generated through CRISPR/Cas9 methods (Bawden et al. 2024). To further enrich the gene-disrupted cells in the polyclonal cultures, MHC-II-negative proportions were sorted via flow cytometry following IFN-γ stimulation (Figure 3.8C). The control cell line used for subsequent experiments were generated through transfection with a Px459 empty vector, which lacks the *Ciita*-targeting RNA sequences (B16.gD.Px459; $CIITA^{WT}$) (Figure 3.8D). Similar to the parental B16.gD, the B16.gD.Px459 cells upregulated both MHC-I and -II expression following IFN-γ stimulation.

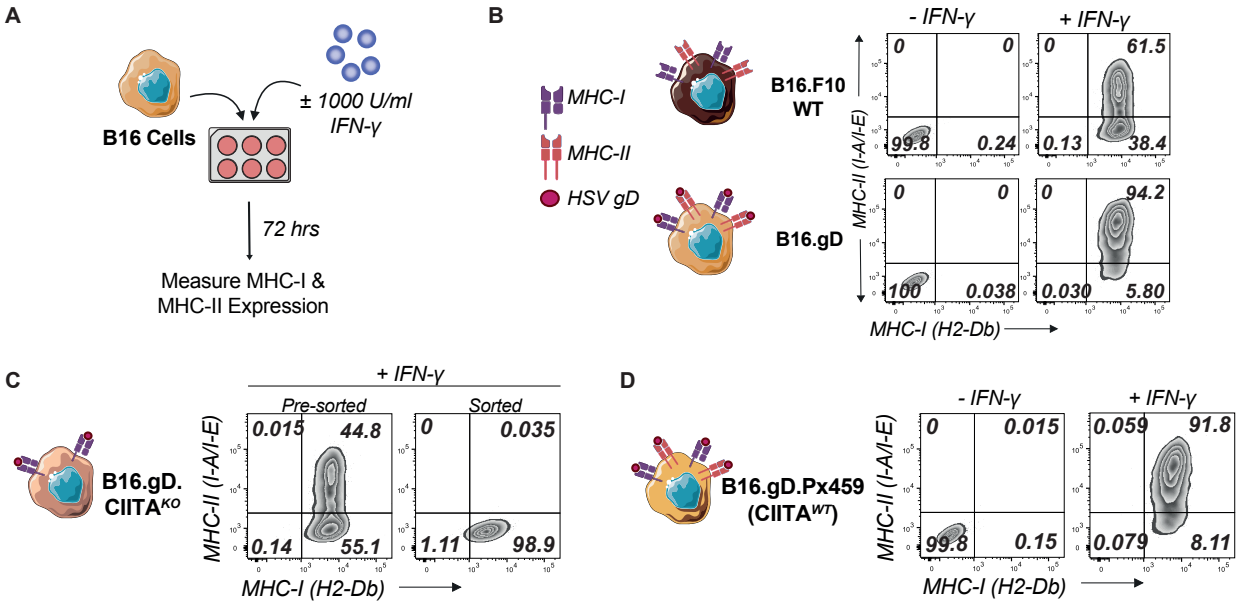

Figure 3.8: MHC-I and MHC-II expression of B16 cells
(A) Schematic depicting stimulation of B16 cells with mouse IFN-γ (1000U/ml). **(B)** MHC-I and MHC-II expression from parental B16.F10 WT and B16.gD ± IFN-γ stimulation *in-vitro*. **(C)** MHC-I and MHC-II expression of IFN-γ-stimulated MHC-II-deficient B16.gD (B16.gD.*Ciita*^{KO}, CIITA^{KO}) before and after flow sorting, to enrich for MHC-I^{+} MHC-II^{-} population. (**D)** MHC-I and MHC-II expression on the control cell line B16.gD.Px459 (CIITA^{WT}), ± IFN-γ stimulation *in-vitro*.

3.9 gDT-II CD4^{+} T cells can specifically recognise the HSV-gD epitope

Following *in-vitro* protocol establishment and assessing the B16 targets, we next determined the antigen specificity of gDT-II T cells towards the gD epitope. Primed gDT-II CD4^{+} T cells were sorted through flow cytometry and restimulated in co-cultures with WT splenocytes pulsed with either the gD peptide or an irrelevant CD4^{+} T cell peptide using the Lymphocytic choriomeningitis virus (LCMV) peptide (Figure 3.9A). gD-primed CD4^{+} T cells displayed significantly higher levels of both TNF-α and IFN-γ upon re-encounter with the gD peptide, but not with the LCMV peptide (Figure 3.9B). We further validated the specificity through priming the gDT-II cells with either the gD or the LCMV peptide, and subsequently co-culturing the cells with IFN-γ-stimulated parental B16.F10 WT or B16.gD cells (Figure 3.9C). As expected, the gD-primed cells produced significantly higher levels of both TNF-α and IFN-γ when co-cultured with B16.gD and not with the parental B16.F10 cell line (Figure 3.9D and 3.9E). Of note, this response was only exhibited with IFN-γ-pre-stimulated B16.gD cells (data not shown). Conversely, no

responses were triggered from the LCMV-primed CD4⁺ T cells following co-cultures with either of the B16 cell lines. Collectively, these data validated the antigen specificity of the transgenic CD4⁺ T cells towards the gD epitope.

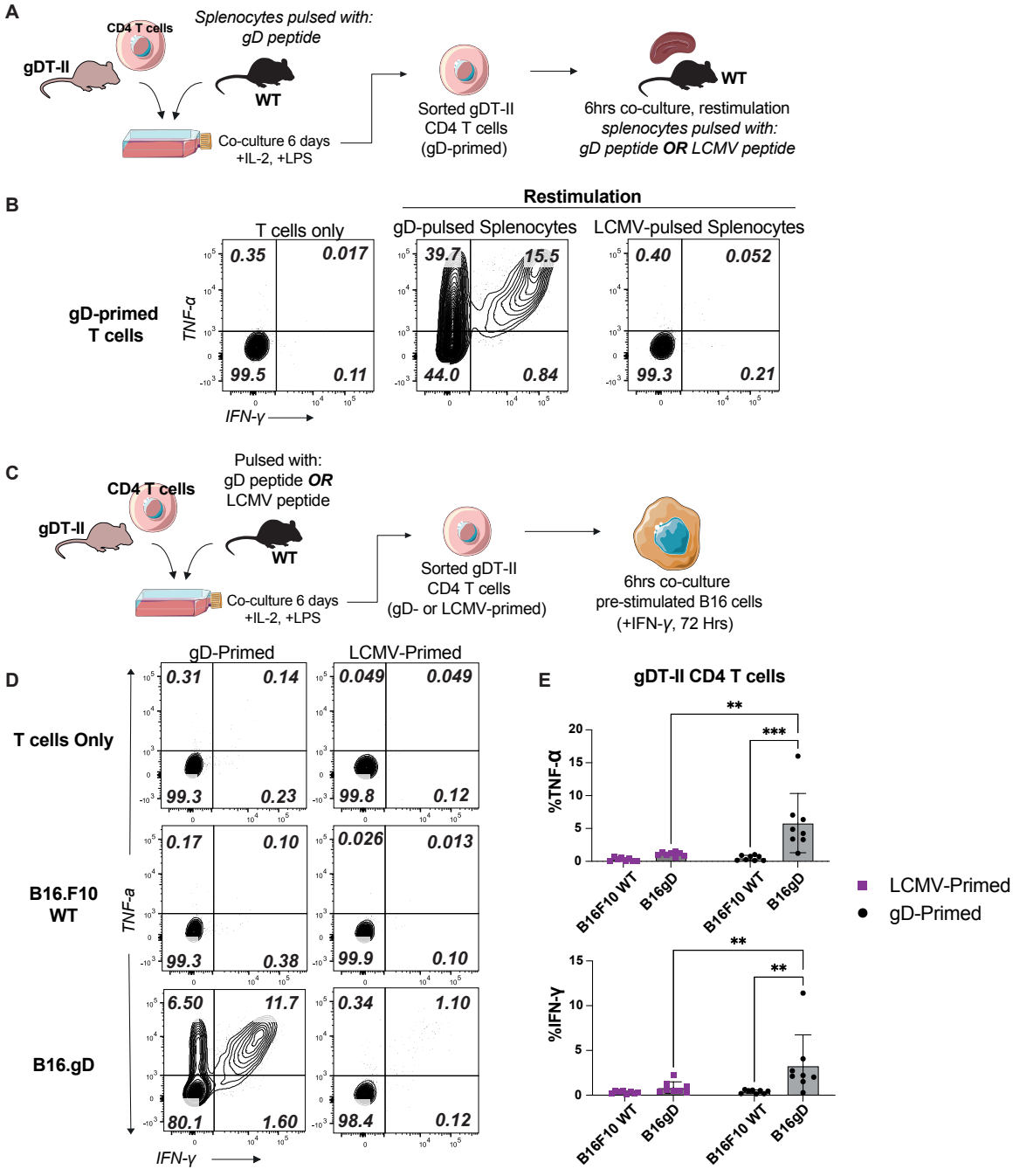

Figure 3.9: Antigen-specific activation and functional profiling of gDT-II CD4⁺ T cells **(A)** Experimental workflow for *in-vitro* priming and activation of gDT-II CD4⁺ T cells. For restimulation, primed T cells were co-cultured WT splenocytes (as APCs) pulsed with gD peptides. **(B)** Representative flow plots showing TNF-α and IFN-γ production from gD-primed gDT-II CD4⁺ T cells following restimulation with peptide-pulsed splenocytes. **(C)**

Schematic of co-culture assay of gD- or -LCMV-peptide primed gDT-II $CD4^+$ T cells with B16 melanoma cells (pre-stimulated with IFN-γ, 72 hours) (**D)** Representative dot plots showing TNF-α and IFN-γ production from the respective peptide-primed gDT-II $CD4^+$ T cells, following a 6-hour co-culture B16 cells (pre-stimulated with IFN-γ, 72 hours), and its respective quantification **(E)** (n= 8, mean ± SD, data cumulative of two experiments). Statistics: one-way ANOVA with post hoc Tukey's for multiple comparisons. *p < 0.05, **p < 0.01, ***p < 0.001, ****p < 0.0001.

3.10 MHC-II is required for an effective immune response against gD-expressing melanoma cells

As mentioned, the response from gD-primed $CD4^+$ T cells was only invoked in co-cultures with pre-stimulated B16.gD cells; bearing upregulated MHC-II expression post-stimulation. This aligns with various studies demonstrating the importance of MHC-II expression in antigen recognition by $CD4^+$ T cells in various cancers (Hunder et al. 2008; Tran et al. 2014; Leko et al. 2019). To confirm that direct antigen recognition is MHC-II dependant, we repeated the described co-culture experiment with MHC-II-deficient $CIITA^{KO}$ cells with $CIITA^{WT}$ controls (Figure 3.10A). Predictably, co-cultures with IFN-γ-stimulated $CIITA^{KO}$ cells did not induce any TNF-α or IFN-γ responses, nor upregulate CD25 expression from the gDT-II cells, as compared to co-culture with B16.gD or the $CIITA^{WT}$ cells (Figure 3.10B and 3.10C). Thereby, validating that MHC-II expression is essential for gD antigen recognition by gDT-II $CD4^+$ T cells in the neoantigen model.

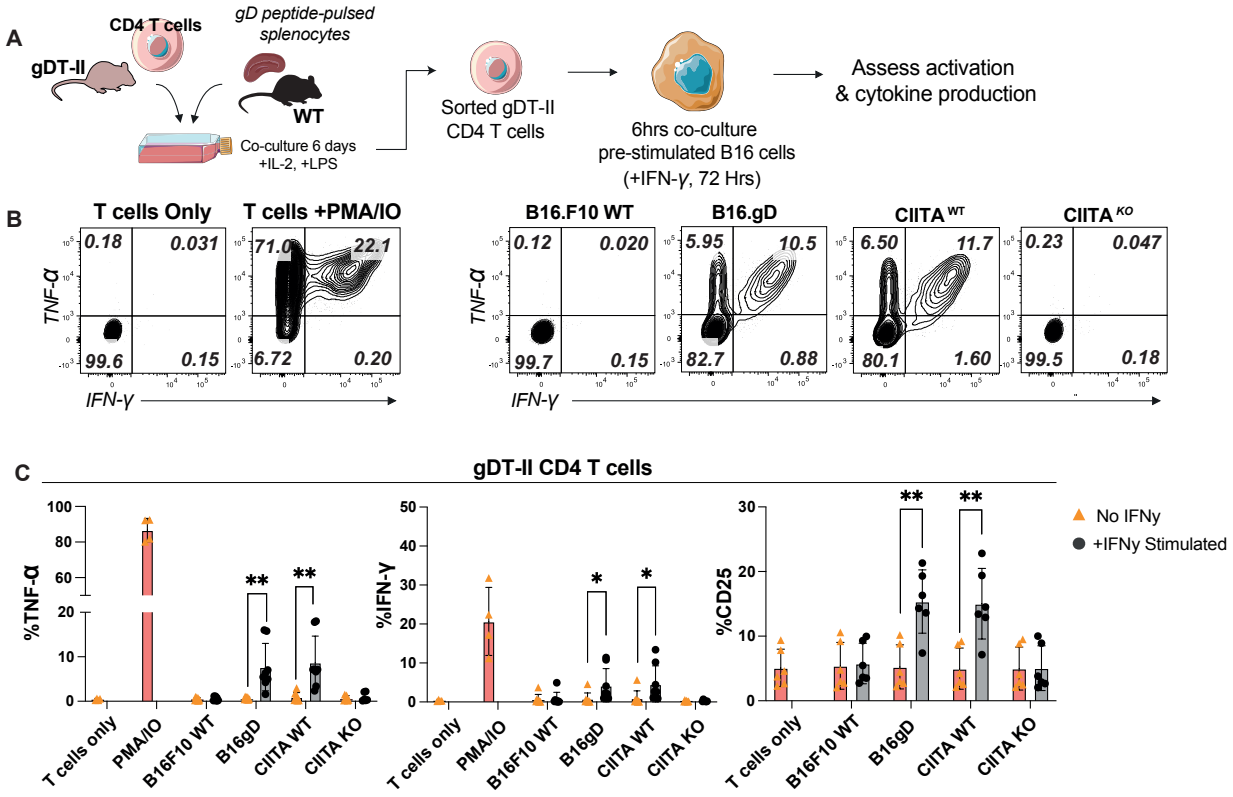

Figure 3.10: MHC-II expression is required for gDT-II CD4⁺ T cell recall response to the gD antigen
(A) Schematic for *in-vitro* gDT-II activation through gD-peptide priming with splenocytes. Primed gDT-II CD4⁺ T cells were sorted, and co-cultured with B16 melanoma cells (pre-stimulated with IFN-γ, 72 hours). **(B)** Representative flow cytometry plots showing TNF-α and IFN-γ by gD-primed gDT-II CD4⁺ T cells following co-culture with various B16 cells, including the MHC-II-expressing (B16.gD.Px459; $CIITA^{WT}$) or MHC-II-deficient (B16.gD.*Ciita*^{KO}; $CIITA^{KO}$) cells. **(C)** Corresponding quantification of TNF-α, IFN-γ and expression of CD25 by gDT-II CD4⁺ T cells after co-culture with the respective B16 melanoma cells (pre-stimulated with IFN-γ, 72 hours) (n= 6, mean ± SD, data cumulative of two experiments). Statistics: one-way ANOVA with post hoc Tukey's for multiple comparisons. *p < 0.05, **p < 0.01, ***p < 0.001, ****p < 0.0001.

3.11 Cytokine production from gD-primed CD4⁺ T cells requires CD226

Following the establishment and functional validation of the gDT-II model, we next addressed the importance of CD226 in anti-tumour responses from gD-primed CD4⁺ T cells in an antigen-specific setting. CD226-deficient gD-primed CD4⁺ T cells ($CD226^{KO}$) was firstly generated with CRISPR/Cas9 approach through nucleofection, subsequently flow-sorted, and subjected to co-cultures experiments with the B16 variants (Figure 3.11A). From the three designed CD226-targeting single-guide RNAs (sgRNA), sgRNA

#80 exhibited the highest knockout efficiency in WT $CD4^+$ T cells when compared to Mock controls, which did not receive any targeting sgRNA (Figure 3.11B). Hence, sgRNA #80 was chosen for the generation of $CD226^{KO}$ gDT-II cells for subsequent experiments. To enrich for $CD226^+$ and $CD226^-$ gD-primed cells, the nucleofected cells were flow-sorted accordingly – $CD226^{KO}$ cells from CD226-negative population; Mock from CD226-positive population – and rested overnight, before subsequent B16 co-cultures (Figure 3.11C and 3.11D). Notably, the Mock cells showed a gradual decrease of CD226 levels following overnight rest. $CD226^{KO}$ gDT-II cells displayed markedly lower TNF-α and IFN-γ production in contrast to the Mock cells in response against the B16.gD cells (Figure 3.11E-3.11H). Predictably, both $CD226^{KO}$ and Mock cells displayed limited responses when co-cultured with $CIITA^{KO}$ cells as compared to control $CIITA^{WT}$ or the parental B16.F10 cells (Figure 3.11G and 3.11H). Upon stratification of the homogenous $CD226^+$ and $CD226^-$ population within the Mock cells, the significant increase in cytokine levels observed upon gD antigen encounter, were predominantly driven by the $CD226^+$ population (Figure 3.11I and 3.11J). Taken together, these data suggest functional necessities for CD226 on antigen-primed $CD4^+$ T cells in executing MHC-II-restricted responses.

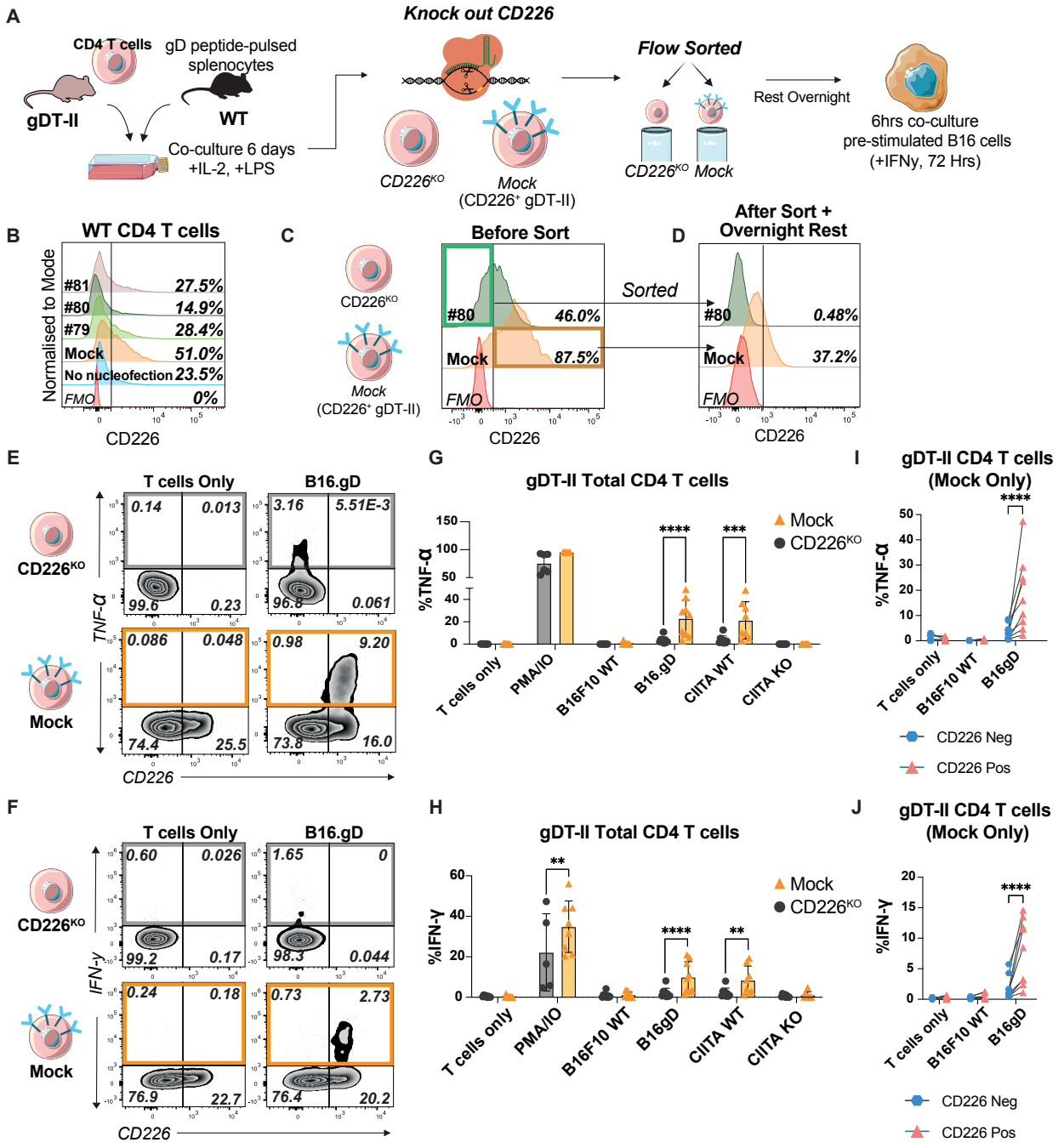

Figure 3.11: Antigen-primed CD226⁺ CD4⁺ T cells mediate cytokine production in tumour response

(A) Schematic for CRISPR-cas9 generation of $CD226^{KO}$ gDT-II $CD4^+$ T cells, followed by flow sorting and co-culture with IFN-γ-pre-treated B16 melanoma cells. **(B)** Representative histogram plots showing CD226 knockout efficacies of different sgRNAs in WT $CD4^+$ T cells. **(C)** Representative histogram showing CD226 knockout efficacy of selected guide RNA (#80) in gDT-II $CD4^+$ T cells. Cells were sorted accordingly ($CD226^{KO}$: $CD45.1^+$, $CD4^+$, $CD226^{neg}$; Mock: $CD45.1^+$, $CD4^+$, $CD226^{pos}$). **(D)** Representative histogram plots of CD226 expression from sorted samples post-sort following an overnight rest. **(E, F)** Representative dot plots showing TNF-α **(E)** IFN-γ production (F) from

$CD226^{KO}$ or Mock $CD4^+$ T cells after a 6-hour co-culture with IFN-γ-stimulated B16.gD cells. (**G, H)** Corresponding quantification of TNF-α **(G)** and IFN-γ **(H)** production from the $CD226^{KO}$ and Mock gDT-II $CD4^+$ T cells after a 6-hour co-culture with B16 cells (pre-stimulated with IFN-γ, 72 hours). **(I, J)** Cytokine production by $CD226^+$ vs $CD226^-$ subsets within Mock cells (n= 9, mean ± SD, data cumulative of 3 experiments). Statistics: paired Student's t test (G and J), one-way ANOVA with post hoc Tukey's for multiple comparisons (F and I). *p < 0.05, **p < 0.01, ***p < 0.001, ****p < 0.0001.

3.12 Human $CD226^+$ $CD4^+$ T cells produces IFN-γ upon TCR stimulation

Expanding upon previous observation in mice, we extended our analysis to human T cells to investigate if CD226 expression patterns on human $CD4^+$ T cells are similar to mice at baseline. Consistent with previous observations with mouse T cells, $CD8^+$ T cells from human PBMCs displayed higher CD226 expression level as compared to $CD4^+$ T cells (Figure 3.12A). Within the memory subsets, Tn from both $CD4^+$ and $CD8^+$ T cells showed limited surface CD226 expression relative to its respective memory groups (Tcm, Tem, Temra) (Figure 3.12B). Next, we investigated if surface CD226 expression on human $CD4^+$ T cells similarly identifies cytokine-secreting population as previously observed in mice, following comparable TCR stimulation conditions (Figure 3.12C). CD226 expression levels showed gradual upregulation across all time points as compared to baseline (Day 0), peaking at 72 hours post-stimulation (Figure 3.12D). Alongside the observed upregulated CD226 expression, we profiled characteristic Th cytokines (Th1: TNF-α, IFN-γ; Th2: IL-13; Th17: IL-17A; Tregs: IL-10). Production of IFN-γ levels increased significantly post-stimulation, with uniform levels across all time points (Figure 3.12E and 3.12F). Conversely, low levels were detected for IL-13, IL-17A and IL-10, relative to baseline (Figure 3.12G-3.12J). However, albeit the low level of cytokine production, IL-10 levels showed a mild significant upregulation at 24- and 48-hours post-stimulation (Figure 3.12K and 3.12L). Further analyses of CD226-negative and -positive population within the $CD4^+$ T cells at 72 hours post-stimulation revealed that cytokine production was driven mainly by the CD226-positive $CD4^+$ T cells (Figure 3.12M-3.12P).

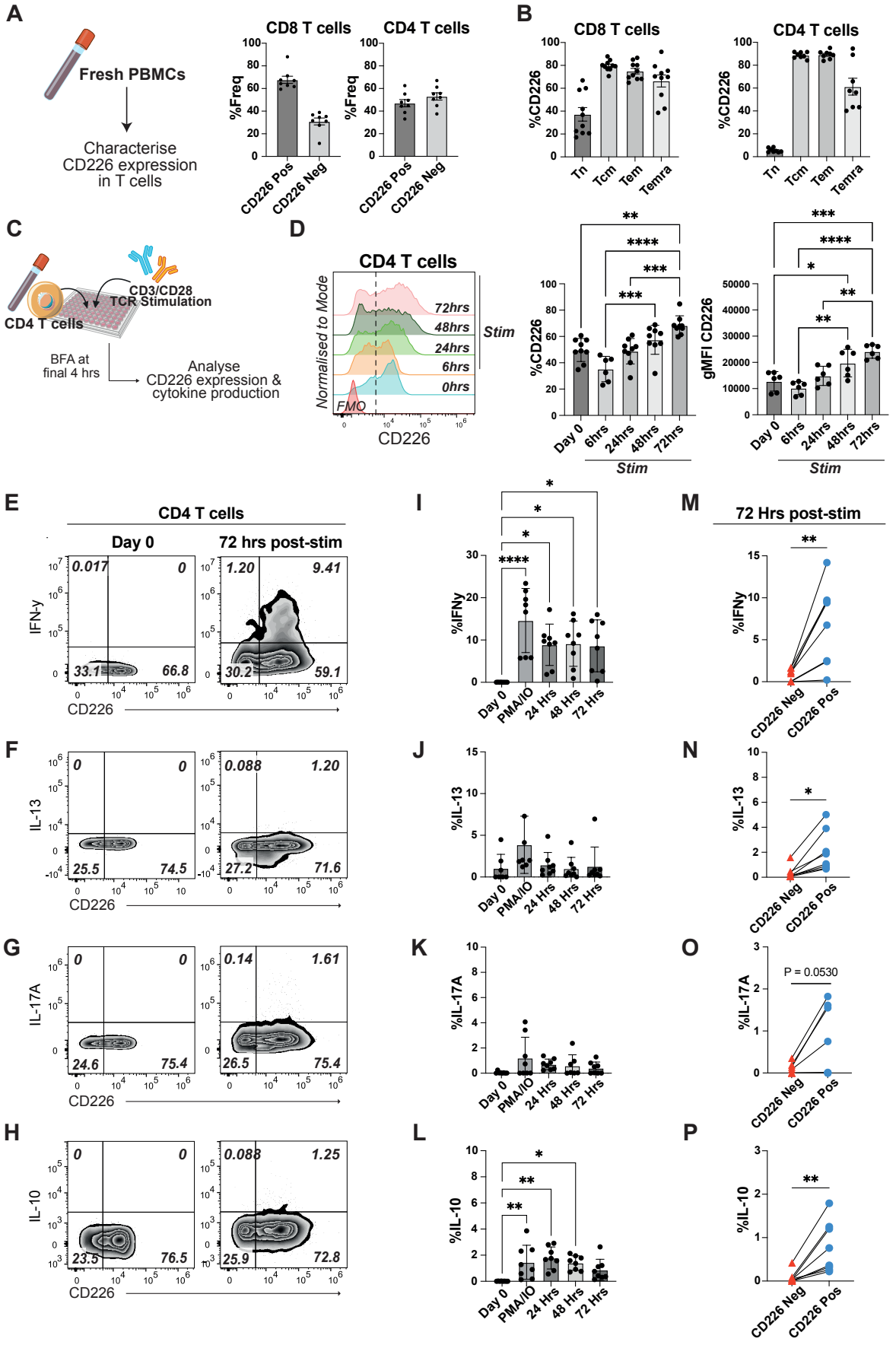
A
Fresh PBMCs
Characterise CD226 expression in T cells
CD8 T cells
CD4 T cells
%Freq
CD226 Pos
CD226 Neg
B
CD8 T cells
CD4 T cells
%CD226
Tn
Tcm
Tem
Temra
C
CD3/CD28 TCR Stimulation
CD4 T cells
BFA at final 4 hrs
Analyse CD226 expression & cytokine production
D
CD4 T cells
Normalised to Mode
72hrs
48hrs
24hrs
6hrs
0hrs
FMO
Stim
CD226
%CD226
gMFI CD226
Day 0
6hrs
24hrs
48hrs
72hrs
Stim
E
CD4 T cells
Day 0
72 hrs post-stim
IFN-γ
0.017
0
33.1
66.8
1.20
9.41
30.2
59.1
CD226
I
%IFNγ
Day 0
PMA/IO
24 Hrs
48 Hrs
72 Hrs
M
72 Hrs post-stim
CD226 Neg
CD226 Pos
F
IL-13
0
0
25.5
74.5
0.088
1.20
27.2
71.6
J
N
G
IL-17A
0
0
24.6
75.4
0.14
1.61
26.5
75.4
K
O
P = 0.0530
H
IL-10
0
0
23.5
76.5
0.088
1.25
25.9
72.8
L
P

Figure 3.12: CD226 surface expression correlates with cytokine production in human CD4$^+$ T cells
(A) Frequencies of CD4$^+$ and CD8$^+$ T cells from human PBMCs. **(B)** Quantification of CD226$^+$ populations among CD4$^+$ and CD8$^+$ T cells (n=8, mean ± SEM, one experiment). **(C)** Schematic illustration of *in-vitro* stimulation of human T cells isolated from PBMCs. **(D)** Representative histograms and quantification of surface CD226 expression on CD4$^+$ T cells following TCR stimulation (n= 6-9; mean ± SD, data cumulative of 2 experiments). **(E-H)** Representative flow cytometry plots showing cytokine production (IFN-γ, IL-13, IL-17A, IL-10) by CD4$^+$ T cells at baseline (Day 0) and 72 hours post-stimulation. (I-L) Corresponding quantification of the respective cytokines produced by total CD4$^+$ T cells. PMA/ionomycin (PMA/IO) control values were taken from the 48-hour timepoint of the experiments. **(M-P)** Cytokine production by CD226$^-$ and CD226$^+$ CD4$^+$ T cells at 72 hours post-stimulation (n=8; mean ± SD, cumulative of 2 experiments). Statistics: one-way ANOVA with post hoc Tukey's for multiple comparisons (I-L), paired Student's T-test (M-P); *p < 0.05, **p < 0.01.

3.13 CD226 deficiency in human CD4$^+$ T cells does not impair cytokine output

To investigate if CD226 is involved in cytokine production, we generated CD226KO from primary CD4$^+$ T cells using CRISPR/Cas9 as previously described, followed by TCR restimulation (Figure 3.13A). This constitutes as a restimulation because a prior activation of T cells was required for the generation of CD226^{KO} cells. Among the three designed CD226-targeting sgRNA, sgRNA #74 displayed the greatest knockout efficiency and utilised for subsequent generation of CD226^{KO} CD4$^+$ T cells (Figure 3.13B). Upon restimulation, both CD226^{KO} and Mock cells displayed limited levels of cytokines of lower than 8%, across all time points. Despite the modest increase in IFN-γ levels at 24 hours post-restimulation as compared to baseline, no differences were observed between the two cell groups across all time points (Figure 3.13C). Similar kinetics were displayed for the other cytokines (IL-13, IL-17A, IL-10) investigated in these experiments (Figure 3.13C-3.13F). Collectively, CD226 impairment in human CD4$^+$ T cells does not seem to significantly alter cytokine output following restimulation. However, given the low levels of cytokines detected, the data still remains inconclusive.

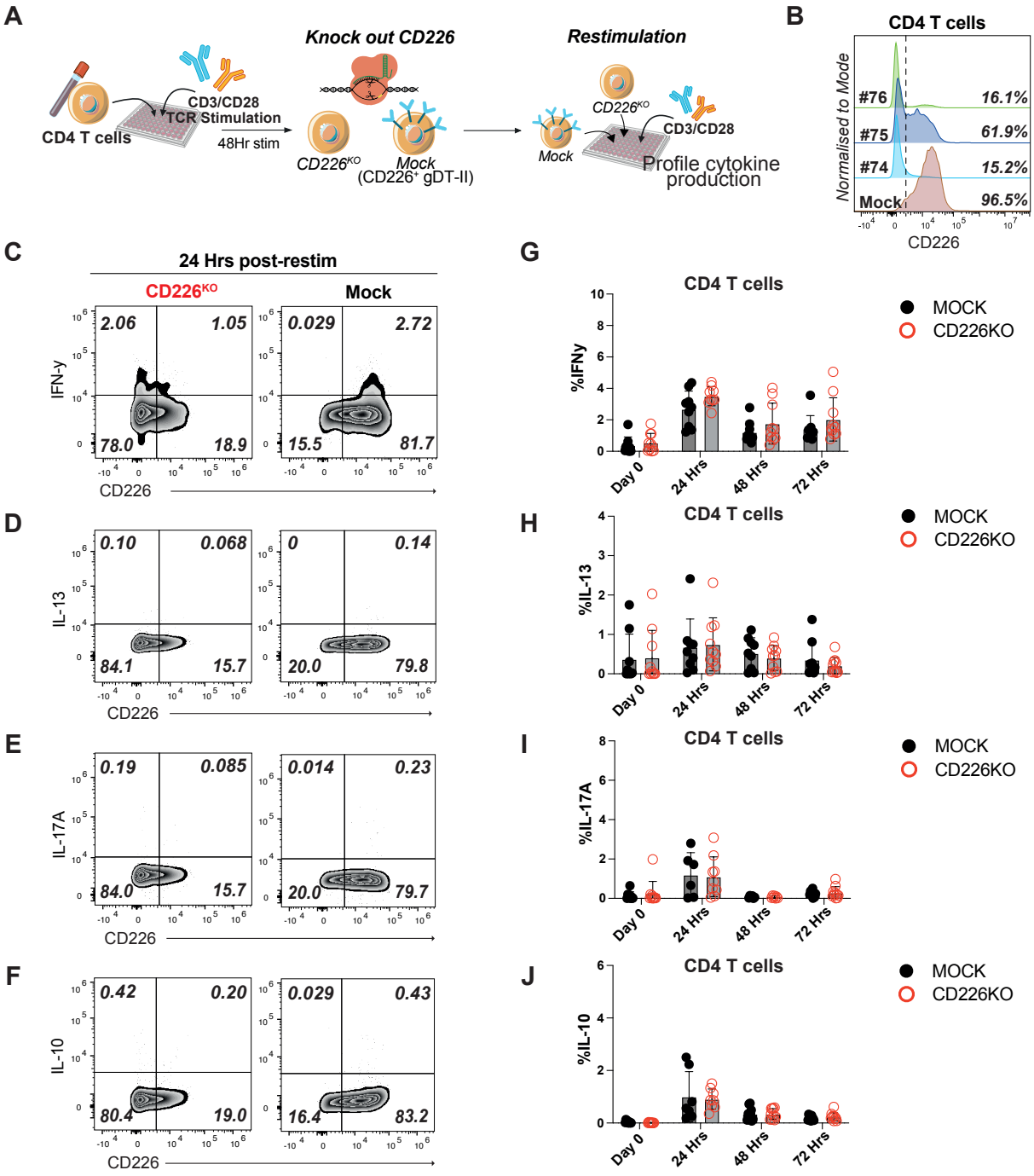

Figure 3.13: CD226 deficiency does not substantially alter cytokine production upon restimulation

(A) Schematic for CRISPR-cas9-mediated generation of CD226KO primary human CD4$^+$ T cells, followed by TCR restimulation with anti-CD3/CD28. **(B)** Representative histogram plots showing CD226 knockout efficiency of different CD226-targeting guide RNAs, with guide RNA #74 selected for subsequent experiments. **(C-F)** Representative flow cytometry plots showing cytokine production (IFN-γ, IL-13, IL-17A, IL-10) by CD226^{KO} and Mock CD4$^+$ T cells at 24 hours post-restimulation. **(G-J)** Corresponding quantification of cytokine production by CD226^{KO} and Mock CD4$^+$ T cells across all time points (n=9; mean

± SD, cumulative of 3 experiments). Statistics: one-way ANOVA with post hoc Tukey's for multiple comparisons (G-J); no significant differences observed between $CD226^{KO}$ and Mock cells at any time point.

3.14 CD226 is expressed on $CD4^+$ tumour-infiltrating lymphocytes

Many studies have demonstrated that high CD226-expressing $CD8^+$ TILs yields potent anti-tumour function and favourable prognosis (Weulersse et al. 2020; Huang et al. 2023; Viot et al. 2023). However, direct investigation of CD226 expression in human $CD4^+$ TILs remain limited. To explore this, the Tumour Immune Cell Atlas dataset was utilised (Nieto et al. 2021), consisting of TILs (n = 314,679) from 177 patients across multiple tumour subtypes (Figure 3.14A and 3.14B). CD226 is found to be expressed across all tumour entities within the dataset, with breast cancer (BC) displaying the highest level of expression. Immune cell type stratification showed that CD226 is expressed on a broad range of immune population within the tumour (Figure 3.14C). Further stratification of the $CD4^+$ TILs within the tumour subtypes revealed distinct clustering of subsets, with dense CD226 signal corresponding to Th cells (Figure 3.14D and 3.14E). Notably, the highest CD226 expression level was displayed in the $CD4^+$ T cells annotated as recently activated cells (Figure 3.14E). Taken together, this dataset demonstrates that $CD4^+$ T cells within the tumour displayed varying CD226 expression, which may suggest functional heterogeneity within the tumour microenvironment.

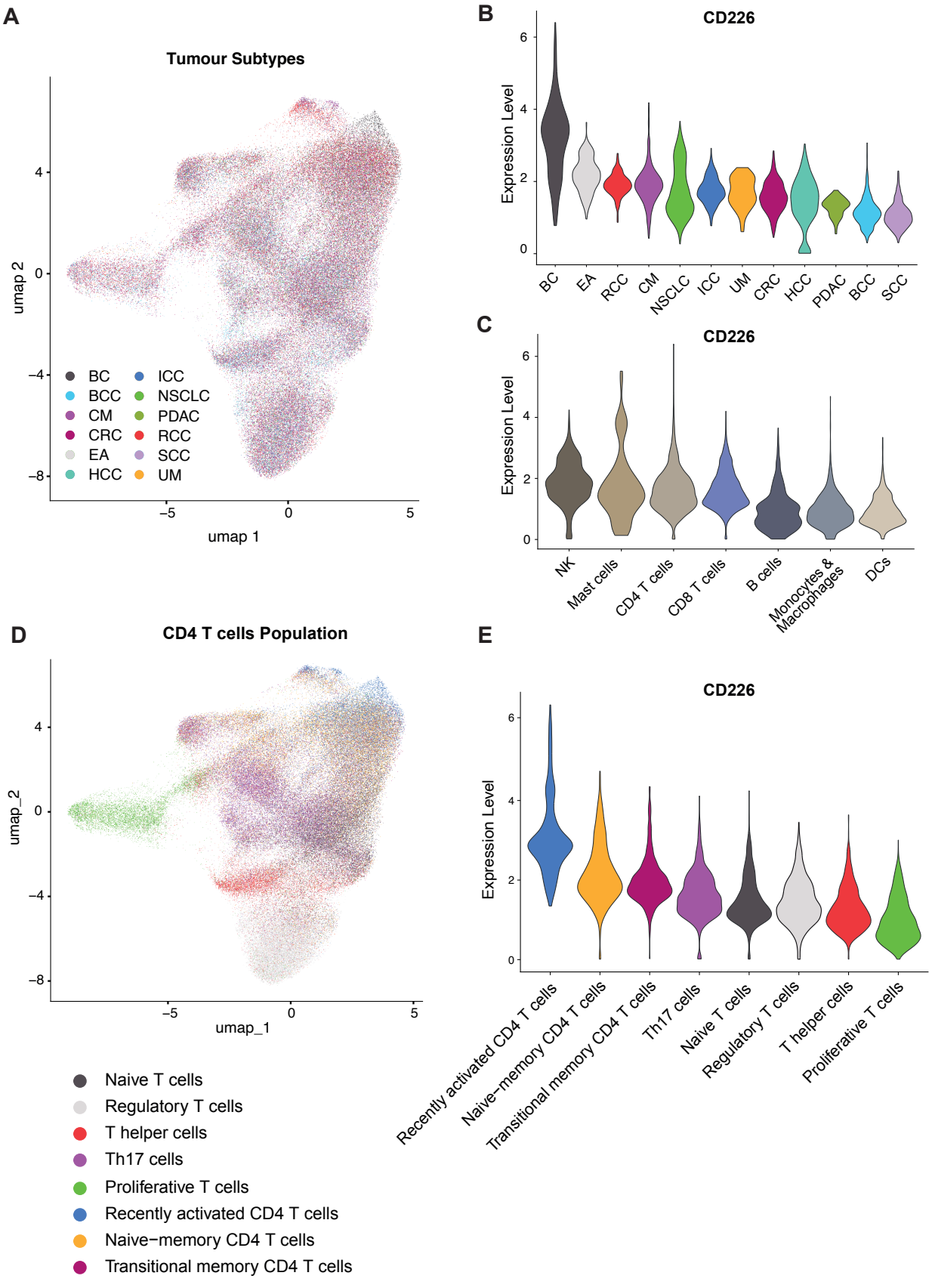
A
Tumour Subtypes
umap 2
umap 1
BC
BCC
CM
CRC
EA
HCC
ICC
NSCLC
PDAC
RCC
SCC
UM
B
CD226
Expression Level
BC
EA
RCC
CM
NSCLC
ICC
UM
CRC
HCC
PDAC
BCC
SCC
C
CD226
Expression Level
NK
Mast cells
CD4 T cells
CD8 T cells
B cells
Monocytes & Macrophages
DCs
D
CD4 T cells Population
umap_2
umap_1
Naive T cells
Regulatory T cells
T helper cells
Th17 cells
Proliferative T cells
Recently activated CD4 T cells
Naive−memory CD4 T cells
Transitional memory CD4 T cells
E
CD226
Expression Level
Recently activated CD4 T cells
Naive−memory CD4 T cells
Transitional memory CD4 T cells
Th17 cells
Naive T cells
Regulatory T cells
T helper cells
Proliferative T cells

Figure 3.14: CD226 is expressed on CD4$^+$ tumour-infiltrating lymphocytes across multiple cancer entities
(A) UMAP plot of the different tumour subtypes identified within the Tumor Immune Cell Atlas dataset. BC: Breast Cancer, BCC: Basal Cell Carcinoma, CM: Cutaneous Melanoma, CRC: Colorectal Cancer, EA: Esophageal Adenocarcinoma, HCC: Hepatocellular Carcinoma, ICC: Intrahepatic Cholangiocarcinoma, NSCLC: Non-small Cell Lung Cancer, PDAC: Pancreatic Ductal Adenocarcinoma, RCC: Renal Cell Carcinoma, SCC: Squamous Cell Carcinoma, UM: Uveal Melanoma. **(B)** Violin plot showing total CD226 expression levels across the tumour subtypes as well as **(C)** within intratumoral immune population. (**E)** Violin plot showing CD226 expression across the identified CD4+ T cell population within the dataset. These analyses were performed by Dr. Dillon Corvino**.**

3.15 CD155 and CD112 induces surface CD226 loss in human T cells

Building upon the heterogenous CD226 expression in human CD4$^+$ TILs, we next question whether the CD155-mediated downregulation mechanism – as observed in mice – would similarly impact CD4$^+$ TILs. For this, T cells isolated from PBMCs were co-culture with; CHO cells bearing stable expression of CD3 (CHO-OKT3), or expressing in combination with either CD155 (CHO-OKT3-CD155) or CD112 (CHO-OKT3-CD112) (Figure 3.15A). Co-cultures with OKT3-CD112 and OKT3-CD155 cells showed a significant increase in surface CD69 expression at 16 hours post-co-cultures, which are similar to those stimulated with CHO-OKT3 cells alone (Figure 3.15B). Thus, validating activation through the engagement of the stably expressed OKT3 on the CHO cell variants. Consistent to results observed in murine cells, CD226 expression levels on both human CD4$^+$ and CD8$^+$ T cells were drastically reduced when co-cultured with OKT3-CD155 cells as compared to controls. Interestingly, upon co-cultures with OKT3-CD112 cells, both CD4$^+$ and CD8$^+$ T cells also showed a marked decrease in surface CD226 level, with CD8$^+$ T cells exhibiting the stronger apparent effect (Figure 3.15C and 3.15D). However, prolonged co-cultures with OKT3-CD112 cells till 72 hours did not further exaggerate the CD226 downregulation on both T cells.

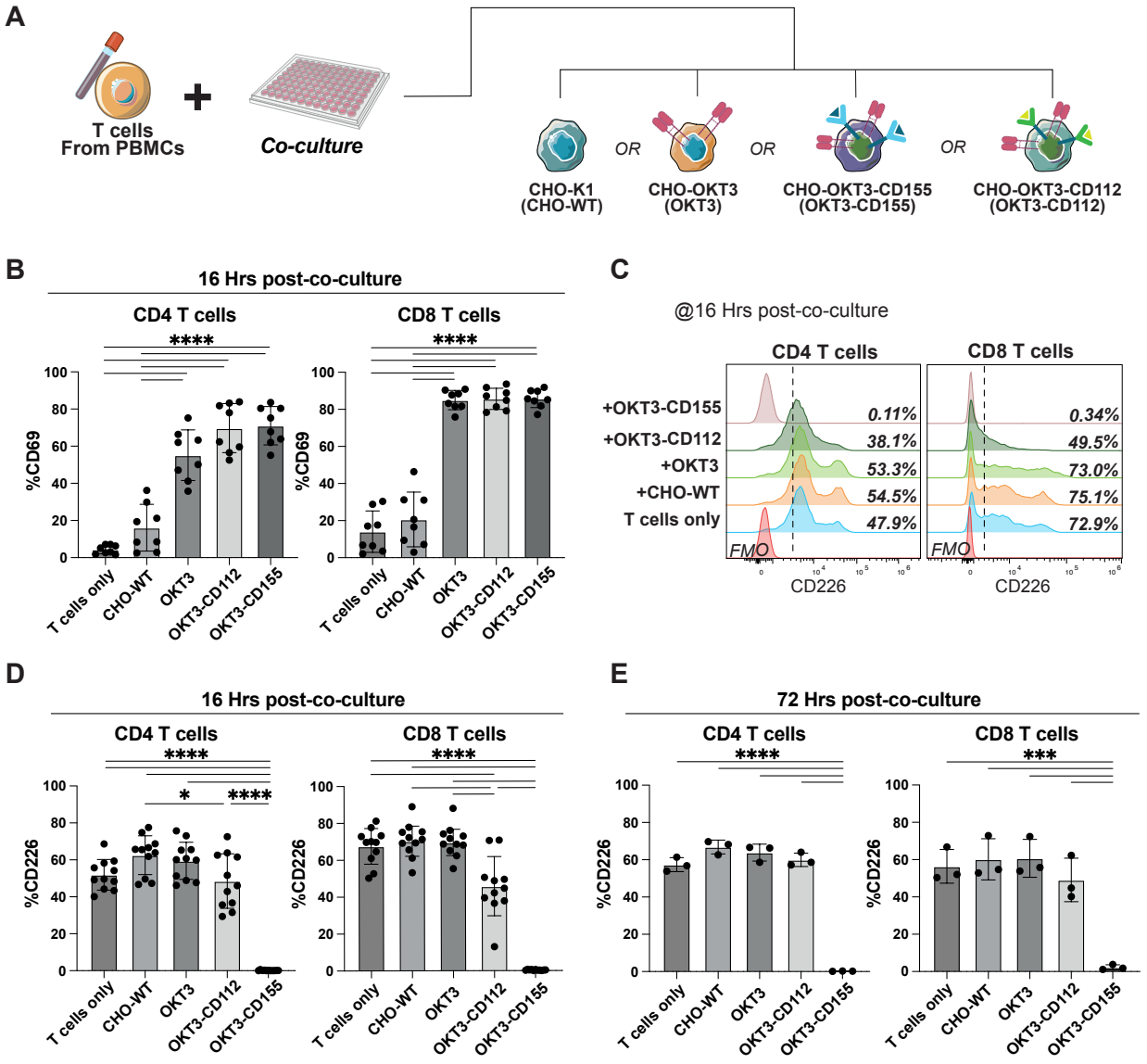

Figure 3.15: CD226 is downregulated on human T cells upon CD155 engagement
(A) Schematic of *in-vitro* co-cultures of T cells from PBMCs with different variants of CHO-K1 cell line. **(B)** Corresponding quantification of CD69 expression on T cells after a 16-hour co-culture with CHO-K1 variants. **(C)** Representative histogram plots showing surface CD226 expression on T cells after 16-hour co-cultures with CHO-K1 variants, with **(D)** corresponding quantification (n=11; mean ± SD, cumulative of 3 experiments). **(E)** Quantification of surface CD226 expression on T cells after 72 hours post co-cultures with CHO-K1 variants (n=3, mean ± SEM, one experiment). Statistics: one-way ANOVA with post hoc Tukey's for multiple comparisons (B, D, E). Experiments performed by Johannes Siewert.

4. Discussion

Immunotherapy investigations largely leveraged $CD8^+$ CTLs. However, this dismisses the role of $CD4^+$ T cells in anti-tumour immunity. Beyond the well-characterised suppressive mechanisms of Tregs, accumulating evidences underscores the crucial contribution of $CD4^+$ T cells towards overall anti-tumour immunity. Several studies have shown that adoptive co-transfer of both $CD4^+$ and $CD8^+$ T cells, resulted in significantly enhanced overall anti-tumour responses as compared to transfer of either subset alone (Böhm et al. 1998; Huang et al. 2005). Due to the diverse subsets within the $CD4^+$ T cells, delineating their exact mechanism within the already complex TME, proves to be challenging. Additionally, although inhibitory receptors on TILs have been extensively characterised, the function and regulation of activating receptors in the context of the TME remains unexplored. The activating receptor CD226 is crucial for NK and T cell function, especially in cancer (Gilfillan et al. 2008; Iguchi-Manaka et al. 2008). However, its role and regulation specifically in tumour-infiltrating $CD4^+$ T cells remains poorly understood. Given the emerging roles of $CD4^+$ T cells in anti-tumour immune responses and the importance of CD226 for $CD8^+$ T cell function, we hypothesised that optimal anti-tumour responses require CD226 surface expression on $CD4^+$ T cells.

4.1 Functional role of CD226 in $CD4^+$ T cells at baseline and in tumour

We showed that activated $CD4^+$ T cells displayed upregulated CD226 expression, a phenomenon of many co-stimulatory molecules. However, through anti-CD3/CD28 activation, we found that CD226 may be dispensable for cytokine production. Although, IFN-γ and TNF-α were predominantly detected, indicative of a Th1-skewed response. It is important to note that the TCR stimulation was performed in non-polarising conditions, and hence the cytokines profiles observed reflects the intrinsic default pathway of Th0 cells, instead of a committed Th1 lineage. This intrinsic default cytokine production was similarly reported in early studies, where Th1-related cytokines are among the first to be detected, and other lineage-characteristic cytokines detected later time points, following similar activation conditions (Webb and Feldmann 1995; Rostaing et al. 1999). Therefore, to properly evaluate the role of CD226 in $CD4^+$ T cell subset function, further investigation in polarised defined $CD4^+$ Th subsets is required or in Th-dependant cancer contexts.

To characterise the expression of CD226 in $CD4^+$ TILs, we injected WT mice with B16F1 melanoma cells, expressing high levels of CD155. Upon phenotypic characterisation, $CD4^+$ TILs were predominantly Th1 cells. Albeit the relatively high proportion of Th1 cells detected, they are limited in their CD226 expression. Given that CD226 has been described to be highly expressing on Th1 cells due to its role in differentiation and effector function (Smits et al. 2002); this limited CD226 expression in the tumour-derived Th1 cells may suggest a failure to maintain or a progressive loss in CD226 expression. This was further exhibited when we observed a trend towards an inverse correlation between $CD226^+$ $CD4^+$ TILs and tumour volume; with larger tumours showing fewer $CD226^+$ $CD4^+$ TILs. Similar findings have been reported; where $CD226^-$ $CD8^+$ TILs accumulated in both mouse and human tumours, involving the transcriptional regulator Eomes, yielding loss of surface CD226, suppressed effector functions as well as reduced T cell fitness, after chronic exposure to tumours (Braun et al. 2020; Weulersse et al. 2020). However, it is still unclear if the accumulation of the $CD226^-$ $CD8^+$ T cells is due to the outgrowth of $CD226^-$ T cells, death of $CD226^+$ T cells, or active downregulation. Further clonal tracing or fate-mapping approach would be required for further clarification. Nevertheless, our data suggests that $CD226^-$ $CD4^+$ T cells similarly accumulate in tumours, with plausible dysfunction states, akin to that seen with $CD8^+$ T cell responses.

To assess functionality of the $CD4^+$ TILs, we attempted ex-vivo restimulation of the $CD4^+$ TILs via anti-CD3/CD28 antibodies to elicit a recall response. However, only limited levels of IFN-γ responses was detected (data not shown); reflecting either sub-optimal restimulation conditions or a true physiological exhausted or dysfunctional state of the $CD4^+$ TILs. These primary data prompt further investigation into the functional state and differential status of the CD226-expressing or non-expressing $CD4^+$ TILs subsets.

Future studies should explore how CD226 can function in different tumour contexts. Our scRNA-seq analysis of public human tumour atlases showed varying expression patterns of $CD4^+$ TILs as well as their corresponding CD226 expression across tumour types. In our *in-vivo* study, we utilised the B16F1 melanoma model, which is considered a “cold” tumour due to its low immunogenicity and limited lymphocytes infiltration. Given that $CD4^+$ T cell subset differentiation is influenced by the cytokine milieu of the TME and that TMEs can vary between cancers, some TME might favour certain subsets of $CD4^+$ T cells.

Therefore incorporating “hot” tumours, such as the murine colon adenocarcinoma cell line (MC38), which are more permissible to lymphocyte infiltration would be important to determine if CD226$^+$ CD4$^+$ T cells would function differently.

Collectively, we have shown that CD226$^+$ CD4$^+$ T cells represent a functionally active subset that coincides with Th1-related cytokine production, and potential anti-tumour mechanisms. Further investigation involving different tumour models would enable insights to the role of CD226 in CD4$^+$ TILs in different TME.

4.2 Regulation of CD226 on CD4$^+$ T cells upon ligand engagement

Others have previously shown that tumour cells can impair CD8$^+$ CTL fitness through CD155-mediated internalisation and degradation of CD226, yielding dysfunctional T cells – revealing potential mechanism of immune escape (Braun et al. 2020). We questioned if CD226$^+$ CD4$^+$ T cells have similar mechanisms. Here, we showed that CD155 ligation similarly displayed a loss of surface CD226 on both mouse and human CD4$^+$ T cells. Utilising *Cd226*^{Y319F} and *Cbl-b*$^{\Delta DR}$ mice, we further verified that phosphorylation of CD226 at tyrosine Y319, recruits the E3 ubiquitin ligase, Cbl-b, resulting in ubiquitination and proteasomal degradation of CD226. Although the functional consequence of this degradation was not explored in our study, these data illustrate that CD155-induced CD226 degradation is not exclusive to CD8$^+$ T cells, but may also impair CD4$^+$ T cells and thus could contribute to reduced anti-tumour functions. This is of relevance especially considering multiple cancer studies from others, and our earlier findings showing that CD226$^+$ CD4$^+$ T cells are predominantly the cytokine-producing population.

The role of Cbl-b in T cell activation and cancer has been well established (Chiang et al. 2000; Loeser et al. 2007). As a negative regulator, Cbl-b maintains T cell anergy until co-stimulation is engaged, acting as a checkpoint in TCR signaling (Paolino and Penninger 2010). Cbl-b targets multiple substrates involved in the T cell activation cascade, including the guanine nucleotide exchange factor, Vav-1. Vav-1 was implicated in CD226 downstream signalling leading to production of IL-17 by CD4$^+$ T cells, implying a relationship between Cbl-b acitivity and CD4$^+$ T cell functionality (Gaud et al. 2018).In this study, we have further validated that Cbl-b is also involved in the regulation of CD226$^+$ in CD4$^+$ T cells. However, the precise molecular mechanisms and downstream pathways underlying this regulation still remains unclear. Further investigation in this pathway may

unveil how Cbl-b further modulates effector functions through CD226-dependant signaling in the TME.

Apart from ubiquitination and proteasomal degradation, other regulatory pathways may converge to regulate CD226 surface expression on $CD4^+$ T cells, prompting further detailed investigation. PD-1 has been shown to promote CD226 dephosphorylation via recruitment of the protein tyrosine phosphatase Shp2, whereas TIGIT regulates CD226 activation through competitive ligand binding (Banta et al. 2022). Moreover, the transcription factor Eomes, is mostly enriched in $CD226^{neg}$ T cells due to its recruitment to the regulatory region of CD226, suggesting direct regulation (Weulersse et al. 2020). These insights suggests that a single pathway may not be solely responsible for CD226 regulation. Therefore, although these regulatory effectors have been described, the extent of their intrinsic interaction, hierarchical regulation, as well as their interplay within the CD226 signaling in $CD4^+$ T cells is yet to be fully demonstrated and prompts future investigation.

Several studies have explored the structures of human CD226, unveiling key features that are required for efficient ligand binding (Ralston et al. 2004; Deuss et al. 2019; Wang et al. 2019). However, comparative studies between mouse and human CD226 remains limited. In our study, we showed that CD112 ligation yielded CD226 downregulation on human T cells, which was not recapitulated in mouse T cells under similar conditions. We speculate that this could stem from the species-specific structural differences between mouse and human, and affinity binding differences between CD155 and CD112. An earlier study demonstrated that human CD226 interacts with both CD155 and CD112, while mouse CD226 primarily interacts with CD155, with limited CD112 interaction (Stanietsky et al. 2013). The extracellular domain of CD226 consists of two Ig-like domains - referred to as CD226-D1 and CD226-D2 (Figure 4.1). In humans, CD226-D1 has been shown to mediate binding to CD155, whereas the CD226-D2 provides structural stability for the receptor, and interacts minimally to CD155 (Deuss et al. 2019). Although the overall CD226 architecture and binding affinities are conserved, both mouse and human CD226 only share 54% homology, resulting to different ligand-binding interfaces (Figure 4.1) (Wang et al. 2019). Studies investigating the CD226-CD112 interactions remains limited; with one study showing that CD112 homophilic interactions in humans, results in CD226

accumulation at the immunological synapse, boosting avidity (Tahara-Hanaoka et al. 2004). Therefore, limited CD226-CD112 interactions may impair effective immunological synapse formation, potentially dampening overall immune responses of T cells.

Taken together, highlighted that species-specific differences occur which may stem from distinct structural or architectural features. Hence, these differences should be considered in functional studies, and future investigation should further interrogate the molecular relevance of CD112.

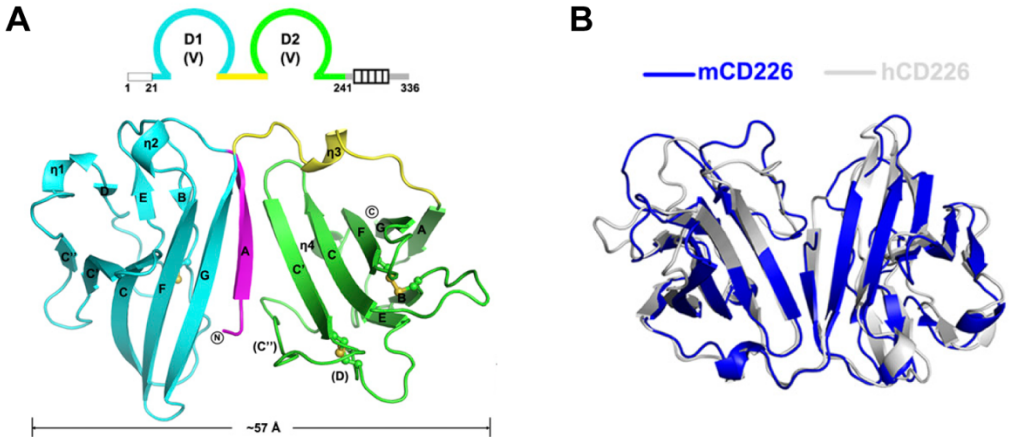

Figure 4.1: Overview of human and mouse CD226 structures
A) Ribbon representation of the extracellular domain of human CD226. CD226-D1 and CD226-D2 depicted through cyan and green colours respectively. Both domains are connected via arm linkers, coloured in magenta and yellow. **B)** Superimposed ectodomain structures of mouse (blue) and human (white) CD226. Figure taken from Wang et al. 2019.

4.3 CD226 as a prerequisite for cytotoxicity in CD4$^+$ T cells

Studies have reported CD4$^+$ T cell infiltration in various cancers can express cytotoxic markers. They can perform direct eradication of tumour cells or enhance overall anti-tumour responses through various mechanisms (Haabeth et al. 2018; Cachot et al. 2021; Kruse et al. 2023). Incorporating the gD antigen model, we demonstrated that CD226-deficiency in gDT-II CD4$^+$ T cells abolished cytokine production upon encountering B16.F10 presenting the gD epitope. This emphasises a critical role of CD226 in invoking tumour antigen-specific responses. Many tumours, including melanoma, expresses high levels of CD226 ligands (Braun et al. 2020). Additionally, CD226 has been reported to synergize with the adhesion molecule, LFA-1, which propagates downstream TCR signals, cytokine production and effector functions (Shibuya et al. 1999). Our initial *in-vitro*

experimental assays using anti-CD3/CD28 stimulation bypassed LFA-1 and CD226 engagement and therefore showed that CD226 deficiency may be equally capable of cytokine production. This suggests that under artificial TCR stimulation, CD226 may be dispensable; as similarly shown in a study which described that CD226-deficient naïve T cells concurred comparable activation milieu under similar activation conditions, but formed sub-optimal immunological synapses with APCs (Gilfillan et al. 2008). In contrast, in the more physiological context of tumour antigen recognition through the gD model, CD226 engagement with its ligands on the melanoma cells, likely prompted synergy with LFA-1 to amplify downstream TCR signalling, stabilise the immunological synapse, and subsequently driving effector functions. This is aligns with previous findings demonstrating the CD226-LFA-1 association and stable synapse formation are crucial for effective T cells responses (Ralston et al. 2004; Gilfillan et al. 2008). Moreover, previous work have also demonstrated that CD226-LFA-1 association influences Th1 differentiation from naïve $CD4^+$ T cells in an IL-12 independent manner (Smits et al. 2002); underscoring the ligand-dependant role for CD226 in Th1 expansion under physiological conditions.

Others have also shown that tumoricidal $CD4^+$ T cells can perform direct tumour eradication through TNF-α and FasL mechanisms (Bawden et al. 2024). Our findings further integrate into this, positioning CD226 as a potential key contributor to functional mechanisms. The loss of function exhibited by the CD226-deficient gDT-II CD4+ T cells underscores its importance in direct anti-tumour immunity.

Future assays should investigate if CD226-deficiency could potentially impair killing capacities through various cytolytic pathways involving perforin, granzymes, FasL and TNF-α; both *in-vitro* and *in-vivo*. Moreover, although $CD226^{KO}$ cells were generated using CRISPR-cas9 protocols, knockout efficiency was only confirmed via flow cytometric analysis and *in-vitro* assays. Future assays should also include genomic validation to confirm deletion integrity and obviate off-target effects.

We also demonstrated that the gD-specific $CD4^+$ T cells were only further activated when the melanoma cells were pre-treated with IFN-γ, which upregulated MHC-II expression. This aligns with previous studies that showed tumour-intrinsic MHC-II expression orchestrates $CD4^+$ T cells-mediated tumour control in the TME (Mumberg et al. 1999; Perez-Diez et al. 2007; Haabeth et al. 2018) and that its expression correlates with

favourable outcome with immunotherapy (Johnson et al. 2016; Oliveira et al. 2022). However, whether the tumour-intrinsic MHC-II is redundant remains unclear, as antigen presentation could potentially be compensated by professional APCs. This is of relevance for future experiments, considering TCR signalling strength and quality can differ between APCs and tumour due to the variation of co-stimulatory molecules (Driessens et al. 2009). It is established that an absence or weak co-stimulation may lead to T cell exhaustion or promote Treg functions instead (Driessens et al. 2009), or inhibit T and NK cell function through ligation of the immune checkpoint receptor Lag-3, which also can bind MHC-II (Johnson et al. 2018). The B7-CD28 pathway represents the primary and strongest costimulatory signal delivered by APCs to amplify T-cell activation. Positive costimulatory molecules, including the B7-1 and B7-2, are often absent in many tumours, despite these tumour cells conserving their ability for antigen presentation (Driessens et al. 2009). Earlier studies demonstrated that expression of B7-1 on tumours trigger robust CD8+ T cell-mediated anti-tumour responses and confer long-term protection upon rechallenge in several models (Chen et al. 1992; Baskar et al. 1993; Townsend and Allison 1993). However, in the context of non-immunogenic tumours, B7 expression was insufficient to elicit effective immune responses, indicating that other or additional tumour-intrinsic factors were required to overcome immune resistance (Chen et al. 1994). While we have shown that CD226-expressing gDT-II cells concurred response against the melanoma cells *in-vitro*, it is still unclear if a sub-optimal co-stimulation can trigger CD226-mediate co-stimulation, or if CD155/CD112 engagement alone is insufficient. Given that CD226 associates with LFA-1 for stable synapse formation and amplify downstream TCR signalling, the effectiveness of the CD226 axis in physiological conditions may further depend on cell-intrinsic properties such as adhesion molecules, synapse formation as well as ligand density.

Hence future studies concerning CD226's role on tumoricidal $CD4^+$ T cells should investigate the mechanisms concerning direct or indirect antigen presentation mechanisms, including cross-talk with intratumoral APCs and other immune cells.

5. Abstract

Activating receptors on T cells, such as CD226 (DNAM-1), play an important role for anti-cancer responses. Tumour cells can downregulate CD226 on $CD8^+$ T cells in mouse and human tumours and that the success of immune checkpoint blockade in melanoma patients correlates with the presence of $CD226^+$ $CD8^+$ T cells. While there is a growing recognition for the role of $CD4^+$ T cells in anti-tumour immunity, the role of CD226 in $CD4^+$ T cells functions remains unclear. In both mouse and human, CD226 expression is upregulated during activation and correlates with the functionality of $CD4^+$ T cells. Furthermore, a rapid downregulation of CD226 is observed upon ligation with its ligand, CD155. In tumour infiltrating $CD4^+$ T cells, we also observed reduced CD226 surface expression. A mutation at the tyrosine 319 (Y319) residue showed resistance to CD155-driven downregulation. Mechanistically, CD155 induced Y319 phosphorylation, which led to Cbl-b mediated ubiquitination, internalisation, and ultimately proteasomal degradation of CD226. To further investigate the role of CD226 in tumour immunity, the herpes simplex glycoprotein D (gD) was utilised as a model antigen, because it harbours an epitope ($gD_{315–327}$) recognized by $CD4^+$ T cells from the transgenic gDT-II mice. *In-vitro* co-culture studies using CRISPR/Cas9 generated $CD226^{KO}$ $CD4^+$ gDT-II cells, showed limited cytokine production and activation as compared to WT controls. Hence, suggesting a role for $CD226^+$ $CD4^+$ T cells in anti-tumour function.

In summary, our findings provide insights to CD226 dynamics and its contribution to anti-tumour capacity of $CD4^+$ T cells. While therapeutic implications of CD226 on $CD4^+$ T cells remain to be fully explored, our study prompts future investigation into its functional and potential therapeutic significance.

6. List of figures

7. List of tables

8. References

Ahrends T, Spanjaard A, Pilzecker B, Bąbała N, Bovens A, Xiao Y, et al. CD4+ T Cell Help Confers a Cytotoxic T Cell Effector Program Including Coinhibitory Receptor Downregulation and Increased Tissue Invasiveness. Immunity. 2017 Nov 21;47(5):848-861.e5.

Akhmetzyanova I, Zelinskyy G, Littwitz-Salomon E, Malyshkina A, Dietze KK, Streeck H, et al. CD137 Agonist Therapy Can Reprogram Regulatory T Cells into Cytotoxic CD4+ T Cells with Antitumor Activity. J Immunol. 2016 Jan 1;196(1):484–492.

Azizi E, Carr AJ, Plitas G, Cornish AE, Konopacki C, Prabhakaran S, et al. Single-Cell Map of Diverse Immune Phenotypes in the Breast Tumor Microenvironment. Cell. 2018 Aug 23;174(5):1293-1308.e36.

Banta KL, Xu X, Chitre AS, Au-Yeung A, Takahashi C, O'Gorman WE, et al. Mechanistic convergence of the TIGIT and PD-1 inhibitory pathways necessitates co-blockade to optimize anti-tumor CD8+ T cell responses. Immunity. 2022 Mar 8;55(3):512-526.e9.

Baskar S, Ostrand-Rosenberg S, Nabavi N, Nadler LM, Freeman GJ, Glimcher LH. Constitutive expression of B7 restores immunogenicity of tumor cells expressing truncated major histocompatibility complex class II molecules. Proc Natl Acad Sci U S A. 1993 Jun 15;90(12):5687–5690.

Bawden EG, Wagner T, Schröder J, Effern M, Hinze D, Newland L, et al. CD4+ T cell immunity against cutaneous melanoma encompasses multifaceted MHC II–dependent responses. Sci Immunol. 2024 Jan 19;9(91):eadi9517.

Bedoui S, Whitney PG, Waithman J, Eidsmo L, Wakim L, Caminschi I, et al. Cross-presentation of viral and self antigens by skin-derived CD103+ dendritic cells. Nat Immunol. 2009 May;10(5):488–495.

Bekes I, Löb S, Holzheu I, Janni W, Baumann L, Wöckel A, et al. Nectin-2 in ovarian cancer: How is it expressed and what might be its functional role? Cancer Sci. 2019;110(6):1872–1882.

Bindea G, Mlecnik B, Tosolini M, Kirilovsky A, Waldner M, Obenauf AC, et al. Spatiotemporal Dynamics of Intratumoral Immune Cells Reveal the Immune Landscape in Human Cancer. Immunity. 2013 Oct 17;39(4):782–795.

Blomberg OS, Spagnuolo L, Garner H, Voorwerk L, Isaeva OI, van Dyk E, et al. IL-5-producing CD4+ T cells and eosinophils cooperate to enhance response to immune checkpoint blockade in breast cancer. Cancer Cell. 2023 Jan 9;41(1):106-123.e10.

Böhm W, Thoma S, Leithäuser F, Möller P, Schirmbeck R, Reimann J. T Cell-Mediated, IFN-γ-Facilitated Rejection of Murine B16 Melanomas1. J Immunol. 1998 Jul 15;161(2):897–908.

Boyman O, Sprent J. The role of interleukin-2 during homeostasis and activation of the immune system. Nat Rev Immunol. 2012 Mar;12(3):180–190.

Braun M, Aguilera AR, Sundarrajan A, Corvino D, Stannard K, Krumeich S, et al. CD155 on Tumor Cells Drives Resistance to Immunotherapy by Inducing the Degradation of the Activating Receptor CD226 in CD8+ T Cells. Immunity. 2020 Oct 13;53(4):805-823.e15.

Burnet FM. Immunological surveillance in neoplasia. Transplant Rev. 1971;7:3–25.

Burns GF, Triglia T, Werkmeister JA, Begley CG, Boyd AW. TLiSA1, a human T lineage-specific activation antigen involved in the differentiation of cytotoxic T lymphocytes and anomalous killer cells from their precursors. J Exp Med. 1985 May 1;161(5):1063–1078.

Cachot A, Bilous M, Liu YC, Li X, Saillard M, Cenerenti M, et al. Tumor-specific cytolytic CD4 T cells mediate immunity against human cancer. Sci Adv. 2021 Feb 26;7(9):eabe3348.

Cenerenti M, Saillard M, Romero P, Jandus C. The Era of Cytotoxic CD4 T Cells. Front Immunol. 2022 Apr 27;13.

Chang SH. T helper 17 (Th17) cells and interleukin-17 (IL-17) in cancer. Arch Pharm Res. 2019 Jul 1;42(7):549–559.

Chen L, Ashe S, Brady WA, Hellström I, Hellström KE, Ledbetter JA, et al. Costimulation of antitumor immunity by the B7 counterreceptor for the T lymphocyte molecules CD28 and CTLA-4. Cell. 1992 Dec 24;71(7):1093–1102.

Chen L, McGowan P, Ashe S, Johnston J, Li Y, Hellström I, et al. Tumor immunogenicity determines the effect of B7 costimulation on T cell-mediated tumor immunity. J Exp Med. 1994 Feb 1;179(2):523–532.

Chen X, Wan J, Liu J, Xie W, Diao X, Xu J, et al. Increased IL-17-producing cells correlate with poor survival and lymphangiogenesis in NSCLC patients. Lung Cancer. 2010 Sep 1;69(3):348–354.

Chiang YJ, Kole HK, Brown K, Naramura M, Fukuhara S, Hu RJ, et al. Cbl-b regulates the CD28 dependence of T-cell activation. Nature. 2000 Jan;403(6766):216–220.

Chraa D, Naim A, Olive D, Badou A. T lymphocyte subsets in cancer immunity: Friends or foes. J Leukoc Biol. 2019 Jan 31;105(2):243–255.

Conner M, Hance KW, Yadavilli S, Smothers J, Waight JD. Emergence of the CD226 Axis in Cancer Immunotherapy. Front Immunol. 2022 Jun 24;13:914406.

Corthay A, Skovseth DK, Lundin KU, Røsjø E, Omholt H, Hofgaard PO, et al. Primary Antitumor Immune Response Mediated by CD4+ T Cells. Immunity. 2005 Mar 1;22(3):371–383.

Dardalhon V, Schubart AS, Reddy J, Meyers JH, Monney L, Sabatos CA, et al. CD226 Is Specifically Expressed on the Surface of Th1 Cells and Regulates Their Expansion and Effector Functions1. J Immunol. 2005 Aug 1;175(3):1558–1565.

Deuss FA, Watson GM, Goodall KJ, Leece I, Chatterjee S, Fu Z, et al. Structural basis for the recognition of nectin-like protein-5 by the human-activating immune receptor, DNAM-1. J Biol Chem. 2019 Aug 16;294(33):12534–12546.

Dobrzanski MJ. Expanding Roles for CD4 T Cells and Their Subpopulations in Tumor Immunity and Therapy. Front Oncol. 2013 Mar 26;3.

Driessens G, Kline J, Gajewski TF. Costimulatory and coinhibitory receptors in anti-tumor immunity. Immunol Rev. 2009;229(1):126–144.

Du X, de Almeida P, Manieri N, de Almeida Nagata D, Wu TD, Harden Bowles K, et al. CD226 regulates natural killer cell antitumor responses via phosphorylation-mediated inactivation of transcription factor FOXO1. Proc Natl Acad Sci. 2018 Dec 11;115(50):E11731–E11740.

Dunn GP, Bruce AT, Ikeda H, Old LJ, Schreiber RD. Cancer immunoediting: from immunosurveillance to tumor escape. Nat Immunol. 2002 Nov;3(11):991–998.

Filipe-Santos O, Bustamante J, Chapgier A, Vogt G, de Beaucoudrey L, Feinberg J, et al. Inborn errors of IL-12/23- and IFN-gamma-mediated immunity: molecular, cellular, and clinical features. Semin Immunol. 2006 Dec;18(6):347–361.

Foulds KE, Zenewicz LA, Shedlock DJ, Jiang J, Troy AE, Shen H. Cutting Edge: CD4 and CD8 T Cells Are Intrinsically Different in Their Proliferative Responses1. J Immunol. 2002 Feb 15;168(4):1528–1532.

Fourcade J, Sun Z, Chauvin JM, Ka M, Davar D, Pagliano O, et al. CD226 opposes TIGIT to disrupt Tregs in melanoma. JCI Insight. 2018 Jul 25;3(14).

Freeman AJ, Vervoort SJ, Michie J, Ramsbottom KM, Silke J, Kearney CJ, et al. HOIP limits anti-tumor immunity by protecting against combined TNF and IFN-gamma-induced apoptosis. EMBO Rep. 2021 Nov 4;22(11):e53391.

Fridman WH, Zitvogel L, Sautès-Fridman C, Kroemer G. The immune contexture in cancer prognosis and treatment. Nat Rev Clin Oncol. 2017 Dec;14(12):717–734.

Gaud G, Roncagalli R, Chaoui K, Bernard I, Familiades J, Colacios C, et al. The costimulatory molecule CD226 signals through VAV1 to amplify TCR signals and promote IL-17 production by CD4 T cells. Sci Signal. 2018 Jul 10;11(538).

Gilfillan S, Chan CJ, Cella M, Haynes NM, Rapaport AS, Boles KS, et al. DNAM-1 promotes activation of cytotoxic lymphocytes by nonprofessional antigen-presenting cells and tumors. J Exp Med. 2008 Nov 24;205(13):2965–2973.

Gobert M, Treilleux I, Bendriss-Vermare N, Bachelot T, Goddard-Leon S, Arfi V, et al. Regulatory T Cells Recruited through CCL22/CCR4 Are Selectively Activated in Lymphoid Infiltrates Surrounding Primary Breast Tumors and Lead to an Adverse Clinical Outcome. Cancer Res. 2009 Mar 2;69(5):2000–2009.

Golubovskaya V, Wu L. Different Subsets of T Cells, Memory, Effector Functions, and CAR-T Immunotherapy. Cancers. 2016 Mar;8(3):36.

Guo X, Zhang Y, Zheng L, Zheng C, Song J, Zhang Q, et al. Global characterization of T cells in non-small-cell lung cancer by single-cell sequencing. Nat Med. 2018 Jul;24(7):978–985.

Haabeth OAW, Fauskanger M, Manzke M, Lundin KU, Corthay A, Bogen B, et al. CD4+ T-cell–Mediated Rejection of MHC Class II–Positive Tumor Cells Is Dependent on Antigen Secretion and Indirect Presentation on Host APCs. Cancer Res. 2018 Aug 14;78(16):4573–4585.

Hirschhorn-Cymerman D, Budhu S, Kitano S, Liu C, Zhao F, Zhong H, et al. Induction of tumoricidal function in CD4+ T cells is associated with concomitant memory and terminally differentiated phenotype. J Exp Med. 2012 Oct 22;209(11):2113–2126.

Hoepner S, Loh JMS, Riccadonna C, Derouazi M, Maroun CY, Dietrich PY, et al. Synergy between CD8 T Cells and Th1 or Th2 Polarised CD4 T Cells for Adoptive Immunotherapy of Brain Tumours. PLOS ONE. 2013 May 23;8(5):e63933.

Huang H, Bi XG, Yuan JY, Xu SL, Guo XL, Xiang J. Combined CD4+ Th1 effect and lymphotactin transgene expression enhance CD8+ Tc1 tumor localization and therapy. Gene Ther. 2005 Jun;12(12):999–1010.

Huang H, Huang Z, Ge J, Yang J, Chen J, Xu B, et al. CD226 identifies functional CD8+T cells in the tumor microenvironment and predicts a better outcome for human gastric cancer. Front Immunol. 2023 Mar 28;14.

Hunder NN, Wallen H, Cao J, Hendricks DW, Reilly JZ, Rodmyre R, et al. Treatment of metastatic melanoma with autologous CD4+ T cells against NY-ESO-1. N Engl J Med. 2008 Jun 19;358(25):2698–2703.

Iguchi-Manaka A, Kai H, Yamashita Y, Shibata K, Tahara-Hanaoka S, Honda S ichiro, et al. Accelerated tumor growth in mice deficient in DNAM-1 receptor. J Exp Med. 2008 Dec 22;205(13):2959–2964.

Johnson DB, Estrada MV, Salgado R, Sanchez V, Doxie DB, Opalenik SR, et al. Melanoma-specific MHC-II expression represents a tumour-autonomous phenotype and predicts response to anti-PD-1/PD-L1 therapy. Nat Commun. 2016 Jan 29;7:10582.

Johnson DB, Nixon MJ, Wang Y, Wang DY, Castellanos E, Estrada MV, et al. Tumor-specific MHC-II expression drives a unique pattern of resistance to immunotherapy via LAG-3/FCRL6 engagement. JCI Insight. 2018 Dec 20;3(24):e120360K.

Kim HS, Long EO. Complementary phosphorylation sites in the adaptor protein SLP-76 promote synergistic activation of natural killer cells. Sci Signal. 2012 Jul 10;5(232):ra49.

Kim JS, Shin ,Bo Ram, Lee ,Hong Kyung, Lee ,Jae Hee, Kim ,Ki Hun, Choi ,Jeong Eun, et al. Cd226−/− natural killer cells fail to establish stable contacts with cancer cells and show impaired control of tumor metastasis in vivo. OncoImmunology. 2017 Aug 3;6(8):e1338994.

Kim S, Iizuka K, Aguila HL, Weissman IL, Yokoyama WM. In vivo natural killer cell activities revealed by natural killer cell-deficient mice. Proc Natl Acad Sci U S A. 2000 Mar 14;97(6):2731–2736.

Kitano S, Tsuji T, Liu C, Hirschhorn-Cymerman D, Kyi C, Mu Z, et al. Enhancement of tumor-reactive cytotoxic CD4+ T cell responses after ipilimumab treatment in four advanced melanoma patients. Cancer Immunol Res. 2013 Oct;1(4):235–244.

Kruse B, Buzzai AC, Shridhar N, Braun AD, Gellert S, Knauth K, et al. CD4+ T cell-induced inflammatory cell death controls immune-evasive tumours. Nature. 2023 Jun;618(7967):1033–1040.

Kryczek I, Banerjee M, Cheng P, Vatan L, Szeliga W, Wei S, et al. Phenotype, distribution, generation, and functional and clinical relevance of Th17 cells in the human tumor environments. Blood. 2009 Aug 6;114(6):1141–1149.

Lee JR, Dalton RR, Messina JL, Sharma MD, Smith DM, Burgess RE, et al. Pattern of recruitment of immunoregulatory antigen-presenting cells in malignant melanoma. Lab Investig J Tech Methods Pathol. 2003 Oct;83(10):1457–1466.

Leko V, McDuffie LA, Zheng Z, Gartner JJ, Prickett TD, Apolo AB, et al. Identification of Neoantigen-Reactive Tumor-Infiltrating Lymphocytes in Primary Bladder Cancer. J Immunol Baltim Md 1950. 2019 Jun 15;202(12):3458–3467.

Liew FY. TH1 and TH2 cells: a historical perspective. Nat Rev Immunol. 2002 Jan;2(1):55–60.

Liu C, Wu S, Meng X, Liu G, Chen D, Cong Y, et al. Predictive value of peripheral regulatory T cells in non-small cell lung cancer patients undergoing radiotherapy. Oncotarget. 2017 Feb 9;8(26):43427–43438.

Liu J, Zhang N, Li Q, Zhang W, Ke F, Leng Q, et al. Tumor-Associated Macrophages Recruit CCR6+ Regulatory T Cells and Promote the Development of Colorectal Cancer via Enhancing CCL20 Production in Mice. PLOS ONE. 2011 Apr 29;6(4):e19495.

Loeser S, Loser K, Bijker MS, Rangachari M, van der Burg SH, Wada T, et al. Spontaneous tumor rejection by cbl-b–deficient CD8+ T cells. J Exp Med. 2007 Apr 16;204(4):879–891.

Lukacher AE, Morrison LA, Braciale VL, Malissen B, Braciale TJ. Expression of specific cytolytic activity by H-2I region-restricted, influenza virus-specific T lymphocyte clones. J Exp Med. 1985 Jul 1;162(1):171–187.

Ma H, Whitters MJ, Jacobson BA, Donaldson DD, Collins M, Dunussi-Joannopoulos K. Tumor cells secreting IL-13 but not IL-13Rα2 fusion protein have reduced tumorigenicity in vivo. Int Immunol. 2004 Jul 1;16(7):1009–1017.

Ma J, Hu W, Liu Y, Duan C, Zhang D, Wang Y, et al. CD226 maintains regulatory T cell phenotype stability and metabolism by the mTOR/Myc pathway under inflammatory conditions. Cell Rep. 2023 Oct 31;42(10):113306.

Maimela NR, Liu S, Zhang Y. Fates of CD8+ T cells in Tumor Microenvironment. Comput Struct Biotechnol J. 2019 Jan 1;17:1–13.

Maimone MM, Morrison LA, Braciale VL, Braciale TJ. Features of target cell lysis by class I and class II MHC-restricted cytolytic T lymphocytes. J Immunol Baltim Md 1950. 1986 Dec 1;137(11):3639–3643.

Miao X, Yang ZL, Xiong L, Zou Q, Yuan Y, Li J, et al. Nectin-2 and DDX3 are biomarkers for metastasis and poor prognosis of squamous cell/adenosquamous carcinomas and adenocarcinoma of gallbladder. Int J Clin Exp Pathol. 2013;6(2):179–190.

Mocikat R, Braumüller H, Gumy A, Egeter O, Ziegler H, Reusch U, et al. Natural killer cells activated by MHC class I(low) targets prime dendritic cells to induce protective CD8 T cell responses. Immunity. 2003 Oct;19(4):561–569.

Montauti E, Oh DY, Fong L. CD4+ T cells in antitumor immunity. Trends Cancer. 2024 Oct 1;10(10):969–985.

Mucida D, Husain MM, Muroi S, van Wijk F, Shinnakasu R, Naoe Y, et al. Transcriptional reprogramming of mature CD4^{+} helper T cells generates distinct MHC class II-restricted cytotoxic T lymphocytes. Nat Immunol. 2013 Mar;14(3):281–289.

Muller AJ, Sharma MD, Chandler PR, DuHadaway JB, Everhart ME, Johnson BA, et al. Chronic inflammation that facilitates tumor progression creates local immune suppression by inducing indoleamine 2,3 dioxygenase. Proc Natl Acad Sci. 2008 Nov 4;105(44):17073–17078.

Mumberg D, Monach PA, Wanderling S, Philip M, Toledano AY, Schreiber RD, et al. CD4+ T cells eliminate MHC class II-negative cancer cells in vivo by indirect effects of IFN-γ. Proc Natl Acad Sci. 1999 Jul 20;96(15):8633–8638.

Nieto P, Elosua-Bayes M, Trincado JL, Marchese D, Massoni-Badosa R, Salvany M, et al. A single-cell tumor immune atlas for precision oncology. Genome Res. 2021 Oct;31(10):1913–1926.

Oh DY, Fong L. Cytotoxic CD4+ T cells in cancer: Expanding the immune effector toolbox. Immunity. 2021 Dec 14;54(12):2701–2711.

Oliveira G, Stromhaug K, Cieri N, Iorgulescu JB, Klaeger S, Wolff JO, et al. Landscape of helper and regulatory antitumour CD4+ T cells in melanoma. Nature. 2022 May;605(7910):532–538.

Oshima T, Sato S, Kato J, Ito Y, Watanabe T, Tsuji I, et al. Nectin-2 is a potential target for antibody therapy of breast and ovarian cancers. Mol Cancer. 2013 Jun 12;12(1):60.

Ouyang W, Liao W, Luo CT, Yin N, Huse M, Kim MV, et al. Novel Foxo1-dependent transcriptional programs control Treg cell function. Nature. 2012 Nov;491(7425):554–559.

Paolino M, Penninger JM. Cbl-b in T-cell activation. Semin Immunopathol. 2010 Jun 1;32(2):137–148.

Paterson AM, Lovitch SB, Sage PT, Juneja VR, Lee Y, Trombley JD, et al. Deletion of CTLA-4 on regulatory T cells during adulthood leads to resistance to autoimmunity. J Exp Med. 2015 Sep 21;212(10):1603–1621.

Perez-Diez A, Joncker NT, Choi K, Chan WFN, Anderson CC, Lantz O, et al. CD4 cells can be more efficient at tumor rejection than CD8 cells. Blood. 2007 Jun 15;109(12):5346–5354.

Poncette L, Bluhm J, Blankenstein T. The role of CD4 T cells in rejection of solid tumors. Curr Opin Immunol. 2022 Feb 1;74:18–24.

Punt S, Langenhoff ,Jessica M, Putter ,H, Fleuren ,Gert Jan, Gorter ,Arko, and Jordanova ES. The correlations between IL-17 vs. Th17 cells and cancer patient survival: a systematic review. OncoImmunology. 2015 Feb 1;4(2):e984547.

Puram SV, Tirosh I, Parikh AS, Patel AP, Yizhak K, Gillespie S, et al. Single-Cell Transcriptomic Analysis of Primary and Metastatic Tumor Ecosystems in Head and Neck Cancer. Cell. 2017 Dec 14;171(7):1611-1624.e24.

Quezada SA, Peggs KS, Curran MA, Allison JP. CTLA4 blockade and GM-CSF combination immunotherapy alters the intratumor balance of effector and regulatory T cells. J Clin Invest. 2006 Jul 3;116(7):1935–1945.

Quezada SA, Simpson TR, Peggs KS, Merghoub T, Vider J, Fan X, et al. Tumor-reactive CD4+ T cells develop cytotoxic activity and eradicate large established melanoma after transfer into lymphopenic hosts. J Exp Med. 2010 Feb 15;207(3):637–650.

Qui HZ, Hagymasi AT, Bandyopadhyay S, St Rose MC, Ramanarasimhaiah R, Ménoret A, et al. CD134 plus CD137 dual costimulation induces Eomesodermin in CD4 T cells to program cytotoxic Th1 differentiation. J Immunol Baltim Md 1950. 2011 Oct 1;187(7):3555–3564.

Ralston KJ, Hird SL, Zhang X, Scott JL, Jin B, Thorne RF, et al. The LFA-1-associated Molecule PTA-1 (CD226) on T Cells Forms a Dynamic Molecular Complex with Protein 4.1G and Human Discs Large*. J Biol Chem. 2004 Aug 6;279(32):33816–33828.

Rostaing L, Tkaczuk J, Durand M, Peres C, Durand D, de Préval C, et al. Kinetics of intracytoplasmic Th1 and Th2 cytokine production assessed by flow cytometry following in vitro activation of peripheral blood mononuclear cells. Cytometry. 1999;35(4):318–328.

Sakuishi K, Ngiow ,Shin Foong, Sullivan ,Jenna M., Teng ,Michele W. L., Kuchroo ,Vijay K., Smyth ,Mark J, et al. TIM3+FOXP3+ regulatory T cells are tissue-specific promoters of T-cell dysfunction in cancer. OncoImmunology. 2013 Apr 1;2(4):e23849.

Saleh M, Davis ID, Wilks AF. The paracrine role of tumour-derived mIL-4 on tumour-associated endothelium. Int J Cancer. 1997;72(4):664–672.

Sato K, Yamashita-Kanemaru Y, Abe F, Murata R, Nakamura-Shinya Y, Kanemaru K, et al. DNAM-1 regulates Foxp3 expression in regulatory T cells by interfering with TIGIT under inflammatory conditions. Proc Natl Acad Sci. 2021 May 25;118(21):e2021309118.

Schietinger A, Philip M, Liu RB, Schreiber K, Schreiber H. Bystander killing of cancer requires the cooperation of CD4+ and CD8+ T cells during the effector phase. J Exp Med. 2010 Oct 25;207(11):2469–2477.

Serroukh Y, Gu-Trantien C, Hooshiar Kashani B, Defrance M, Vu Manh TP, Azouz A, et al. The transcription factors Runx3 and ThPOK cross-regulate acquisition of cytotoxic function by human Th1 lymphocytes. eLife. 2018 Feb 28;7:e30496.

Shankaran V, Ikeda H, Bruce AT, White JM, Swanson PE, Old LJ, et al. IFNgamma and lymphocytes prevent primary tumour development and shape tumour immunogenicity. Nature. 2001 Apr 26;410(6832):1107–1111.

Shibuya A, Campbell D, Hannum C, Yssel H, Franz-Bacon K, McClanahan T, et al. DNAM-1, A Novel Adhesion Molecule Involved in the Cytolytic Function of T Lymphocytes. Immunity. 1996 Jun;4(6):573–581.

Shibuya A, Lanier LL, Phillips JH. Protein kinase C is involved in the regulation of both signaling and adhesion mediated by DNAX accessory molecule-1 receptor. J Immunol Baltim Md 1950. 1998 Aug 15;161(4):1671–1676.

Shibuya K, Lanier LL, Phillips JH, Ochs HD, Shimizu K, Nakayama E, et al. Physical and Functional Association of LFA-1 with DNAM-1 Adhesion Molecule. Immunity. 1999 Nov;11(5):615–623.

Shibuya K, Shirakawa J, Kameyama T, Honda S ichiro, Tahara-Hanaoka S, Miyamoto A, et al. CD226 (DNAM-1) Is Involved in Lymphocyte Function–associated Antigen 1 Costimulatory Signal for Naive T Cell Differentiation and Proliferation. J Exp Med. 2003 Dec 15;198(12):1829–1839.

Śledzińska A, Vila de Mucha M, Bergerhoff K, Hotblack A, Demane DF, Ghorani E, et al. Regulatory T Cells Restrain Interleukin-2- and Blimp-1-Dependent Acquisition of Cytotoxic Function by CD4+ T Cells. Immunity. 2020 Jan 14;52(1):151-166.e6.

Smits HH, de Jong EC, Schuitemaker JHN, Geijtenbeek TBH, van Kooyk Y, Kapsenberg ML, et al. Intercellular Adhesion Molecule-1/LFA-1 Ligation Favors Human Th1 Development1. J Immunol. 2002 Feb 15;168(4):1710–1716.

Spranger S, Spaapen RM, Zha Y, Williams J, Meng Y, Ha TT, et al. Up-Regulation of PD-L1, IDO, and Tregs in the Melanoma Tumor Microenvironment Is Driven by CD8+ T Cells. Sci Transl Med. 2013 Aug 28;5(200):200ra116-200ra116.

Stamm H, Wellbrock J, Fiedler W. Interaction of PVR/PVRL2 with TIGIT/DNAM-1 as a novel immune checkpoint axis and therapeutic target in cancer. Mamm Genome. 2018 Dec 1;29(11):694–702.

Stanietsky N, Rovis TL, Glasner A, Seidel E, Tsukerman P, Yamin R, et al. Mouse TIGIT inhibits NK-cell cytotoxicity upon interaction with PVR. Eur J Immunol. 2013;43(8):2138–2150.

Stengel KF, Harden-Bowles K, Yu X, Rouge L, Yin J, Comps-Agrar L, et al. Structure of TIGIT immunoreceptor bound to poliovirus receptor reveals a cell–cell adhesion and signaling mechanism that requires cis-trans receptor clustering. Proc Natl Acad Sci. 2012 Apr 3;109(14):5399–5404.

Tahara-Hanaoka S, Shibuya K, Onoda Y, Zhang H, Yamazaki S, Miyamoto A, et al. Functional characterization of DNAM-1 (CD226) interaction with its ligands PVR (CD155) and nectin-2 (PRR-2/CD112). Int Immunol. 2004 Apr 1;16(4):533–538.

Takeda K, Smyth MJ, Cretney E, Hayakawa Y, Kayagaki N, Yagita H, et al. Critical Role for Tumor Necrosis Factor–related Apoptosis-inducing Ligand in Immune Surveillance Against Tumor Development. J Exp Med. 2002 Jan 14;195(2):161–169.

Tan CL, Kuchroo JR, Sage PT, Liang D, Francisco LM, Buck J, et al. PD-1 restraint of regulatory T cell suppressive activity is critical for immune tolerance. J Exp Med. 2020 Oct 6;218(1):e20182232.

Tataroğlu C, Kargi A, Ozkal S, Eşrefoğlu N, Akkoçlu A. Association of macrophages, mast cells and eosinophil leukocytes with angiogenesis and tumor stage in non-small cell lung carcinomas (NSCLC). Lung Cancer Amst Neth. 2004 Jan;43(1):47–54.

Tau GZ, Cowan SN, Weisburg J, Braunstein NS, Rothman PB. Regulation of IFN-γ Signaling Is Essential for the Cytotoxic Activity of CD8+ T Cells1. J Immunol. 2001 Nov 15;167(10):5574–5582.

Tepper RI, Coffman RL, Leder P. An Eosinophil-Dependent Mechanism for the Antitumor Effect of Interleukin-4. Science. 1992 Jul 24;257(5069):548–551.

Terabe M, Matsui S, Noben-Trauth N, Chen H, Watson C, Donaldson DD, et al. NKT cell–mediated repression of tumor immunosurveillance by IL-13 and the IL-4R–STAT6 pathway. Nat Immunol. 2000 Dec;1(6):515–520.

Thomas L. On immunosurveillance in human cancer. Yale J Biol Med. 1982;55(3–4):329–333.

Tosolini M, Kirilovsky A, Mlecnik B, Fredriksen T, Mauger S, Bindea G, et al. Clinical Impact of Different Classes of Infiltrating T Cytotoxic and Helper Cells (Th1, Th2, Treg, Th17) in Patients with Colorectal Cancer. Cancer Res. 2011 Feb 14;71(4):1263–1271.

Townsend SE, Allison JP. Tumor Rejection After Direct Costimulation of CD8+ T Cells by B7-Transfected Melanoma Cells. Science. 1993 Jan 15;259(5093):368–370.

Tran E, Turcotte S, Gros A, Robbins PF, Lu YC, Dudley ME, et al. Cancer immunotherapy based on mutation-specific CD4+ T cells in a patient with epithelial cancer. Science. 2014 May 9;344(6184):641–645.

Viot J, Abdeljaoued S, Vienot A, Seffar E, Spehner L, Bouard A, et al. CD8+ CD226high T cells in liver metastases dictate the prognosis of colorectal cancer patients treated with chemotherapy and radical surgery. Cell Mol Immunol. 2023 Apr;20(4):365–378.

Volpert OV, Fong T, Koch AE, Peterson JD, Waltenbaugh C, Tepper RI, et al. Inhibition of Angiogenesis by Interleukin 4. J Exp Med. 1998 Sep 21;188(6):1039–1046.

Wang B, Zhang W, Jankovic V, Golubov J, Poon P, Oswald EM, et al. Combination cancer immunotherapy targeting PD-1 and GITR can rescue CD8+ T cell dysfunction and maintain memory phenotype. Sci Immunol. 2018 Nov 2;3(29):eaat7061.

Wang H, Qi J, Zhang S, Li Y, Tan S, Gao GF. Binding mode of the side-by-side two-IgV molecule CD226/DNAM-1 to its ligand CD155/Necl-5. Proc Natl Acad Sci. 2019 Jan 15;116(3):988–996.

Wang Y, Ma Y, Fang Y, Wu S, Liu L, Fu D, et al. Regulatory T cell: a protection for tumour cells. J Cell Mol Med. 2012;16(3):425–436.

Webb LMC, Feldmann M. Critical Role of CD28/B7 Costimulation in the Development of Human Th2 Cytokine-Producing Cells. Blood. 1995 Nov 1;86(9):3479–3486.

Weiskopf D, Bangs DJ, Sidney J, Kolla RV, De Silva AD, de Silva AM, et al. Dengue virus infection elicits highly polarized CX3CR1+ cytotoxic CD4+ T cells associated with protective immunity. Proc Natl Acad Sci U S A. 2015 Aug 4;112(31):E4256-4263.

Weulersse M, Asrir A, Pichler AC, Lemaitre L, Braun M, Carrié N, et al. Eomes-Dependent Loss of the Co-activating Receptor CD226 Restrains CD8+ T Cell Anti-tumor Functions and Limits the Efficacy of Cancer Immunotherapy. Immunity. 2020 Oct 13;53(4):824-839.e10.

Whelan S, Ophir E, Kotturi MF, Levy O, Ganguly S, Leung L, et al. PVRIG and PVRL2 Are Induced in Cancer and Inhibit CD8+ T-cell Function. Cancer Immunol Res. 2019 Feb 1;7(2):257–268.

Wing JB, Tanaka A, Sakaguchi S. Human FOXP3+ Regulatory T Cell Heterogeneity and Function in Autoimmunity and Cancer. Immunity. 2019 Feb 19;50(2):302–316.

Woo EY, Yeh H, Chu CS, Schlienger K, Carroll RG, Riley JL, et al. Cutting Edge: Regulatory T Cells from Lung Cancer Patients Directly Inhibit Autologous T Cell Proliferation1. J Immunol. 2002 May 1;168(9):4272–4276.

Yamada Y, Saito H, Ikeguchi M. Prevalence and clinical relevance of Th17 cells in patients with gastric cancer. J Surg Res. 2012 Dec 1;178(2):685–691.

Yeap WH, Wong KL, Shimasaki N, Teo ECY, Quek JKS, Yong HX, et al. CD16 is indispensable for antibody-dependent cellular cytotoxicity by human monocytes. Sci Rep. 2016 Sep 27;6(1):34310.

Yu X, Harden K, C Gonzalez L, Francesco M, Chiang E, Irving B, et al. The surface protein TIGIT suppresses T cell activation by promoting the generation of mature immunoregulatory dendritic cells. Nat Immunol. 2009 Jan;10(1):48–57.

Zeng T, Cao Y, Jin T, Tian Y, Dai C, Xu F. The CD112R/CD112 axis: a breakthrough in cancer immunotherapy. J Exp Clin Cancer Res. 2021 Sep 10;40(1):285.

Zhang JP, Yan J, Xu J, Pang XH, Chen MS, Li L, et al. Increased intratumoral IL-17-producing cells correlate with poor survival in hepatocellular carcinoma patients. J Hepatol. 2009 May 1;50(5):980–989.

Zhang L, Yu X, Zheng L, Zhang Y, Li Y, Fang Q, et al. Lineage tracking reveals dynamic relationships of T cells in colorectal cancer. Nature. 2018 Dec;564(7735):268–272.

Zhang Q, He Y, Luo N, Patel SJ, Han Y, Gao R, et al. Landscape and Dynamics of Single Immune Cells in Hepatocellular Carcinoma. Cell. 2019 Oct 31;179(4):829-845.e20.

Zhang Z, Wu N, Lu Y, Davidson D, Colonna M, Veillette A. DNAM-1 controls NK cell activation via an ITT-like motif. J Exp Med. 2015 Nov 16;212(12):2165–2182.

Zhou Y, Yang D, Yang Q, Lv X, Huang W, Zhou Z, et al. Single-cell RNA landscape of intratumoral heterogeneity and immunosuppressive microenvironment in advanced osteosarcoma. Nat Commun. 2020 Dec 10;11(1):6322.

9. Statement on own contribution

The work was carried out at the Institute of Experimental Oncology (IEO) at the University Hospital Bonn, under the supervision of Prof. rer. nat. Tobias Bald.

The experiment from Figure 3.3 was performed in collaboration with Franziska Schneppenhein and Carolin Birr at the IEO. Analyses of the Tumour Immune Cell Atlas dataset in figure 3.14 was performed and compiled by Dr. Dillon Corvino. The following experiments from figure 3.15 was carried out by Johannes Siewert (IEO).

All other experiments were carried out independently by me.

In preparing this work, I used ChatGPT to improve readibility and language of the manuscript. After using this tool, I reviewed and edited relevant sentences. I take full responsibility for the content of the published dissertation.

I confirm that I have written this thesis independently and have not used any sources or aids other than those specified by me.

I hereby confirm that my thesis complies with the Statement by the Executive Committee of the Deutsche Forschungsgemeinschaft (DFG, German Research Foundation) on the Influence of Generative Models of Text and Image Creation on Science and the Humanities and on the DFG’s Funding Activities.

10. Acknowledgements

The completion of this dissertation would not have been possible without the strong foundation built over the past five academic years. Firstly, I am deeply grateful for my supervisor, Prof. Dr. Tobias Bald, for the extraordinary opportunity to move from Brisbane to Bonn, to continue my academic journey. Your belief in me was often more than I had in myself, and this has been truly transformative. Your mentorship, scientific inputs, and endearing support (along with your positive energy!) have shaped my growth as a young scientist. My sincere appreciation goes to Prof. Dr. Michael Hölzel for his continued scientific support through the years, and for the establishment of the Institute of Experimental Oncology (IEO), which has been a vital academic and research environment during my PhD journey,

Additionally, I would also like to thank Prof. Dr. Christian Kurts, Prof. and Prof. Dr. Lukas Flatz for generously agreeing to be part of my dissertation committee and for their support in this process. I am also grateful to the ImmunoSensation^2 for their invaluable support they have provided for the academic growth for me and my peers.

I extend my sincere thanks to my colleagues at IEO for their all-rounding support throughout my academic and personal journey. Special thanks to Johannes Siewart and Dr. Dillon Corvino for generously sharing their findings in support of my project. I am also grateful to the technicians and post-docs of IEO, both present and alumni. Your beaming friendship and professional mentorship shaped Bonn to be home. To my wonderful office mates – Benjamin, Denise, Anu, & Fenna – Thanks for making lab life extremely enjoyable and memorable. I will truly miss our random office distractions and friendly banters.

Finally, I would like to express my deepest gratitude towards my friends and family for their unwavering support through this journey. This work is dedicated to my late father, who had sacrificed unconditionally for my success. I hope he would be proud wherever he is! To my Singaporean family: your constant encouragement has meant the world to me. Terima kasih banyak-banyak Ibu, Abang dan Kakak! Tak sabar nak balik! To my Porschen family; Danke, dass ihr mich in eure Familie aufgenommen habt und mich so bedingungslos liebt. And to Marcel; my greatest partner in crime, thank you for walking with me every step of the way. I am forever grateful to have you by my side – now, for life!